Magnetic dipole excitations in nuclei: Elementary modes of nucleonic motion

Kris Heyde*

Department of Subatomic and Radiation Physics, University of Gent, Proeftuinstraat 86, B-9000 Gent, Belgium

Peter von Neumann-Cosel†

Institut für Kernphysik, Technische Universität Darmstadt, Schlossgartenstraße 9, D-64289 Darmstadt, Germany

Achim Richter‡

Institut für Kernphysik, Technische Universität Darmstadt, Schlossgartenstraße 9, D-64289 Darmstadt, Germany
and ECT, Villa Tambosi, I-38123 Villazzano (Trento), Italy*

(Published 9 September 2010)

The nucleus is one of the most multifaceted many-body systems in the Universe. It exhibits a multitude of responses depending on the way one "probes" it. With increasing technical advancements of beams at the various accelerators and of detection systems the nucleus has, over and over again, surprised us by expressing always new ways of "organized" structures and layers of complexity. Nuclear magnetism is one of those fascinating faces of the atomic nucleus discussed in the present review. We shall not just limit ourselves to presenting the by now large data set that has been obtained in the past two decades using various probes, electromagnetic and hadronic alike and that presents ample evidence for a low-lying orbital scissors mode around 3 MeV, albeit fragmented over an energy interval of the order of 1.5 MeV, and higher-lying spin-flip strength in the energy region 5–9 MeV in deformed nuclei nor to the presently discovered evidence for low-lying proton-neutron isovector quadrupole excitations in spherical nuclei. To the contrary, the experimental evidence is put in the perspectives of understanding the atomic nucleus and its various structures of well-organized modes of motion and thus enlarges the discussion to more general fermion and bosonic many-body systems.

DOI: 10.1103/RevModPhys.82.2365 PACS number(s): 21.10.Pc, 21.60.−n

CONTENTS

*kris.heyde@ugent.be
†vnc@ikp.tu-darmstadt.de
‡richter@ikp.tu-darmstadt.de

I. INTRODUCTION

A. General remarks

Nucleons moving inside the atomic nucleus naturally generate orbital and spin magnetism. In certain mass regions—in particular, for nuclei between closed shells—the orbital magnetism can give rise to cooperative effects between the many nucleons in the nucleus. Collective modes might result from the out-of-phase motion of protons and neutrons and of those, magnetic dipole modes at fairly low energies ($0\hbar\omega$ excitations) excited with electromagnetic probes are one of the most pronounced ones. Besides these, at higher excitation energies, cooperative effects may even lead to collective spin-flip modes, as well as to even higher-lying genuine collective dipole modes ($2\hbar\omega$ excitations) which so far have not even been seen directly in experiments. In the present article, we start from a discussion of the early attempts in order to describe nucleonic out-of-phase motion leading to magnetic collective excitations (Sec. II) before entering into a discussion of magnetic dipole excitations in heavy nuclei (Sec. III). The experimental evidence that has been accumulated over the years concerning the observation of a so-called scissors mode in which the neutrons and protons in a deformed nucleus perform small angle vibrations in a scissorslike motion with respect to each other, using both electromagnetic and hadronic probes, is listed. Theoretical concepts concerning the description of the low-lying orbital scissors strength in even-even nuclei are presented. Collective (geometric and algebraic) and microscopic [shell-model and quasiparticle random phase approximation (QRPA) studies] models are discussed and they are related to one another in order to better understand both the complementarity and the specific model effects. The difficult problem of addressing the observed fragmentation of orbital magnetic strength will also be looked in the light of collective and microscopic approaches.

The aspects related to the experimental evidence and the derivation of a theoretical description of the concentration of spin-flip strength at higher excitation energies is presented in Sec. III as well, using mainly QRPA and shell-model calculations. In Sec. IV magnetic dipole excitations in heavy odd-mass nuclei are discussed. There the problem of missing strength in the measured spectra is looked at in some detail and the need for a better theoretical description of the fragmented transition strength is pointed out. Section V discusses experimental examples from magnetic dipole excitations in light and medium-heavy nuclei and their theoretical treatment in terms of the shell model and the QRPA. In Sec. VI we discuss the magnetic dipole isovector transitions in vibrational nuclei, illuminating the intimate connection with the scissors mode typical to rotational nuclei. In Sec. VII we bring the former discussion within a broader context of general many-body systems, e.g., deformed metallic clusters, quantum dots, and scissors motion in trapped Bose-Einstein condensates. In the final Sec. VIII, conclusions and an outlook are given concerning the issue of magnetic dipole excitations within the broader context of past and future nuclear physics research. Relevant literature on the subject that appeared until the end of 2009 has been considered in this review.

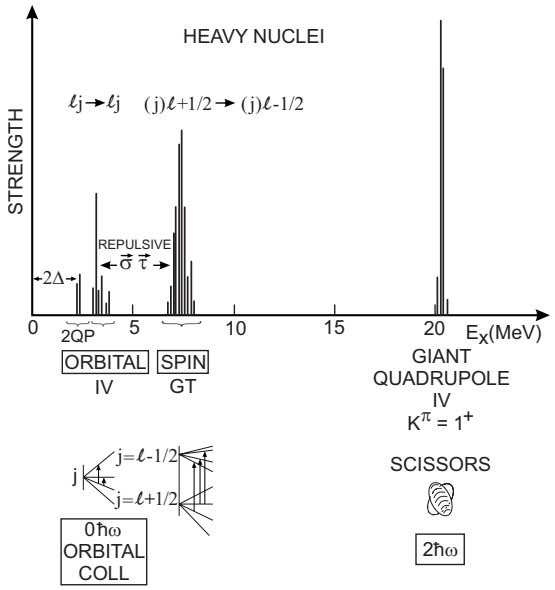

FIG. 1. Schematic representation of the magnetic dipole strength distribution in even-even heavy deformed nuclei and its model character. From Richter, 1990.

B. Magnetic dipole response in atomic nuclei: A qualitative overview

Even on rather general grounds, one can make a fingerprint figure for the magnetic dipole response in heavy rare-earth deformed nuclei on one side and more spherical and light nuclei on the other side. We illustrate the salient features of this response in two figures that shall be referred to quite often in the present review.

In even-even strongly deformed (rare-earth and actinide) nuclei, particularly due to the lifting of the spherical symmetry and the associated degeneracy in the various m components for a spherical orbital with angular momentum j, one can separate four different energies regions (see Fig. 1):

(i) At the excitation energy of about twice the pairing gap ($2\Delta \simeq 2-2.5$ MeV), two quasiparticle (2qp) $J^\pi = 1^+$ excitations show up with a very specific shell-model structure and thus, if these stay rather pure, can be detected in electromagnetic decay and selective transfer reactions.

(ii) At the excitation energy around 3 MeV, one observes a concentration of orbital magnetic dipole strength, built up from various 2qp configurations, into a weakly collective $0\hbar\omega$ mode, called the scissors mode. Here a number of proton and neutron 2qp configurations $(lj) \rightarrow (lj)$ contribute in a more or less coherent way, depending on external quantities such as nuclear deformation and the position of the Fermi level (number of protons Z and the number of neutrons N) in the Nilsson deformed single-particle spectrum.

(iii) In the excitation energy interval of 6–8 MeV, one starts observing the spin Gamow-Teller giant resonance (with a bound part, depending on the precise location in energy, and a resonance part) resulting from particle-hole (p-h) excitations across the major closed shells. In particular, shell-model transitions of the type $(j=l+\frac{1}{2}) \rightarrow (j=l-\frac{1}{2})$ play a major role. In the rare-earth region, depending on the precise proton and neutron number, the $1g_{9/2} \rightarrow 1g_{7/2}$, $1h_{11/2} \rightarrow 1h_{9/2}$, and $1i_{11/2} \rightarrow 1i_{11/2}$ transitions contribute most to the 1^+ spin mode. Moreover, the residual $\vec{\sigma}\cdot\vec{\sigma}\vec{\tau}\cdot\vec{\tau}$ repulsive part of the effective nucleon-nucleon interaction concentrates the spin strength from the lower-lying 2qp states around 2–4 MeV into this state. The final result is a large concentration of spin $M1$ strength.

(iv) Still higher in excitation energy, near 20 MeV, the $K^\pi = 1^+$ component of the isovector giant quadrupole resonance should eventually show up. This particular mode, built in a microscopic way from a coherent superposition of $2\hbar\omega$ configurations, has originally been studied in macroscopic collective models and this state would correspond to the "real scissors mode" in strongly deformed, rotational nuclei. Unfortunately, due to the very high excitation energy and due to the fact that its transition strength vanishes at the photon point because the $M1$ operator contains no radial dependence, such a state in the continuum is difficult to observe unambiguously.

The excitation mechanisms described in (i)–(iv) should thus lead to the typical fingerprint pattern of the magnetic dipole response in deformed rare-earth nuclei, in the actinides, and partly also in the medium-heavy deformed nuclei in the fp-shell region as shown schematically in Fig. 1. In the following discussion, we concentrate on these various patterns and give a thorough but succinct discussion of the experimental facts validating this former, more "idealized" picture, emerging from the basic underlying shell structure in deformed nuclei in combination with the essential multipole components of the residual two-body interactions: the pairing component, the repulsive $\vec{\sigma}\cdot\vec{\sigma}\vec{\tau}\cdot\vec{\tau}$ component, and the long-range quadrupole force.

In the spherical, lighter fp-shell nuclei but also in the region of lighter rare-earth nuclei (nuclei with neutron number N near to 82, and proton number Z between 50 to 66), a somewhat different and slightly simpler structure emerges (see Fig. 2):

(i) On the lower excitation energy side, one observes a rather stable (in energy) predominantly orbital 1^+ excitation which is produced through coupling the lowest proton 2^+_π excitation with the lowest neutron 2^+_ν excitation. Depending on the precise shell structure, one can also find some higher-lying $4^+_\pi \otimes 4^+_\nu$, $6^+_\pi \otimes 6^+_\nu$ fragments, in general, with rapidly decreasing $M1$ excitation strength. This feature is particularly evident in the light nuclei

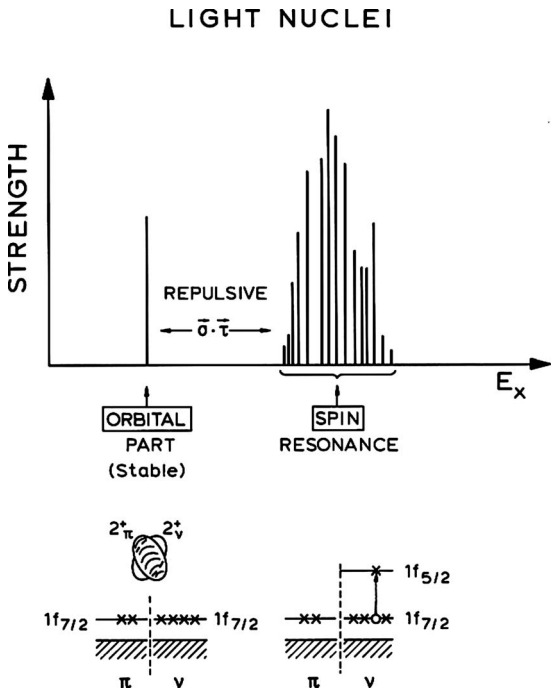

FIG. 2. Schematic representation of the magnetic dipole strength distribution in even-even light nuclei and its interpretation in terms of the shell model. The subscripts π and ν denotes the proton and neutron contributions, respectively. From Richter, 1990.

with protons and neutrons filling the spherical $1f_{7/2}$ shell-model orbital.

(ii) Removed from this lower state by several MeV and near to 10 MeV of excitation energy for the nuclei in the mass $A=50$ region, one finds the spin Gamow-Teller giant resonance. Here the repulsive spin-isospin force component is responsible for a coherent state made of $1p$-$1h$ excitations, mainly. For nuclei around mass $A=50$, this will predominantly be a $1f_{7/2}\rightarrow 1f_{5/2}$ excitation, whereas in the somewhat heavier mass $A=90$ region, one will encounter $1g_{9/2}\rightarrow 1g_{7/2}$ transitions.

The particular magnetic dipole response shown schematically in Fig. 2 forms the salient features amply discussed in the present article when highlighting $J^\pi=1^+$ states and the associated $M1$ strength for light and medium-heavy even-even nuclei. Besides the extensive exploration of the magnetic dipole response in deformed nuclei and also in the region of light to medium-heavy nuclei, uncovering the presence of a scissors mode (Sec. I.B), during the last decades, much progress has been made lately in the study of proton-neutron 2^+ excited states in vibrational and transitional nuclei, corresponding with mixed-symmetry wave functions in the proton and neutron building blocks. Here small amplitude quadrupole oscillations (phonons) dominate the low-energy nuclear structure properties. Coupling the proton 2^+_π and neutron 2^+_ν phonons can result in multiphonon

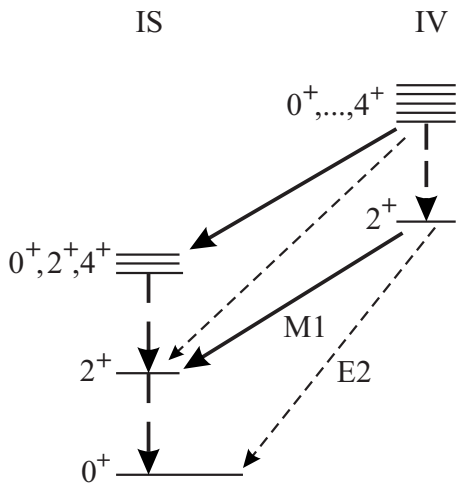

FIG. 3. Schematic representation of the $M1$ and associated $E2$ transitions of states with symmetric (lhs) and mixed-symmetric (rhs) wave functions in vibrational nuclei near closed shells.

states where the phonons move in phase (characterized by symmetric wave functions with shorthand notation S) but also with out-of-phase motion [with mixed-symmetry (MS) wave functions]. This is shown in Fig. 3. Recent review articles (Kneissl *et al.*, 2006; Pietralla, von Brentano, and Lisetsky, 2008) discussed the regions in which such 2^+ states have been observed as well as presented the experimental techniques needed to characterize unambiguously those isovector excitations (photon scattering, electron scattering, Coulomb excitation, β decay, inelastic neutron scattering, and light-ion fusion reactions as the major probes).

In view of the isoscalar and isovector components of the magnetic dipole operator (see also Secs. III.B.1 and VI for its precise structure and a more detailed discussion), the experimental identification of these isovector excitations, shown schematically in Fig. 3, is characterized by (i) strong $M1$ transitions (matrix element of $\simeq 1\mu_N$) between the MS and S states (thick full lines), (ii) weakly collective $E2$ transitions [a few percent of the large isoscalar $B(E2;2^+_1\rightarrow 0^+_1)$ transition probability, typical for vibrational and transitional nuclei] between the MS and S states (thin dashed lines), and (iii) strongly collective $E2$ transitions in between states with MS character, with strength typical for the collective $E2$ transitions between symmetric states (thick dashed lines).

These particular fingerprints properties result from a systematic exploration of isovector excitations in vibrational and transitional regions during the last decade (Pietralla, von Brentano, and Lisetsky, 2008) and clear-cut evidence for the observation of the lowest 2^+_{ms} (both of a one-phonon and two-phonon nature) as well as two-phonon 3^+_{ms} and 1^+_{ms} isovector excitations exists now for the mass regions with $Z\sim 40$, $N\sim 50$ and $Z\sim 50$, $50<N<82$, rare-earth nuclei in the region $54<Z\leqslant 82$, $72<N\leqslant 82$ (i.e., Xe, Ba, Ce, Nd, and Sm nuclei), as well

as nuclei in the $A\sim60$ mass region, and heavy nuclei near ^{208}Pb.

C. Scissors modes in other many-body systems

In the Introduction we have pointed out that the magnetic dipole response in strongly deformed atomic nuclei is characterized by a clearly separated orbital scissors mode (small-angle vibration of neutrons versus protons) at the lower energies and at the higher-energy side by a resonancelike structure comprised of proton and neutron spin-flip excitations. In nuclei with vibrational and transitional character, near to closed shells, mixed-symmetry excitations result from the isovector coupling of the lowest one-phonon proton and neutron 2_1^+ excitations. The essential ingredient in both cases is the presence of two distinguishable components, proton and neutron fluids, in the atomic nucleus.

It turns out that in other many-body systems very similar rotational oscillatory scissors motion has been discussed and, in certain cases, also been observed experimentally. The presence of a two-component or two-fluid quantum system is essential in this respect. In Sec. VII we address the main results obtained in the study of (i) metallic clusters (Lipparini and Stringari, 1989a; Nesterenko *et al.*, 1999), (ii) elliptically deformed quantum dots (Serra *et al.*, 1999; Alhassid, 2000), and (iii) the oscillatory behavior induced by the rotation of the atomic cloud in a deformed trap and the corresponding superfluid effects caused by Bose-Einstein condensation (Guéry-Odelin and Stringari, 1999; Maragò *et al.*, 2000, 2001), as well as their connections with the study of magnetic dipole excitations in atomic nuclei. The underlying common mechanism as well as some typical illustrations will also be presented.

II. EARLY THEORETICAL SUGGESTIONS FOR THE MAGNETIC SCISSORS MODE AND ITS EXPERIMENTAL DISCOVERY

A. Overview: A piece of history

Low-energy collective modes in atomic nuclei, for both spherical and deformed nuclei, displaying nuclear density oscillations or more permanently deformed structures of the density have been well described within the Bohr-Mottelson model (Bohr and Mottelson, 1975). In those excitations both the proton density $\rho_\pi(\vec{r})$ and the neutron density $\rho_\nu(\vec{r})$ exhibit variations that act in phase, i.e., isoscalar collective modes are obtained. It was soon realized that, besides these symmetric collective modes, nonsymmetric density variations might also show up. The latter excitations are expected to occur at much higher excitation energies, though, because of the symmetry energy term, coupling the proton and neutron density oscillations preferentially in a symmetric way. The giant electric-dipole mode—which in even-even nuclei excites negative parity states—is the best-known and well-documented example for such isovector excitations, the mode in which the center-of-mass for the charge and mass distributions do not coincide but perform an out-of-phase motion around the equilibrium value.

Nonsymmetric collective modes were considered quite early by Greiner (1965, 1966) and Faessler (1966), independently, at the end of the 1960s for spherical nuclei and this on the basis of isovector quadrupole collective excitations. Somewhat later but again, about at the same time and independently, Hilton (1976), Suzuki and Rowe (1977), and Lo Iudice and Palumbo (1978, 1979) suggested an extension of the Bohr-Mottelson description of rotational motion. The latter treated the nucleus in terms of a geometrical two-rotor model (TRM), in which a collective magnetic dipole ($M1$) mode could be formed by a rotational oscillation of the proton versus the neutron deformed density distribution (or fluids giving a rotational flow that is strongly excited as an orbital magnetic excitation). The name "scissors mode" was suggested much later after the experimental discovery of this mode originating in the peculiar nature of its geometrical picture (Richter, 1983; Bohle, Richter, *et al.*, 1984).

At that time, these nonsymmetric excitations, in particular the scissors mode in deformed systems, were a mere theoretical suggestion built on the strong fundament in describing nuclear collective motion (for both spherical and deformed nuclei). A determining factor in order to estimate the excitation energy and the strength was of course knowledge of the symmetry energy connected to the nonsymmetric motion. In the early calculations, the full symmetry energy term, known from a liquid-drop model treatment of global nuclear structure properties, was considered giving rise to energies and $B(M1)$ values much too large. It was only when the excitation energy of the scissors mode (having both a mass parameter and a restoring force strength) was adjusted to the observed experimental low-lying $B(E2)$ values including also pairing correlation in the protons and neutrons participating in the scissors motion that excitation energies of about 3–5 MeV (Suzuki and Rowe, 1977; De Franceschi *et al.*, 1983, 1984; Lipparini and Stringari, 1983) but still fairly high $B(M1)$ values of 9–18 μ_N^2 were obtained (De Franceschi *et al.*, 1983, 1984; Lipparini and Stringari, 1983).

Strong support for the above idea came from a different way of treating collective modes of motion in the nuclear many-body problem. Working in an algebraic framework and using the concepts of symmetry, Arima and Iachello (1975a, 1975b) formulated a model in which the interacting fermion problem is replaced by an interacting boson problem, only considering s ($L=0$) and d ($L=2$) boson degrees of freedom [interacting boson model (IBM)]. It was known from standard shell-model two-body interactions that the 0^+ coupled pair state and, to a much lesser extent, the 2^+ coupled pair dominate the binding of two-nucleon systems. By studying the symmetries of such an interacting boson model with the U(6) symmetry (the symmetry describing an interacting system of s and d bosons) and at the same time incorpo-

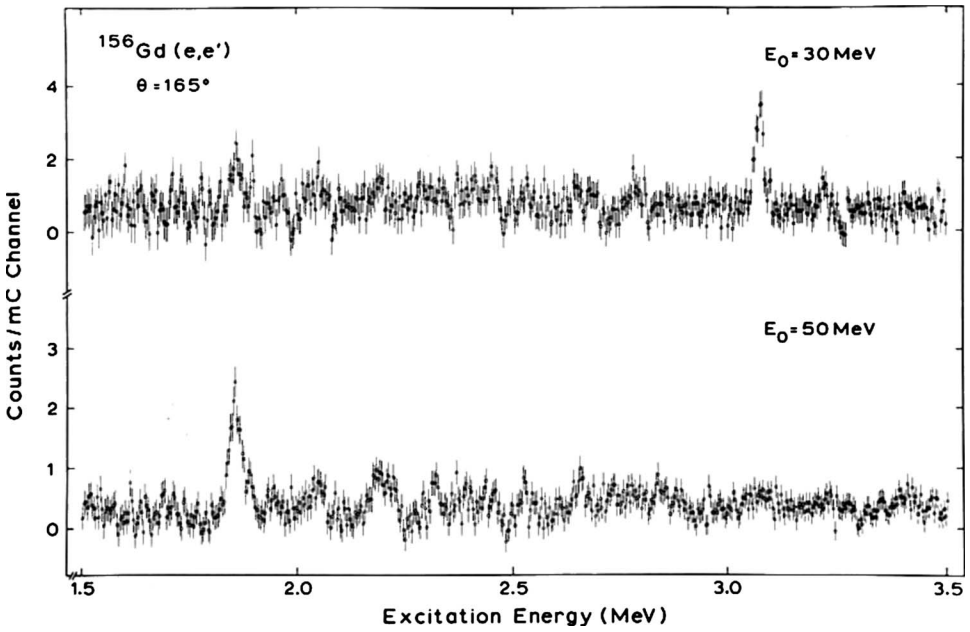

FIG. 4. Backward angle ^{156}Gd(e,e') spectra indicating the almost uniform excitation of many low-spin states in the measured energy region except for a strongly excited $J^\pi=1^+$ state seen in the 30 MeV spectrum at $E_x=3.075$ MeV and a known $J^\pi=3^-$ state at $E_x=1.825$ MeV in the 50 MeV spectrum. The excitation of the state at $E_x=3.075$ MeV is due to the scissors mode (Bohle, Richter, *et al.*, 1984).

rating the proton and neutron degrees of freedom (IBM-2), a class of states with nonsymmetric spatial and also nonsymmetric charge structure (mixed-symmetry states) showed up naturally. By fitting the parameters in the IBM-2 model to known fermionic properties, a $B(M1)$ value for a scissorslike mode of about 2–3 μ_N^2 has been predicted (Iachello, 1981).

B. Experimental discovery

Both the predictions of Lo Iudice and Palumbo (1978, 1979) within the TRM and of Iachello (1981) and Dieperink (1983) within the IBM-2 formed the essential basis for high-resolution inelastic electron scattering experiments at the Darmstadt Electron Linear Accelerator (DALINAC) to search for this mode. And indeed after much experimental efforts it has first been detected in the strongly deformed nucleus ^{156}Gd with essentially all the properties that were predicted (Richter, 1983).

Figure 4 from the work of Bohle, Richter, *et al.* (1984) displays two of the original spectra measured at a backward angle of $\theta=165°$ where magnetic excitations are expected to show up strongly. The spectrum, taken at the low bombarding energy $E_0=30$ MeV (corresponding to a low momentum transfer), reveals a rich fine structure of excited low-spin states with known experimental levels up to about 2.5 MeV of excitation energy. The only strong transition is to a state at $E_x=3.075$ MeV. This state is almost absent in the $E_0=50$ MeV spectrum (i.e., at a higher momentum transfer), in which, however, a well-known collective $J^\pi=3^-$ state at $E_x=1.852$ MeV is strongest. The state at $E_x=3.075$ MeV dominating all measured spectra at low momentum transfer has a form-factor behavior consistent with a $J^\pi=1^+$ assignment and a transition strength $B(M1)\uparrow$ of about $1.5\mu_N^2$.

Immediately after its discovery in ^{156}Gd it has been shown that the newly found $M1$ mode of course is not unique to this particular nucleus but is a general property of heavy deformed nuclei. This has been proven by inelastic electron scattering measurements at the DALINAC on the deformed nuclei ^{154}Sm, ^{158}Gd, ^{164}Dy, ^{168}Er, and ^{174}Yb (Bohle, Küchler, *et al.*, 1984), where also first evidence for the fragmentation of the scissors mode strength has been presented in the nucleus in which it has been discovered, ^{156}Gd. Furthermore, the new mode has also immediately been verified in nuclear resonance fluorescence experiments with real photons (Berg, 1984; Berg, Ackermann, *et al.*, 1984; Berg *et al.*, 1984).

Since then, the experimental evidence for such scissorslike excitations in strongly deformed nuclei but also in vibrational, transitional, and gamma-soft nuclei has become compellingly large. Moreover, the scissors mode has been explored besides the purely electromagnetic probes (electrons and photons) also with hadronic probes (proton scattering, and low-energy neutron-induced compound reactions) all over the nuclear mass table. A rather complete summary of the experimental data from electron and photon scattering can be found in Enders *et al.* (2005). Several articles covering this work from both the experimental and the theoretical point of view have appeared (Richter, 1985, 1990, 1991, 1993, 1994, 1995; Berg and Kneissl, 1987; Heyde, 1989; Kneissl *et al.*, 1996; Lo Iudice, 1997, 2000; Zawischa, 1998). In the next section (Sec. III.A.1), we discuss this experimental evidence for magnetic excitation of states of mixed-symmetric character (spatially and in the proton-neutron charge coordinates) and present all of the salient features in depth although not exhaustively. We put emphasis mainly on the overall and systematic features rather than on each individual case, separately. Thereby, we are able to focus on the essential properties of this mode of motion.

III. MAGNETIC DIPOLE EXCITATIONS IN HEAVY NUCLEI

A. Low-energy scissors mode

1. Experimental evidence

a. Overview

The early systematics of the scissors mode in heavy deformed nuclei known mainly from high-resolution electron and photoexcitation experiments at the DALINAC and the S-DALINAC in Darmstadt and the DYNAMITRON accelerator in Stuttgart was described by Richter (1995) and Kneissl *et al.* (1996). The majority of nuclei studied are even-even ones but the scissors mode has also been detected in a number of heavy odd-mass nuclei (Sec. IV). Very often the transition strength of the scissors mode is fragmented. In order to detect weak transitions, highly efficient gamma-ray detector systems with proper background suppression have to be used in photon scattering [also called nuclear resonance fluorescence (NRF)] experiments as discussed by Kneissl *et al.* (1996). In present-day nuclear resonance fluorescence experiments reduced transition strengths of $B(M1)\uparrow \approx 0.01\mu_N^2$ for magnetic dipole transitions at an energy of about 3 MeV can be detected. The scissors mode has been studied in vibrational and rotational nuclei and in chains of isotopic nuclei. Advances in gamma spectroscopy, e.g., by the use of EUROBALL detector modules (von Neumann-Cosel, 1997), have extended our knowledge of the scissors mode to γ-soft nuclei, ^{194,196}Pt (von Brentano *et al.*, 1996; Linnemann *et al.*, 2003), and the chain of Xe isotopes (von Garrel *et al.*, 2006). For example, in the rare-earth region a total of 42 isotopes ranging from Nd to Pt have been studied providing detailed experimental information on the systematics of the scissors mode. Furthermore, it has been verified in the actinide mass region (Heil *et al.*, 1988; Margraf *et al.*, 1990).

Comparison of different probes for the case of ^{156}Gd is shown in Fig. 5 (Richter, 1990). A combined analysis of the (e,e') and (γ,γ') experiments (Bohle *et al.*, 1986) revealed five more weakly excited $J^\pi=1^+$ states in the vicinity of the strongest one, bringing the total $M1$ strength up to about $2.4\mu_N^2$. The strongest state might be viewed acting as a doorway for the others. A high-resolution inelastic proton-scattering spectrum (Wesselborg *et al.*, 1986) is also shown in Fig. 5 and the absence of any of the states seen in the (e,e') and (γ,γ') reactions is already a strong hint that the scissors mode is excited through the orbital part of the magnetic dipole operator.

The salient features of the scissors mode in heavy deformed nuclei unraveled in high-resolution electron, photon, and proton-scattering experiments (Richter, 1995) are the following:

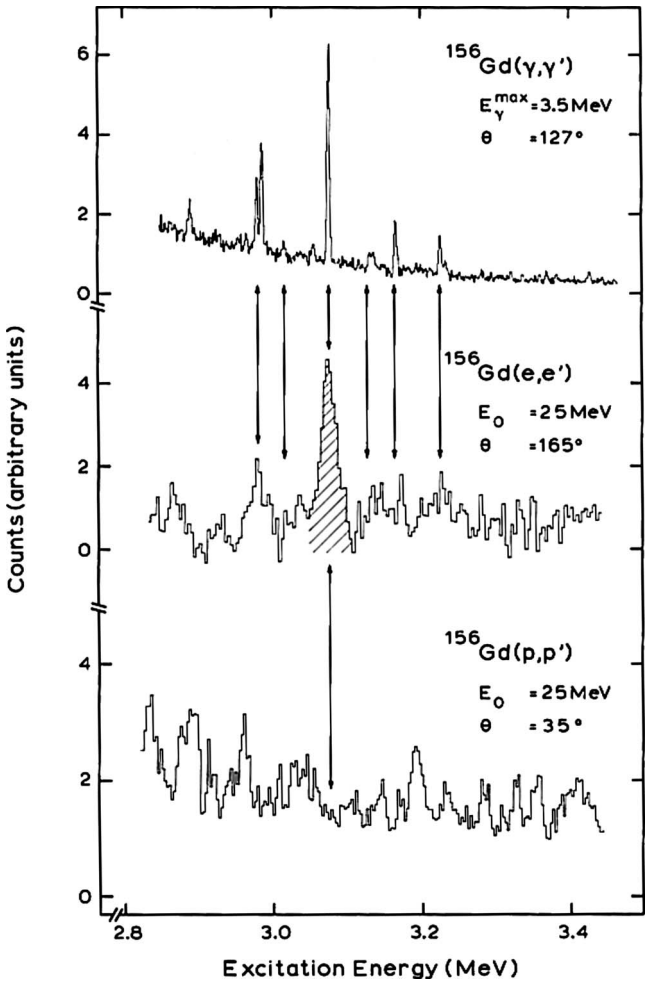

FIG. 5. Comparison of different scattering probes for ^{156}Gd. High-resolution nuclear fluorescence (upper part) and inelastic electron scattering (middle part) spectra showing a strongly excited $J^\pi=1^+$ state (hatched) and several weaker 1^+ states, all marked by arrows. These states are conspicuously absent in the inelastic proton-scattering (lower part) spectrum (Richter, 1990).

(i) Its mean excitation energy scales roughly as $66\delta A^{-1/3}$ MeV with δ being the deformation parameter.[1] This puts the center of gravity of the orbital $M1$ strength distribution in rare-earth nuclei at $E_x \approx 3$ MeV.

(ii) The total transition strength from the ground state into the $J^\pi=1^+$ states is $\Sigma B(M1)\uparrow \approx 3\mu_N^2$ and the maximum strength that is carried in the transition to an individual state is roughly $1.5\mu_N^2$.

(iii) In the nuclear transition current the orbital part dominates over the spin part and one has typically $B_l(M1)/B_\sigma(M1) \approx 10$.

[1]In this article, the quadrupole deformation parameter used is mainly denoted by δ. Slightly different parametrizations (β_2,ϵ_2) exist, which can all be related with each other (Löbner *et al.*, 1970; Hasse and Myers, 1988). To lowest order $\epsilon_2 \approx \delta \approx \frac{3}{4}\sqrt{5/\pi}\beta_2$.

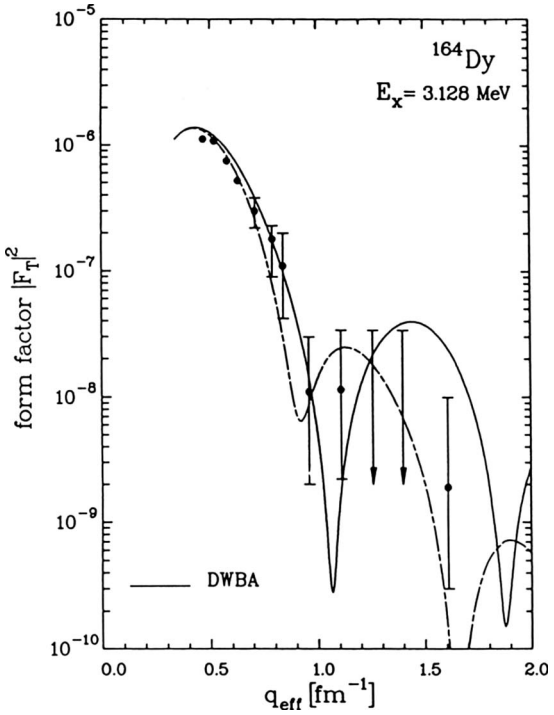

FIG. 6. Comparison of the experimental form factor for the transition into one of the $J^\pi=1^+$ scissors mode states in ^{164}Dy with form factors predicted in QRPA (Scholtz *et al.*, 1989). The dashed curve denotes the orbital part only (Richter, 1990).

(iv) The summed experimental transition strength up to $E_x \approx 4$ MeV varies quadratically with the quadrupole ground state deformation parameter.

Before these observations are compared with various nuclear model predictions in Sec. III.A.2, we concentrate on a few more experimental characteristics of the mode.

b. Form factor

One of the first strong hints that indeed $J^\pi=1^+$ states were excited from the $J^\pi=0^+$ ground state came from the measurements of form factors in inelastic electron scattering at low momentum transfers (Bohle, Küchler, *et al.*, 1984; Bohle, Richter, *et al.*, 1984). In all cases a shape characteristic for a magnetic dipole form factor has been found. As an example, one such form factor (Bohle, Kilgus, *et al.*, 1987) is shown in Fig. 6 for the transition into a scissors mode state in ^{164}Dy at E_x =3.11 MeV. It is compared to a form factor calculated (Scholtz *et al.*, 1989) in the distorted wave Born approximation (DWBA) with a QRPA transition density to a state at E_x=3.128 MeV, i.e., very close to the experimental state. The full curve is the total form factor (orbital plus spin) and the dashed one its orbital part alone. It is evident that the experimental form factor is well described at and above its first maximum by the model, considering the sizable uncertainty due to the smallness of the form-factor values at momentum transfers larger than 1 fm^{-1}. Similarly to the QRPA model, the interacting boson model-2 (IBM-2)—to be discussed later on—

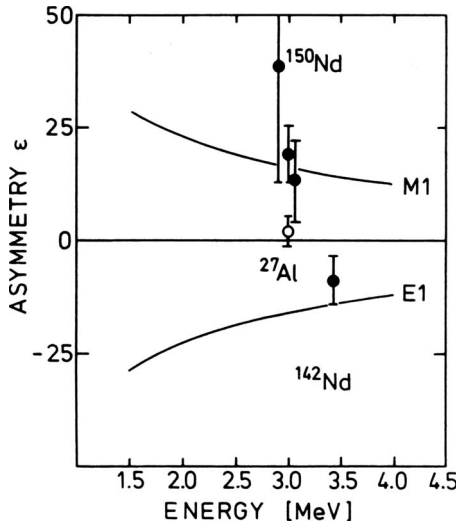

FIG. 7. Experimental asymmetries $\epsilon=(N_\perp-N_\parallel)/(N_\perp+N_\parallel)$ of Compton-scattered photons determined by a five-detector polarimeter. The experimental data are compared with the calculated polarization sensitivity of the setup given by the solid lines. Three strongly excited $M1$ transitions into states around 3 MeV excitation energy in the deformed nucleus ^{150}Nd have been identified. For comparison an $E1$ transition into a state at 3.4 MeV in the spherical nucleus ^{142}Nd is also shown. From Kasten *et al.*, 1989.

describes the data as well and points in particular also to the orbital nature of the transition.

c. Photon polarization and parity assignments

Although the excitation of the scissors mode states by inelastic electron scattering and the measurement of the respective form factors has already provided a clear indication of the magnetic nature of the transition, it can be established beyond any doubt using polarized photons either in the entrance or in the exit channel in NRF experiments [see Kneissl *et al.* (1996) for a detailed discussion]. In the former method of $(\vec{\gamma},\gamma')$, which has been successfully used at the photon scattering facilities at Gent (Govaert *et al.*, 1994) and Rossendorf (Schwengner *et al.*, 2007), the linearly polarized bremsstrahlung causes a positive azimuthal asymmetry for pure electric and a negative one for pure magnetic dipole excitations of the detected photon in the exit channel. In the latter method of $(\gamma,\vec{\gamma}')$, which has been employed recently at Stuttgart (Margraf *et al.*, 1995), the parity assignments for the excited states in the nucleus result from the measurement of the linear polarization of the scattered photons with a Compton polarimeter. In a pioneering experiment (Kasten *et al.*, 1989) in the field of the scissors mode this technique has been used to measure directly (and model independently) the parity of three strongly excited states near 3 MeV in the deformed nucleus ^{150}Nd. They were shown to be of positive parity, i.e., $J^\pi=1^+$ states excited through the scissors mode (Fig. 7).

For transitions into states at excitation energies above 4 MeV, however, the application of this technique will be difficult simply because the already small analyzing

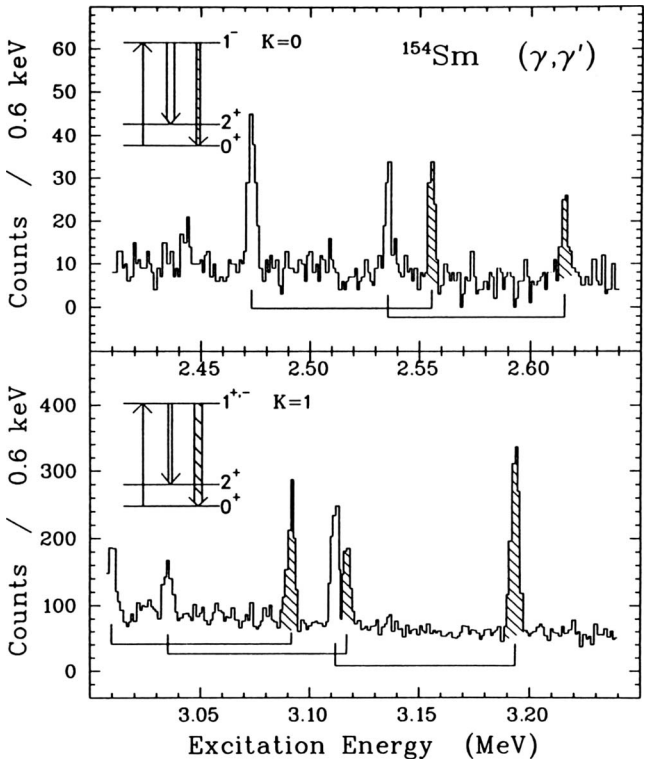

FIG. 8. Two parts of a NRF spectrum of ^{154}Sm. The ratio of the areas of peaks linked by brackets, corresponding to the ground state and the 2^+ transitions, allows the assignment of the K quantum number to the excited spin-one state. In the upper part two examples for $J^\pi;K=1^-;0$, and in the lower part two examples for $J^\pi;K=1^{+,-};1$ assignments are shown (Richter, 1991).

power of the Compton polarimeter at low energies becomes even smaller at higher energies. Here the use of polarized photons in the entrance channel of the reaction and the subsequent measurement of the intensity distribution of the scattered photon is preferable for the parity determination of nuclear dipole transitions. The analyzing power of this process is 100% and independent of the energy of the scattered photon. In a conceptually simple experiment, Pietralla *et al.* (2001) measured unambiguously the parity of a number of dipole excitations in ^{138}Ba in the range $E_x=5.5-6.5$ MeV using photons from the Duke/OK-4 Storage Ring Free Electron Laser backscattered from relativistic electrons, now called the High Intensity Gamma-Ray Source (HIγS) facility (Weller *et al.*, 2009). The produced photon beam has been intense (10^7 photons/s) and nearly monochromatic ($\Delta E_\gamma/E_\gamma \approx 3.8\%$). This very efficient technique indeed will have a future in the study of elementary dipole transitions below threshold for particle emission.

d. Branching ratios of spin-one states in deformed nuclei and the K quantum number

In NRF measurements, spin-one levels of both parities are selectively exited which decay either to the 0^+ ground state or to low-lying excited states. Figure 8 shows two parts of a NRF spectrum taken at a bremsstrahlung end point energy slightly above 4.6 MeV for the strongly deformed ($\delta=0.27$) nucleus ^{154}Sm. A number of transitions clustering around 3 MeV, i.e., the location of the states excited by the scissors mode, are observed (Ziegler *et al.*, 1993). Multipolarities of individual transitions were ascertained by simultaneous two-point angular distribution measurements at 90° and 127° with respect to the direction of the incoming bremsstrahlung beam. Those data sufficed to clearly distinguish between quadrupole and dipole transitions. In the case of ^{154}Sm it has been possible to determine the nature of the dipole transitions ($M1$ or $E1$) by supplementing the present (γ,γ') data with (e,e') form-factor measurements (Ziegler *et al.*, 1993). However, there is still another property attached to the $J=1$ levels excited from the $J^\pi=0^+$ ground state, i.e., its K quantum number. The pairs of the lines connected by brackets in the spectrum of Fig. 8 correspond to the decay of the $J=1$ levels into the ground state or the first excited $J^\pi=2^+$ state of ^{154}Sm. From the observed branching ratio one obtains information on the K quantum number of the $J=1$ state as shown in Fig. 8.

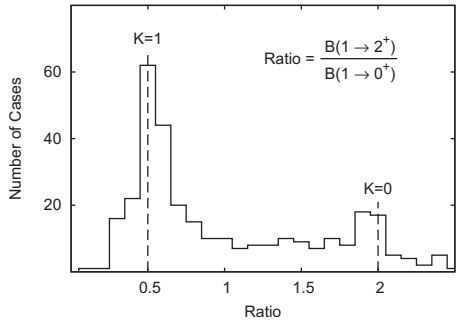

FIG. 9. Frequency distribution of experimental branching ratios for about 320 transitions observed in NRF in deformed rare-earth and actinide nuclei. One notes two distinct maxima at 0.5 for $K=1$ and at 2.0 for $K=0$ spin-one levels. Adapted from Zilges *et al.*, 1990.

The branching ratios for the deexcitation of levels in deformed nuclei to various states of a rotational band are governed by the so-called Alaga rules (Alaga *et al.*, 1955) which yield for the ratio of transition strengths $B(1\rightarrow 2)/B(1\rightarrow 0)=0.5$ for $\Delta K=1$ and 2 for $\Delta K=0$ transitions, respectively.

Examination of the decay of about 200 $J=1$ levels in a number of rare-earth nuclei (Zilges *et al.*, 1990) indeed showed maxima at experimental branching ratios of 0.5 (as expected for states with $K=1$) and of 2.0 (as expected for states with $K=0$). Figure 9 shows an update including additional data which appeared since the original publication (Enders *et al.*, 2005). The number of $K=1$ states is at least twice the number of $K=0$ (note that there are no positive parity states with $K=0$). Thus, the majority of the branching ratios are in good agreement with the Alaga rules. Furthermore, recent parity measurements of strong dipole transitions in ^{172,174}Yb confirm the $E1/M1$ assignments based on the K quantum numbers (Savran *et al.*, 2005).

But what is the reason for a number of cases with branching ratios in between the limits set by the Alaga rules? Some of them are known to result from rather strong $E1$ transitions of $J^\pi=1^-$ states with a strength hitherto still unexplained (Zilges *et al.*, 1996). The deviations, however, may also be taken as evidence for possible K mixing. In fact K mixing matrix elements have been calculated from the measured energies, branching ratios, and absolute transition strengths and are about 50 keV (von Brentano *et al.*, 1994).

e. Evidence for quasiparticle excitations at low energy

The high-resolution (e,e') data, obtained by Bohle, Küchler, *et al.* (1984), as well as NRF results (Wesselborg *et al.*, 1988) on ^{164}Dy have shown, in addition to the strongly excited $J^\pi=1^+$ states around $E_x\approx 3$ MeV, a second group of $J^\pi=1^+$ states about 0.5 MeV lower in excitation energy which carry a much weaker strength. Similar results have been obtained in the ^{168}Er(e,e') spectrum proving that the occurrence of a lower-lying weakly excited group of $J^\pi=1^+$ states seems to be a general phenomenon in heavy deformed nuclei. On the basis of (e,e') form-factor measurements, albeit difficult for the lower group of states because of the smallness of the experimental cross sections and the corresponding large uncertainty, it has been speculated that the two groups of states might be of very different structure (Richter, 1990).

That this is indeed the case has been proven independently in a study of the proton pick-up reaction ^{165}Ho$(\alpha,t)^{164}$Dy (Freeman *et al.*, 1989). As can be seen from the top part of Fig. 10 the $J^\pi=3^+$ to 8^+ members of a $K^\pi=1^+$ rotational band have been identified in this single-particle transfer reaction. The reconstruction of the (not populated) 1^+ bandhead energy resulted in $E_x=2.543(13)$ MeV which can be safely identified with the $J^\pi=1^+$ state energy of $E_x=2.539$ MeV observed in (e,e') scattering (Bohle, Kilgus, *et al.*, 1987) and the NRF experiments (Wesselborg *et al.*, 1988). This 1^+ state thus corresponds most likely to a two-quasiproton configuration (bottom part of Fig. 10) of the form $7/2^-[523]\otimes 5/2^-[523]$, and such a configuration is of course not consistent with a collective magnetic dipole transition from the ground state into it, as pointed out earlier by Hamamoto and Åberg (1984) and later also by Otsuka (1990). Furthermore, no rotational states built upon the $J^\pi=1^+$ scissors mode states around $E_x\approx 3.1$ MeV are seen in the spectrum supporting the collective interpretation of the latter.

f. The scissors mode and deformation

Deformation so far has been mentioned alongside the discussion of the experimental data on the scissors mode. The most important observation made since the discovery of the mode itself has been that the measured orbital magnetic dipole strength increases linearly with the square of the deformation parameter δ. This is shown in Fig. 11, where the summed $M1$ strength is plotted versus δ^2, for a chain of even-even Sm isotopes (Ziegler *et al.*, 1990). This striking result has later been verified in corresponding experiments on a series of even-even Nd isotopes (Margraf *et al.*, 1993). Those observations have been anticipated in a systematic theoret-

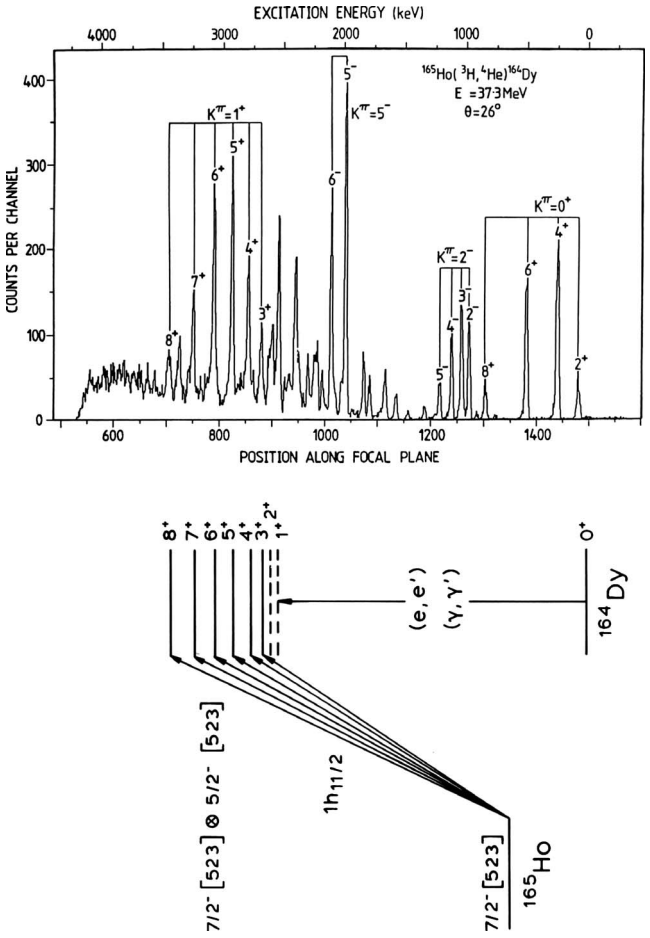

FIG. 10. Members of a $K^\pi=1^+$ rotational band observed in the single-particle transfer reaction ^{165}Ho$(^3$H$,^4$He$)^{164}$Dy. The (not populated) 1^+ bandhead lies at an excitation energy of 2.543(13) MeV which can be identified with the 1^+ state energy of 2.539 MeV, observed in nuclear resonance fluorescence and inelastic electron scattering experiments (Richter, 1990).

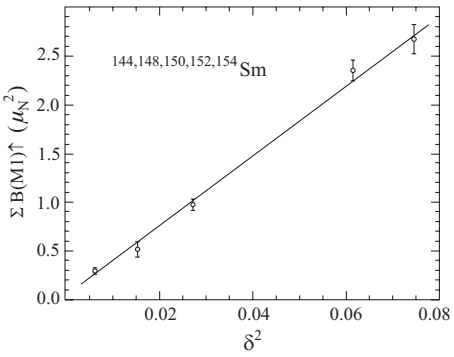

FIG. 11. The summed orbital $M1$ strengths observed in even-even Sm isotopes and plotted versus the square of the deformation parameter δ (Ziegler *et al.*, 1990). See also Fig. 24 for the systematics of rare-earth nuclei including the present data.

ical study (De Coster and Heyde, 1989) of $M1$ strength in nuclei of the rare-earth region within the Nilsson model. Immediately after the experimental results shown in Fig. 11, it was further realized that the orbital $M1$ strength in a given nucleus is also proportional to the strength of the $E2$ transition to the lowest $J^\pi=2^+$ state (Rangacharyulu *et al.*, 1991). The empirical relation

$$\sum_f B_f(M1)\uparrow \sim B(E2;0_1^+ \rightarrow 2_1^+) \sim \delta^2, \tag{1}$$

thus represents [as expressed by Lo Iudice (2000)] the most spectacular manifestation of the scissors nature of the low-lying magnetic dipole transitions and their collectivity. Since the neutron-proton interaction is mainly responsible for the nuclear quadrupole deformation, the experimental observation of the strong $M1/E2$ correlation is of much interest for a test of nuclear models of deformation as shown below.

g. Summary

In Secs. III.A.1.a, III.A.1.b, III.A.1.c, III.A.1.d, III.A.1.e, and III.A.1.f, experimental evidence has been presented for the existence of strong magnetic dipole transitions of orbital character into states at an excitation energy of $E_x \approx 3$ MeV in even-even heavy deformed nuclei. The total *orbital* strength into these states amounts in strongly deformed nuclei to $\Sigma B(M1) \approx 3\mu_N^2$. It hardly moves at all with excitation energy, i.e., it remains low lying, is scissorslike and weakly collective, but strong on the single-particle scale. Its observability is a strong effect as a consequence of the fact that the nuclear particle-hole force has swept the competing stronger spin-flip strength up to higher excitation energy (see Fig. 1 and Sec. III.B). Furthermore, the existence of weakly excited two-quasiparticle $J^\pi=1^+$ excitations at about twice the pairing gap, i.e., below the states associated with the scissors mode, has been shown. Thus, returning to the schematic picture of Fig. 1, the salient experimental features of magnetic dipole excitations below about 4 MeV of excitation energy in heavy deformed nuclei have been demonstrated in this section.

The weakly collective scissors mode excitation has become an ideal test of models, especially microscopic models, of nuclear vibrations. Most models are usually calibrated to reproduce properties of strongly collective excitations (e.g., of $J^\pi=2^+$ or 3^- states, giant resonances, etc.). Weakly-collective phenomena, however, force the models to make genuine predictions and the fact that the transitions in question are strong on the single-particle scale makes it impossible to dismiss failures as a mere detail, especially in light of the overwhelming experimental evidence for them in many nuclei (Richter, 1995; Kneissl *et al.*, 1996). This should be kept in mind in assessing the wide variety of nuclear models which the scissors mode has inspired after its discovery about two and a half decades ago.

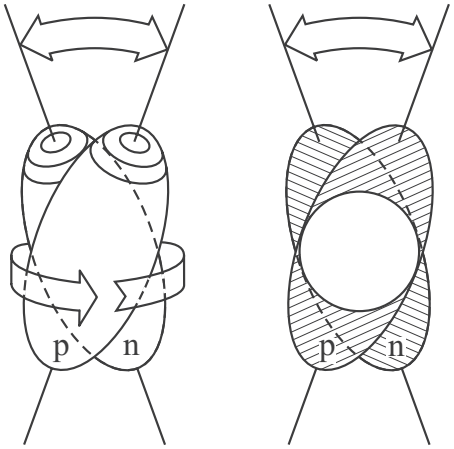

FIG. 12. Pictorial representation of the scissors mode. We view the mode in a proton-neutron two-fluid model (left part) and in a presentation where an inert core exists and only a small part of the proton and neutron fluids take part in the scissors motion (right part). The proton-neutron rotational oscillation is the basis of the two-rotor model which is the rotational analog of the semiclassical model of the giant electric dipole resonance.

2. Theoretical description: From collective to microscopic models

a. Geometric collective models

As a special case of the generalized isovector Bohr-Mottelson model, a TRM considering both proton (π) and neutron (ν) degrees of freedom was worked out by Lo Iudice and Palumbo (1978, 1979). Describing these two systems as axially symmetric rigid rotors that are able to perform rotational oscillations around a common axis orthogonal to their symmetry axes [Fig. 12, left-hand side (lhs)], the following Hamiltonian was defined:

$$H = \frac{(\hat{I}_\pi + \hat{I}_\nu)^2}{2J_{\text{intr}}} + \frac{(\hat{I}_\pi - \hat{I}_\nu)^2}{2J_{\text{intr}}} + \frac{1}{2}C\theta^2, \tag{2}$$

in which the restoring force constant C is related to the symmetry energy constant in the semiempirical mass formula. Using known properties of deformed nuclei: the moment of inertia J_{intr} of the ground-state band, the symmetry energy, and the $B(E2;0_1^+ \rightarrow 2_1^+)$ transition strength, one can determine both the excitation energy $E_{sc}=\hbar\sqrt{C/J_{\text{intr}}}$ and the $B(M1)$ transition strength,

$$B(M1;0^+ \rightarrow 1^+) = \frac{3}{16\pi}\frac{J_{\text{intr}}}{\hbar^2}E_{sc}(g_p - g_n)^2\mu_N^2. \tag{3}$$

Here g_p and g_n denote the orbital gyromagnetic factors associated with the rotation of the deformed proton and neutron systems, respectively. It turned out that the early calculations of both the excitation energy and the $M1$ strength gave too large values compared with the first experimental observations of 1^+ scissors excitations in deformed nuclei [the $B(M1)$ value exceeds experimental values for the strongest 1^+ states by a factor of almost 7]. However, it cannot be emphasized enough how important the seminal work of Lo Iudice and

Palumbo (1978, 1979) has been in the experimental search which finally led to the discovery of the scissors mode in ^{156}Gd (Bohle, Richter, *et al.*, 1984). Moreover, the confrontation of the conceptually simple TRM with the wealth of experimental data having accumulated rapidly in the late 1980s and early 1990s of the last century has led to a steady improvement of the model (Lo Iudice, 1997, 2000) which still allows first insight in the dynamics which causes the scissors mode to show up at all in deformed nuclei.

A geometrical model for strongly deformed nuclei (assuming axial symmetry) with separate proton and neutron deformations has been formulated by Rohozinski and Greiner (1985). There the scissors mode was explained as a relative vibration of the proton and neutron collective surface. Moreover, rotational bands are obtained on top of $K^\pi=0^+$, 1^+, and 2^+ vibrational excitations.

Through the experimental observations, we now know the restoring force constant C in Eq. (2) much better which determines largely the excitation energy E_{sc} of the mode. Furthermore, introducing pairing correlations among the participating protons and neutrons and thus effectively reducing the number of protons and neutrons participating in the scissors motion [Fig. 12, right-hand side (rhs)] resulted in reduced $M1$ strengths, but still too large by factors 4–5 as compared to experiment. In this purely collective approach, all $M1$ strength is concentrated in a single state whereas the data are much more fragmented.

As a consequence of the too high excitation energy and the too large $M1$ strength for the 1^+ scissors excitation, Faessler and Nojarov (1986) concentrated on a more detailed study of the restoring force for this isovector mode (Faessler *et al.*, 1986). Considering the fact that the symmetry energy coefficient exhibits a strong $\rho^{2/3}$ density dependence, the isovector symmetry energy becomes (Nojarov *et al.*, 1986; Faessler and Nojarov, 1987)

$$E_{\mathrm{sym}}^{\mathrm{IV}} = D \int (\rho_p - \rho_n)^2/(\rho_p + \rho_n)^{1/3} d\vec{r}, \tag{4}$$

with $D=91.6$ MeV fm^2. This symmetry energy has been calculated microscopically, using proton and neutron densities ρ_p, ρ_n derived from a deformed Woods-Saxon potential, also including pairing. Identifying the isovector symmetry energy with the scissors potential energy $\frac{1}{2}C\theta^2$, a much improved restoring force constant C could be derived. This reduces the scissors excitation energy by a factor of about 2 but still a too large $B(M1)$ value is obtained. Isovector motion of protons and neutrons has also been discussed (Faessler, 1966; Faessler and Nojarov, 1987) for systems performing harmonic small-amplitude vibrations around a spherical equilibrium shape, using an extended Bohr-Mottelson model. The implications will be studied in Sec. VI.

The collective two-fluid model, both for rotational and for vibrational excitations, has been studied and refined over the years in much detail. The results have been summarized by Lo Iudice (1997, 2000) and partly by Zawischa (1998). We refer the interested reader to these for further details.

b. Algebraic collective models

When discussing the nuclear structure aspects of an interacting fermion system, it is striking that for the low-energy collective modes to develop, the nucleon-nucleon correlations acting in the $L=0$ (paired state) and also in the $L=2$ configuration are particularly important. It has been shown that the $L=0$ correlations among identical nucleons lead to a generalized seniority classification while the addition of the $L=2$ pair component gives rise to the possibility to develop strong collective excitations when both proton and neutron valence particles are present. Considering those two-nucleon pair configurations, it is possible to formulate a model in which these pairs are now treated as genuine bosons: the $L=0$ pair is mapped onto the s boson and the $L=2$ pair onto the d boson (Arima and Iachello, 1975a, 1975b). This system of interacting bosons (IBM concept) has been studied in detail, in particular emphasizing the group structure [which is the group U(6)] and its reductions, by Iachello and Arima (1987).

In examining the model more closely to the shell model with protons and neutrons interacting, the charge degree of freedom was introduced in order to distinguish between s and d proton and neutron bosons, doubling the space of independent degrees of freedom. The fact that for bosons the total wave function needs to be symmetric under the interchange of any two bosons, it is still possible to construct wave functions that have mixed-symmetry character in both the spatial and the charge part separately. Using the group-theoretical formulation, the product irreducible representations (irreps) of $\mathrm{U}_\pi(6)\otimes\mathrm{U}_\nu(6)$ contains, besides the one-row, also two-row irrep or, even more explicitly,

$$[N_\pi]\otimes[N_\nu] = [N_\pi+N_\nu,0]\oplus[N_\pi+N_\nu-1,1]\oplus\cdots. \tag{5}$$

The physics of these mixed-symmetry U(6) irreps becomes clear when studying the energy eigenvalues for a total IBM-2 Hamiltonian which also contains, besides the pure proton and neutron parts, the coupling term between the proton-neutron combined parts. This IBM-2 Hamiltonian can be written as

$$H = \epsilon_{d_\pi}\hat{n}_{d_\pi} + \epsilon_{d_\nu}\hat{n}_{d_\nu} + \kappa(\hat{Q}_\pi+\hat{Q}_\nu)\cdot(\hat{Q}_\pi+\hat{Q}_\nu) + \lambda\hat{M}_{\pi\nu}. \tag{6}$$

We can show the essential results easily in the case of only two bosons (Fig. 13) where one s_π and d_π and one s_ν and d_ν boson are considered.

The symmetric coupling [2,0] corresponds to the 0, 1, and 2 quadrupole phonon structure of the well-known symmetric quadrupole vibrator; the [1,1] irrep gives rise to the nonsymmetric 1^+, 2^+, and 3^+ levels. Here too the energy separation between the 0^+ and 2^+_{ms} states is related to the collective symmetry energy in the interact-

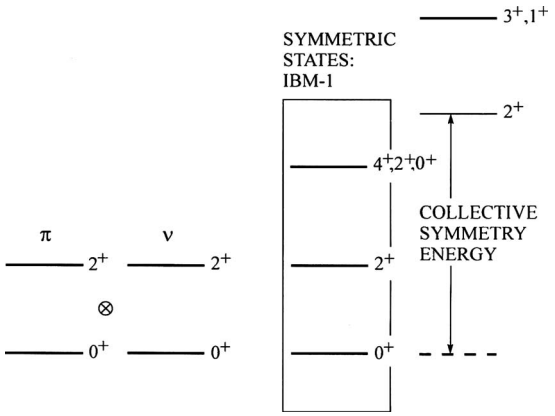

FIG. 13. Schematic representation of a coupled proton-neutron system with boson numbers $N_\pi=1$, $N_\nu=1$. The symmetric states (in the box) and the antisymmetric states are drawn at the right-hand side of the figure. Adapted from Heyde, 1989.

ing boson model, an energy which is governed by the strength λ of the Majorana term $\hat{M}_{\pi\nu}$ in the IBM-2 Hamiltonian of Eq. (6); see Scholten *et al.* (1985). This is very much the same physics underlying the splitting of the various isospin T components resulting from combining protons and neutrons in fermion space, as discussed in the Introduction (Fig. 3). An equivalent two-valued variable (called F spin) has thus been introduced (Arima *et al.*, 1977; Iachello, 1984) to characterize the charge (or spatial) part of the boson wave function. If the proton and neutron bosons are characterized with the help of their F-spin quantum number $F=1/2$, $F_z=+1/2$ and $F=1/2$, $F_z=-1/2$ respectively, a system of N_π proton and N_ν neutron bosons can be classified according to its total F spin. The totally symmetric orbital (sd boson space) states have maximal F spin, i.e., $F_{\max}=\frac{1}{2}(N_\pi+N_\nu)$ while the mixed-symmetric states are labeled by decreasing F-spin values down to $F_{\min}=\frac{1}{2}|N_\pi-N_\nu|$. The class of mixed-symmetry states with $F=F_{\max}-1$ are the lowest lying and can be excited from the ground state of an even-even nucleus by a $\Delta F=1$ transition.

The usual $M1$ operator in fermion space,

$$T^F(M1)=\sqrt{\frac{3}{4\pi}}\sum_i [g_l(i)\hat{l}_i+g_s(i)\hat{s}_i]\mu_N, \tag{7}$$

has its image in boson space

$$T^B(M1)=\sqrt{\frac{3}{4\pi}}(g_\pi\hat{L}_\pi+g_\nu\hat{L}_\nu)\mu_N, \tag{8}$$

with g_l and g_s being the fermion orbital and spin g factors and g_π and g_ν being the respective proton and neutron boson g factors. The quantities $\hat{L}_\pi$ and $\hat{L}_\nu$ are the corresponding orbital angular momentum operators of the proton and neutron boson system.

In IBM-2 studies, concentrating on deformed nuclei, one is using the SU(3) reduction of the U(6) group structure, and for those nuclei it was shown that the lowest-lying states of the family of mixed-symmetry character were characterized by the $F_{\max}-1$, $J^\pi=1^+$ quantum numbers (Iachello, 1981, 1984). These findings corroborate results obtained from a totally different starting point, viz., the TRM. The IBM-2 $J^\pi=1^+$ states are also called scissors states although there is no immediate reference in the algebraic formulation to specific coordinate forms and thus also not of shapes and shape dynamics. Using a coherent-state formalism, Dieperink (1983) showed the correspondence explicitly and, moreover, found indeed that only the valence nucleons contribute to the strength of the scissors mode thus leading in a natural way to a much lower $B(M1)$ strength compared to the early TRM calculations.

In studying the $M1$ excitation properties within the IBM-2, because of the specific difference in magnetization properties for proton and neutron bosons, it was clear that $M1$ transitions could appear naturally now, in contrast to the former IBM-1. Using mapping from fermion magnetic properties onto boson ones, it was possible to also determine the analogous boson g_π and g_ν factors (Sambataro and Dieperink, 1981; Sambataro *et al.*, 1984; Allaart *et al.*, 1988). This item has been a topic of much discussion because the mapping calculations all seem to result with values $g_\pi\simeq 1\mu_N$ and $g_\pi\simeq 0\mu_N$ but empirical fits in various mass regions have indicated quite important deviations (Wolf *et al.*, 1987; Mizusaki *et al.*, 1991; Kuyucak and Stuchbery, 1995). For the pure SU(3) limit, though, an analytically closed form could be derived for the transition strength

$$B(M1)=\frac{3}{4\pi}\frac{8N_\pi N_\nu}{2N-1}(g_\pi-g_\nu)^2\mu_N^2, \tag{9}$$

an expression when applied to ^{156}Gd and using the above boson factors g_π, g_ν gives the result of $B(M1)\simeq 2.8\,\mu_N^2$, quite close to the experimentally observed value. Thus the realistic estimate of Iachello (1981), in the IBM-2, for the transition strength has been equally important in the search for the scissors mode (Bohle, Richter, *et al.*, 1984) as the estimate of Lo Iudice and Palumbo (1978, 1979) in the TRM for the excitation energy.

The subject of mixed-symmetry states appearing as a new class of states in the IBM-2 has been investigated afterwards in much detail. There has been an investigation of the various limiting cases that appear if dynamical symmetries hold (Van Isacker *et al.*, 1986) but also rather extensive numerical studies have been carried out (Scholten *et al.*, 1985). As an illustration, we compare in Fig. 14 the experimental $M1$ transition strengths in Sm isotopes with the results of the pure SU(3) limit and of the numerical IBM-2 calculations (Scholten *et al.*, 1985).

c. Microscopic descriptions

On the opposite side from the collective model concepts, the nuclear shell-model allows for possibilities to describe nuclear coherent motion from first principles using a Hartree-Fock basis and a self-consistent proce-

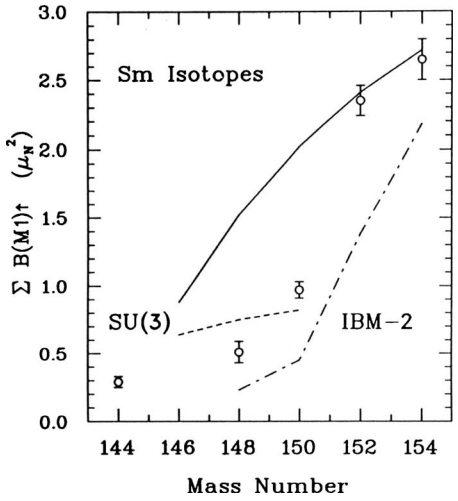

FIG. 14. Orbital $M1$ strength versus mass number of the Sm isotopes. The results from full IBM-2 calculations (dash-dotted line) of Scholten *et al.* (1985) are shown, together with results in the SU(3) limit using a $Z=50$ subshell closure (solid line) and a $Z=64$ subshell closure (dashed line) (Richter, 1991).

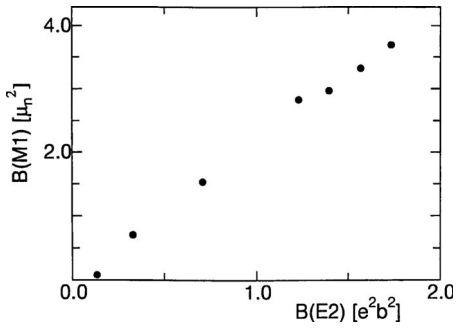

FIG. 15. Summed orbital $B(M1)$ strength from the ground state calculated in a Monte Carlo shell-model approach versus the corresponding $B(E2;0_1^+\rightarrow 2_1^+)$ values in the Ba isotopes with mass numbers $A=138-150$. From Shimizu *et al.*, 2001.

dure in order to determine both global and local nuclear structure properties. The study of scissors motion starting from a microscopic shell-model basis can be separated into two parts. For light and medium-heavy nuclei, regular shell-model calculations have been performed and also $M1$ excitation properties been studied. Once entering the region of heavy and deformed nuclei, the model space to be considered becomes prohibitively large and approximations to the shell model have been used, mainly the QRPA.

Magnetic dipole excitations have, by now, been measured over a large part of the nuclear mass table (Sec. III.A.1). In contrast to most of the purely collective models, the low-lying $M1$ strength is spread out over an energy interval in the region of 2.5–4 MeV, depending on the specific nucleus and thus depending on its proximity to the closed shells.

Large-scale shell-model studies would be an ideal way to probe the presence of concentration and fragmentation of $M1$ strength but this has not been possible for heavy nuclei until recently. Within the context of a Monte Carlo shell-model approach, worked out by Otsuka and collaborators (Honma *et al.*, 1995, 1996; Mizusaki *et al.*, 1996, 1999; Otsuka *et al.*, 1998; Otsuka, Mizusaki, and Honma, 1999; Utsuno *et al.*, 1999; Shimizu *et al.*, 2001), large-scale shell-model studies have been performed in order to study the transition from spherical to deformed shapes with an application to the Ba isotopes. Starting from a given Hamiltonian and for a given single-particle energy spectrum that remains fixed through the Ba isotopes, such microscopic calculations beyond mean-field approaches have given first evidence that shape changes indeed do occur due to a change of the number of interacting protons and neutrons. The $M1$ strength of the scissors mode serves as a good measure of the deformation of the ground state as discussed in Sec. III.A.1, in particular in the context of Fig. 11 and Eq. (1). Shimizu *et al.* (2001) calculated the $M1$ sum rule for the ground state with the orbital g factors having the free nucleon values. The spin contributions have been omitted for simplicity at present. In Fig. 15, the $B(M1)$ sum rule values are plotted versus the corresponding $B(E2;0_1^+\rightarrow 2_1^+)$ values. One notices a nearly perfect linearity between these two quantities first observed experimentally (Ziegler *et al.*, 1990). As mentioned previously, starting from symmetries within the IBM and in the nuclear shell model, such a relation also exists. The Monte Carlo shell-model calculation, however, presents a first microscopic underpinning of the connection between $M1$ and $E2$ properties in nuclei and shows a validity that does not rely any longer on particular symmetries of the nuclear many-body system, i.e., it holds for the whole isotopic series in the Ba nuclei.

Besides the nuclear shell-model explicitly, the QRPA or the quasiparticle Tamm-Dancoff approximation (QDTA), where no ground-state correlations are considered, present an alternative to study the properties and the internal orbital and spin character of the magnetic dipole transitions involving the specific 1^+ states under study. The QRPA and QDTA models in itself will not be discussed here, and we refer the interested reader to the literature for a concise discussion (Rowe, 1970; Ring and Schuck, 1980; Eisenberg and Greiner, 1987; Soloviev, 1992). In the early calculations when applying the QRPA to study the scissors mode excitations, most often rather schematic forces have been used: quadrupole proton-neutron forces and spin-spin and spin-isospin separable interactions, including pairing (both monopole and quadrupole multipoles) in order to study the role of these components (Hamamoto, 1971; Bes and Broglia, 1984; Iwasaki and Hara, 1984; Kurasawa and Suzuki, 1984). Recently (Balbutsev and Schuck, 2004, 2007) a separable quadrupole-quadrupole residual interaction has been used within a time-dependent Hartree-Fock (TDHF) framework and its Wigner transform. Here the aim was to derive a set of equations describing different multipole moments, in particular the scissors and isovector giant quadrupole resonance and their coupling. More recently, the effect of pairing has been incorpo-

rated into the formalism with application to the nuclear scissors mode (Balbutsev *et al.*, 2008, 2009; Balbutsev, 2010). The results obtained are closely related to the earlier work of Lipparini and Stringari (1989b).

The pairing force is particularly important in generating the necessary correlations that relate the overall summed orbital $M1$ strength to the nuclear quadrupole deformation characterizing a given nucleus. Moreover, the spin-isospin parts are determining factors in placing the spin-flip part of the $M1$ response (Fig. 1) at the excitation energy between 5 and 10 MeV. These studies were instrumental in finding out the first and foremost important physics elements that are at the origin of coherent orbital magnetic excitations with a scissors character. It has been pointed out (Heyde and De Coster, 1993; Ikeda and Shimano, 1993) that a correct treatment of the full Coriolis term, and considering the coupling of 2qp excitations to a rotational core, induces specific correlations that concentrate the independent $M1$ components into a single peak.

Realistic application of the QRPA to the study of the scissors mode exciting $J^\pi=1^+$ states has met with some initial problems because the overall rotational motion of an intrinsically deformed nucleus carries the same angular momentum as the scissors mode states themselves. Similar to the case of the electric dipole mode leading to the $J^\pi=1^-$ states, one has to separate the spurious rotational motion of the whole nucleus from the relevant intrinsic 1^+ excitations. This was the origin of the fact that various QRPA calculations gave rise to rather large differences in the 1^+ excitation energy and, more importantly, in the $M1$ response. Removing this spurious rotational motion, however, using various techniques such as (i) constructing a basis orthogonal to the spurious rotational motion, (ii) adding a specific symmetry restoration term to the Hamiltonian, and (iii) using the Pyatov prescription (Baznat and Pyatov, 1975) of replacing the quadrupole field in the Hamiltonian in such a way that rotational invariance is imposed, the results on $J^\pi=1^+$ energies and on $M1$ strengths converge with similar conclusions.

The various QRPA studies are now very close with respect to a number of key issues characterizing the observation of a magnetic scissors type of excitation (Nojarov and Faessler, 1990; Zawischa, Macfarlane, and Speth, 1990; Zawischa and Speth, 1990; Soloviev, Sushkov, and Shirikov, 1997a, 1997b; Soloviev *et al.*, 1997; Beuschel *et al.*, 2000). Examples are shown in Figs. 16–18. Work using variants of QRPA starting from a deformed Woods-Saxon potential, HFB calculations, and schematic forces has also been carried out (Hamamoto and Ronström, 1987; Sugawara-Tanabe and Arima, 1989; Hilton, 1995; Lo Iudice, 1996a, 1996b; Hilton *et al.*, 1998).

(i) A concentration of low-lying $M1$ strength is found close to the energy of 3 MeV, whose overlap with the scissors mode is as large as ≃40% if summed up to 4 MeV (see Fig. 16, upper part). The low-energy $M1$ strength is of dominant orbital character with orbit/spin ratios of the order of 10 or larger (cf. Fig. 16, bottom part as an example). Furthermore, all calculations predict the existence of a higher-lying scissors part. This issue, however, is not closed since many come to largely different conclusions concerning its mean energy and, more importantly, its fragmentation.

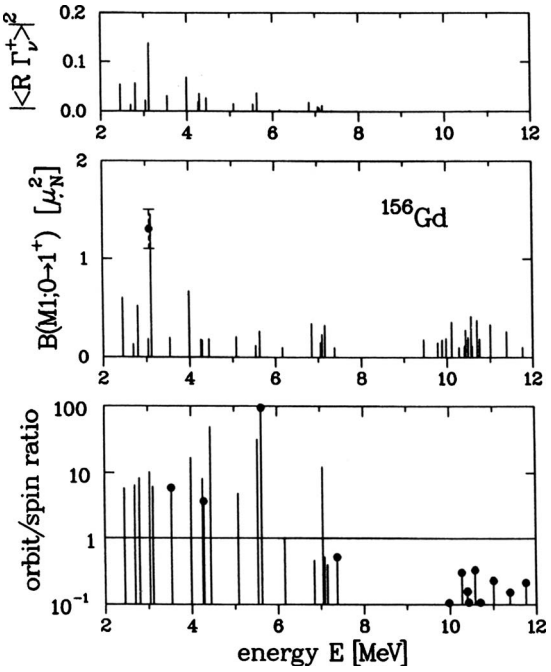

FIG. 16. Calculated QRPA magnetic dipole strength distribution compared to the experimental data point of the strongest transition observed in ^{156}Gd (middle part) and orbit-to-spin ratios of the $M1$ transition matrix elements (bottom part). The magnitude of these ratios is shown and negative ratios are indicated by a dot on the top of the bar. The average overlap of the calculated 1^+ states with the scissors mode state (denoted R) is displayed in the upper part. From Nojarov and Faessler, 1990.

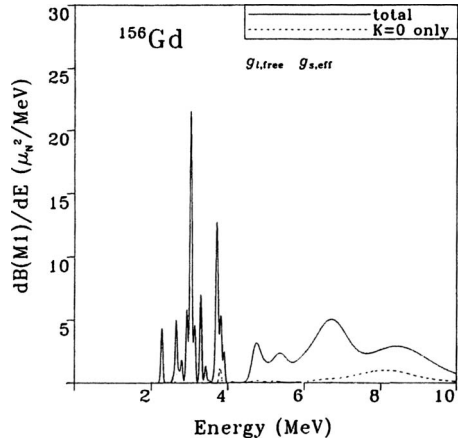

FIG. 17. The complete magnetic dipole response of ^{156}Gd up to 10 MeV excitation energy, calculated using the QRPA approach. The individual levels have been folded with Gaussian functions. From Zawischa, Macfarlane, and Speth, 1990 and Zawischa and Speth, 1990.

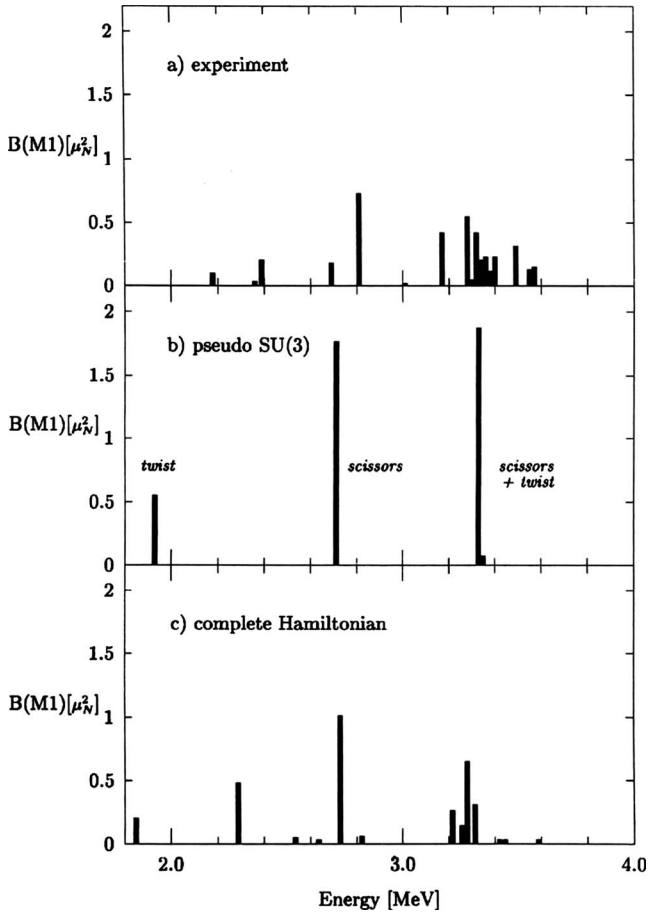

FIG. 18. $M1$ transition strengths in ^{160}Gd. (a) Experimental data, (b) pure pseudo-SU(3) scheme, and (c) complete pseudo-SU(3) calculation. The twist mode results when considering triaxial proton and neutron distributions which allow additional rotation around their principal axes. It can be combined with the scissors mode into a scissors plus twist mode. From Beuschel *et al.*, 2000.

(ii) There is common agreement on the importance of the pairing correlations in establishing a strong relationship between the summed $M1$ strength and nuclear deformation. These at first quite different observables have a deeper connection which is borne out from the microscopic QRPA studies too as discussed below in more detail.

(iii) An important spin-flip $M1$ mode is observed in the strongly deformed rare-earth nuclei in the energy region 5–10 MeV. There is, also here, an open debate on the specific way in which the spin-flip strength is distributed in energy. A two-bump picture shows up but in some calculations the bumps are mainly isoscalar and isovector in character, whereas other calculations comply with a rather definite separation between proton and neutron spin-flip modes. The solution here should come from selective reaction studies (see Sec. III.B for a discussion on this issue).

We cannot provide a complete discussion of the multitude of QRPA and QTDA studies in both the rare-earth and actinide (and even light) nuclei. See Lo Iudice (1997) for a detailed but still succinct presentation of the major results. We note, however, that recently relativistic QRPA calculations within a self-consistent relativistic mean-field (RMF) framework have been carried out for axially deformed nuclei (Peña Arteaga and Ring, 2008). Spin, orbital, and total $M1$ strengths were derived for ^{160}Gd and ^{160}Ne, with clear evidence for a scissors mode in ^{160}Gd (Peña Arteaga and Ring, 2007).

d. Relationship between collective and microscopic models

Starting from collective models, the proton and neutron degrees of freedom form the essential ingredients to generate mixed-symmetry charge (and spatial) wave function of the $J^\pi=1^+$ states. This was the case in the two-rotor geometrical model and also within the proton-neutron interacting boson model (IBM-2).

Because the building blocks constituting the bosons are nucleon pairs, the IBM-2 approach is rooted closely in the nuclear shell model [see, e.g., the studies in the light $1f_{7/2}$ nuclei by McCullen *et al.* (1964), Zamick (1986a, 1986b), and Liu and Zamick (1987a, 1987b, 1987c)]. In the QRPA, on the other hand, the building blocks are highly correlated particle-hole (or 2qp) excitations that make up for a microscopic description to the collective phonon modes in the nucleus. It has been pointed out explicitly (Lo Iudice, 1997) that in schematic models the connection between the microscopic QRPA and the collective two-fluid approaches (TRM) can be shown in detail. An approximate relation for the scissors total summed $M1$ strength is then

$$B(M1)\uparrow \simeq \frac{3}{16\pi}\frac{J_{\mathrm{intr}}}{\hbar^2}E_{sc}\mu_N^2, \tag{10}$$

if all the 1^+ states could be approximated by a single centroid energy E_{sc} as in Eq. (3).

In all of the more detailed microscopic calculations, be it large-scale shell-model studies or QRPA calculations, the immediate connection is not so obvious anymore. Still, the observed spreading (or fragmentation) of the population of 1^+ states is rather well reproduced. The QRPA calculations start mainly from different single-particle structures (Nilsson or Woods-Saxon deformed mean-field, self-consistent energy spectra, etc.) and also have been using differing two-body interactions and as a result a large sensitivity of the 1^+ energy and strength distribution in realistic cases is expected.

There exists a model which tries to give microscopic support of collective magnetic dipole excitations starting from the SU(3) for light nuclei and pseudo-SU(3) for the heavy deformed nuclei. This model goes back to the seminal work of Elliott (1958, 1963) indicating that collective model aspects are inherent in the proton-neutron shell-model structure for light *sd* shell nuclei (Elliott, 1985, 1990). Calculations within this approximation have been carried out in *sd*- and *fp*-shell nuclei for the orbital $M1$ properties and compared to the experimental values (Chaves and Poves, 1986; Poves *et al.*, 1989; Retamosa *et al.*, 1990). The extension to heavier nuclei was hampered

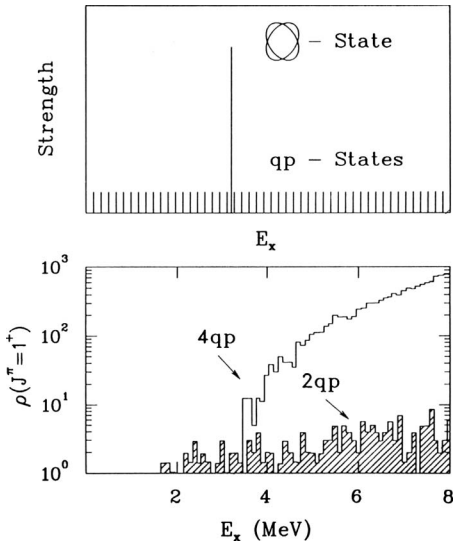

FIG. 19. Doorway picture of the scissors mode. Upper part: Schematic picture of the scissors mode embedded into the background of dense qp states (no coupling). Lower part: Level density for 2qp and 4qp 1^+ states for Gd isotopes calculated using the Nilsson model. Adapted from Heyde, 1989.

for some time as SU(3) is largely broken because of the strong spin-orbit splitting. However, a suggestion has been made in order to reorganize the level structure conform with a pseudo-SU(3) scheme, explicitly incorporating proton and neutron degrees of freedom. In former studies of this type, one had to rely on simple Hamiltonians; this has been overcome and one can now handle general one- and two-body Hamiltonians. So this model, deeply rooted in the shell model, serves as a bridge to connect the underlying microscopic structure to the collective building blocks. Results for Sm, Gd, and Dy nuclei have been obtained (Beuschel *et al.*, 1998, 2000; Rompf *et al.*, 1998) and even a reasonable fragmentation of $M1$ strength is achieved as shown in Fig. 18 for ^{160}Gd.

3. Fragmentation of orbital dipole strength and sum rules

a. Fragmentation of the orbital strength

An important element in discussing relationships, similarities but also complementary aspects of the collective model approaches and shell-model or QRPA studies, is the amount of fragmentation resulting from these various models. As discussed in Sec. III.A.2, in collective models the $M1$ scissors strength is concentrated in a single or very few strongly excited 1^+ states (Scholten *et al.*, 1985) while in the microscopic models strength needs to become concentrated in fewer strong states compared with the unperturbed spectrum of 1^+ states.

What are the major issues here? We present the above elements of fragmenting collective $M1$ strength into a background of microscopic configurations (2qp, 4qp, etc.) much in the same way as fragmentation is generally described in nuclear reaction theory (Fig. 19, upper part). There might remain some structure in the fragmented strength due to interactions with states that are intermediate in complexity between the strongly collective states on one side and the regular shell-model configurations on the other side. Such states could be due to hexadecapole configurations (in certain regions of the nuclear mass table this degree of freedom in the upper part of the rare-earth mass region, particularly, can be important), triaxial shape configurations, etc. that first split the $M1$ scissors strength in the manner of a doorway state before it gets fragmented into the microscopic background of 1^+ states (Scholten *et al.*, 1985). These strength function phenomena have been discussed in Appendix D2 of Bohr and Mottelson (1969). If the average coupling strength $\langle V\rangle$ between a single collective state and the background configurations is larger than the distance between the discrete levels $D=1/\rho$, with ρ denoting the level density, then a Breit-Wigner damping of collective strength over the microscopic background results, given by a width of $\Gamma=2\pi\langle V\rangle^2\rho$. The strength function, i.e., the probability of finding a simple, collective state in a unit energy interval of the spectrum, can subsequently be derived. If, on the other hand, the level density becomes too low for the above conditions to be valid, one has to resort to diagonalizing the coupled system of collective and shell-model configurations. A model where this has been worked out explicitly for the scissors 1^+ state, as obtained in the IBM-2, coupling to the underlying background of 1^+ 2qp and 4qp configurations was described by Heyde *et al.* (1996). The background structure, as calculated using a Nilsson model for the Gd nuclei, is shown in the lower part of Fig. 19. The damping and fragmentation of the scissors mode into this background has been derived using a constant coupling matrix element between the states in the two model spaces (Fig. 20, upper part). For the fragmentation down to the 1% level, a coupling matrix element of about 50 keV is obtained between the scissors mode and the 2qp states. The experimental $M1$ strength plotted in the lower part of Fig. 20 shows a similar fragmentation.

Starting from the opposite side, i.e., a shell-model or QRPA approach, the diagonalization within the unperturbed basis of 2qp, 4qp, etc. states will eventually result in the building up of collective correlations that are reminiscent of a scissors magnetic dipole mode. Examples have been shown in Figs. 16–18 in the heavy deformed rare-earth nuclei. The discussion in Sec. III.A.2 has concentrated on this issue with references to a number of calculations of that type. One can make use of similar arguments as those used at the time by Brown and Bolsterli (1959) in the discussion of how individual 1p-1h 1^- configurations, interacting through a zero-range force, could build a single collective isovector electric dipole mode. In contrast to the study of this giant electric dipole resonant state in which the collective state is mainly built from $1\hbar\omega$ excitations, the orbital magnetic dipole strength is mainly of $0\hbar\omega$ nature. Richter and Knüpfer (1980) showed that the separable characteristics of the two-body matrix elements, which is essential for

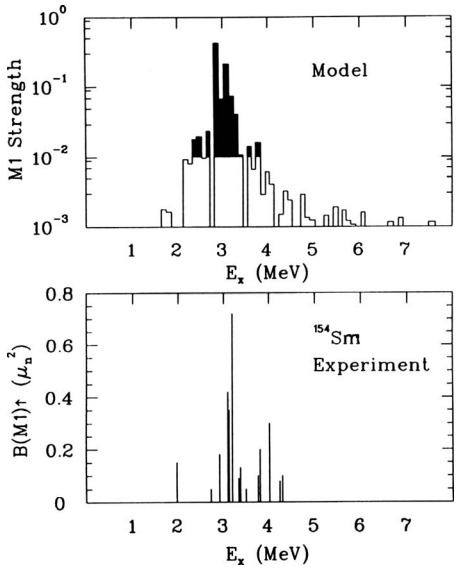

FIG. 20. Damping and fragmentation of the scissors mode. Upper part: Scissors $M1$ strength damped into the background of 2qp and 4qp states shown in lower part of Fig. 19, averaged over intervals of 100 keV. The black part indicates transitions with a relative strength larger than 1%. Adapted from Heyde, 1989. Lower part: Experimentally measured orbital $M1$ strength distribution (Ziegler *et al.*, 1993).

the schematic Brown-Bolsterli model, no longer holds for the magnetic multipole excitations, i.e., the particle-hole matrix elements do not scale with the $M1$ transition amplitudes. As a result, rather small energy shifts show up compared to the unperturbed energy spectrum. Therefore, there remains a concentration of mainly orbital $M1$ strength of $0\hbar\omega$ origin in the energy interval 2.5–4 MeV. An example of the fragmentation process, starting from the pseudo-SU(3) description, but treating a more general Hamiltonian, has been discussed by Draayer and co-workers and a particularly interesting case is ^{196}Pt (Beuschel *et al.*, 2000) which is a prime example of a γ-soft nucleus (von Brentano *et al.*, 1996).

b. Level spacing distribution of scissors mode states

As previously mentioned, the complexity of the nuclear many-body problem is clearly manifest in the fragmentation of the experimental transition strength, which is distributed over several levels of the same spin and parity. This complexity has led Wigner, more than 40 years ago, to the introduction of random-matrix theory (RMT), reviewed by Guhr, Müller-Groeling, and Weidenmüller (1998) and Weidenmüller and Mitchell (2009). This statistical approach models spectral fluctuation properties: if the levels are correlated, one expects a linear repulsion between them and Wigner-Dyson statistics for the nearest-neighbor spacing distribution (NNSD). However, if correlations are absent, there is no level repulsion and the NNSD is of Poisson type, i.e., an exponential distribution. The validity of this ansatz has been confirmed in various data analyses and summarized in the two review articles cited.

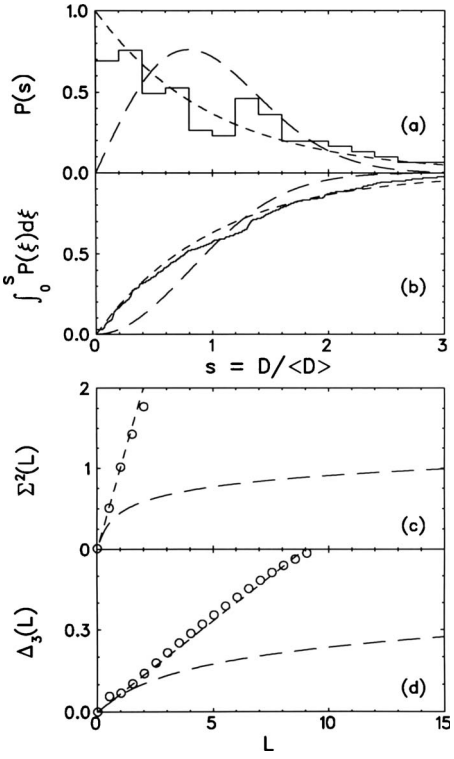

FIG. 21. Level spacing distribution of scissors mode states in heavy deformed nuclei (152 states from 13 nuclei). (a) Nearest-neighbor spacing distribution, (b) cumulative nearest-neighbor distribution, (c) number variance $\Sigma^2(L)$, and (d) spectral rigidity $\Delta_3(L)$, where L denotes the length of the sequence. The histograms and open circles display the data. Poissonian behavior and expectations from the Gaussian orthogonal ensemble (Wigner) are shown as short and long-dashed lines, respectively (Enders *et al.*, 2000).

In heavy nuclei, the picture emerges that high-lying single-particle states containing many complex configurations show Wigner-Dyson statistics (Haq *et al.*, 1982), whereas low-lying collective states of simple structure lack correlations and yield a Poisson distribution (Shriner, Mitchell, and von Egidy, 1991; Garrett *et al.*, 1997). This in turn allows one to use RMT to conclude from spectral statistics if excitations are mainly of single-particle or of collective character. This idea has also been applied to states which belong to the scissors mode (Enders *et al.*, 2000). As discussed in Sec. III.A.1, an unprecedented data set is now available covering doubly even nuclei in the $N=82$–126 major shell. By combining the data sets from 13 heavy deformed nuclei, a data ensemble has been constructed with a total number of 152 states in the excitation energy window of about $2.5<E_x<4.0$ MeV (Fig. 1).

After unfolding the experimental spectra, i.e., removing the energy dependence of the average level spacing, the NNSD, the cumulative NNSD, the number variance Σ^2, and the spectral rigidity Δ_3 (Bohigas, 1991; Guhr, Müller-Groeling, and Weidenmüller, 1998) were extracted from the data ensemble. The results are shown in Fig. 21. All evaluated statistical measures agree very well with the Poissonian behavior of uncorrelated levels.

Although the individual level sequences are rather short (of order of 10 only), the functions Σ^2 and Δ_3 clearly show the lack of long-range correlations. Enders *et al.* (2000) also showed that the influence of missing levels due to the experimental conditions is negligible. Consequently, the remarkable conclusion from the statistics of the level spacings distribution may be drawn that the scissors-mode states all have the same structure and are excited collectively by the same mode.

c. Sum rules and relation to other observables

Even though the magnetic dipole strength appears rather fragmented in the energy region 2.5–4.0 MeV, experimental methods have been set up in order to distinguish those 1^+ states that carry mainly orbital $M1$ strength [see also Kneissl *et al.* (1996)]. The summed experimental strengths show remarkable correlations to collective observables of the low-energy spectrum.

First, as mentioned, the summed $M1$ strength correlates with the square of the equilibrium quadrupole deformation value for series of isotopes such as the Nd and Sm nuclei [Fig. 11, from Ziegler *et al.* (1990)]. Second, the summed $M1$ strength also correlates linearly with the $B(E2;0_1^+ \rightarrow 2_1^+)$ value for most nuclei in this mass region (Richter, 1995). Furthermore, both the summed $M1$ strength and the particular $B(E2)$ value scale in the same way and saturate (Rangacharyulu *et al.*, 1991) when plotted, not as a function of proton (neutron) number (Fig. 22) but using the variable $P=N_pN_n/(N_p+N_n)$ with $N_p/2$, $N_n/2$, the number of proton and neutron pairs, respectively, counted from the nearest closed shells (the number of bosons in the IBM-2 model), introduced by Casten *et al.* (1987). Third, it has been shown that the summed $M1$ strength even scales linearly with the isotopic shift for those nuclei (Nd, Sm, and Dy) where both sets of data are available (Heyde *et al.*, 1993). These three important observations all point toward close interconnections between the $M1$, $E2$, and the $E0$ electromagnetic properties for the rare-earth region.

Before discussing in detail what theoretical models predict for the behavior of the summed $M1$ strength, the deformation dependence of the $B(E2;0_1^+ \rightarrow 2_1^+)$ strength and the radius are rather obvious from a collective geometrical approach (Bohr and Mottelson, 1975). The connection of the latter quantities to the summed magnetic dipole strength, however, was much less expected to appear, in particular the quadratic dependence on deformation and the same saturation behavior when passing through the rare-earth region.

Starting from the generalized Bohr-Mottelson model, Lo Iudice and Richter (1993) worked out a sum rule that holds very generally and is essentially model independent and parameter free. The resulting expression

$$B(M1)\uparrow \simeq 0.0042 E_{sc} A^{5/3} \delta^2 (g_p - g_n)^2 \mu_N^2 \qquad (11)$$

directly contains the dependence on deformation as well as on the gyromagnetic factors associated with the collective motion of the deformed proton and neutron systems. In the region covering transitional and strongly deformed rare-earth nuclei, the ratio of the experimental over the theoretical summed $M1$ strength is close to 1 over a large mass span, with a drop off toward the heavier masses. A specific example in which the sum rule is compared to a number of other models and the data for the Sm nuclei is shown in Fig. 23 (Garrido *et al.*, 1991; Hamamoto and Magnusson, 1991; Heyde and De Coster, 1991; Hilton *et al.*, 1993; Lo Iudice and Richter, 1993). While all of them roughly reproduce the quadratic dependence, the theoretical model results exhibit rather different slopes, in some cases with serious deviations from the data for the more deformed $A=152,154$ nuclei. Lo Iudice (1997) also showed that the TRM and IBM-2 sum rules are very closely related and all can be brought back to the basic sum rule structure as deriving from the QRPA study of collective magnetic dipole excitations.

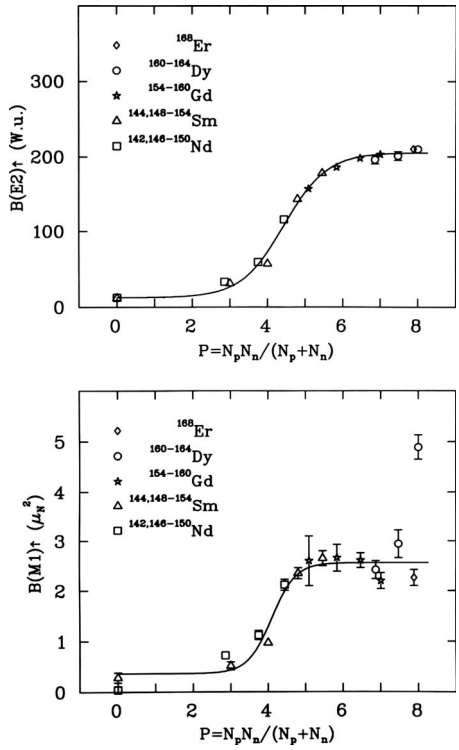

FIG. 22. $E2$ and summed $M1$ strength in the even-even rare-earth nuclei. Upper part: $E2$ transition strengths of the 2_1^+ states indicated in the figure versus P. Lower part: The same for the summed $M1$ strength in the energy range E_x =2.5–4 MeV. The solid lines correspond to fits explained in Rangacharyulu *et al.* (1991).

After the above experimental observations were well established, various theoretical ideas in deriving closed expressions for this summed $M1$ strength, aiming at establishing at the same time a relation to the $E2$ and the $E0$ nuclear properties, have been explored. Here we discuss implications of both non-energy-weighted and energy-weighted sum rules, using collective model as well as shell-model approaches.

Ginocchio (1991) proposed a non-energy-weighted $M1$ sum rule within the IBM for an N-boson system

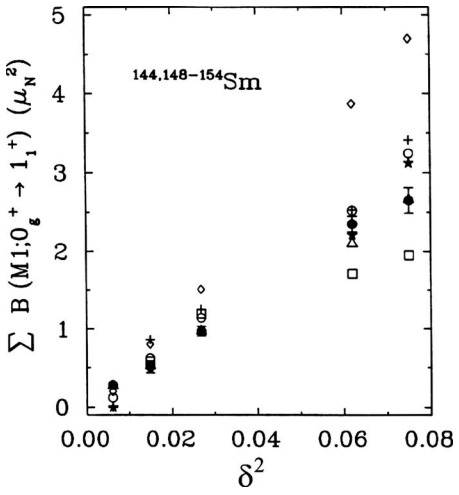

FIG. 23. Orbital $M1$ strength versus the square of deformation in the Sm isotopes. The experimental points (black circles with error bars) are compared to theoretical predictions from Hamamoto and Magnusson (1991) (circles), Garrido *et al.* (1991) (crosses), Hilton *et al.* (1993) (diamonds), Heyde and De Coster (1991) (squares), Lo Iudice and Richter (1993) (triangles), and Sarriguren *et al.* (1994) (stars) (Richter, 1995). Note that the experimental points do overlap with the triangles in a number of cases, making the distinction difficult.

$$\sum B(M1) = \frac{9}{4\pi}(g_\pi - g_\nu)^2 \frac{P}{N-1}\langle 0^+|\hat{n}_d|0^+\rangle, \tag{12}$$

an expression which connects the summed $M1$ strength with the expectation value of the number of d bosons in the nuclear ground state. This latter quantity is also a measure of deformation because the average number of d bosons in the ground state $\langle 0^+|\hat{n}_d|0^+\rangle/N$ can be expressed by a deformation parameter β_{IBM}. A relation was derived (von Neumann-Cosel *et al.*, 1995) between this specific IBM quantity and the corresponding geometrical definition of deformation such as the Bohr-Mottelson parameter β_2 as

$$\beta_{\mathrm{IBM}} = \frac{3\lambda}{2\sqrt{\pi}}\frac{Z}{Z_{\mathrm{val}}}\beta_2. \tag{13}$$

Here Z_{val} describes the number of protons in the valence shell and λ [not to be confused with Majorana strength parameter in Eq. (6)] is a measure of how much of the $E2$ sum rule is exhausted by the transition to the 2_1^+ state. The original sum rule of Ginocchio has thereby been extended and applied to the full range of nuclei spanning the Nd to W region providing an excellent description of the quadratic quadrupole deformation dependence. This is shown in Fig. 24.

Making use of the IBM-2, other sum rules have also been derived (energy-weighted $M1$ sum rule and even sum rules for other multipoles). The energy-weighted sum rule indicates a direct relation between summed $M1$ strength and the $B(E2;0_1^+ \to 2_1^+)$ value when the assumption is made that most $E2$ strength remains in the first

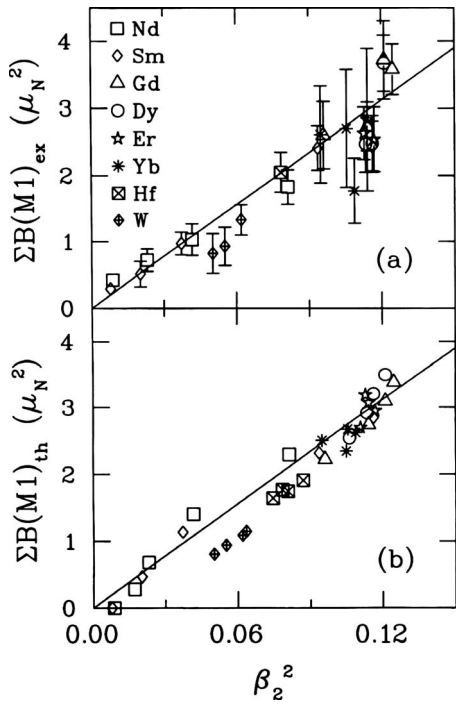

FIG. 24. Experimental $M1$ scissors mode strengths as a function of the deformation parameter β_2^2. (a) The straight line is a least-squares fit assuming intercept zero. (b) Prediction of an IBM-2 sum rule for the scissors mode strength of all even-even stable nuclei from Nd to W (von Neumann-Cosel *et al.*, 1995).

excited 2^+ state (which is a rather good approximation for transitional and definitely so for deformed nuclei) and gives rise to the following relations:

$$\langle 0_1^+|[[\hat{H},\hat{T}(M1)],\hat{T}(M1)]|0_1^+\rangle = \frac{2}{\sqrt{3}}\sum B(M1)\{E_x(1^+) - \lambda N\} \tag{14}$$

or

$$\sum B(M1)\{E_x(1^+) - \lambda N\} = c\sum B(E2) \tag{15}$$

when using F-spin symmetry in evaluating the quadrupole expectation value. Here λ denotes the strength of the Majorana term in Eq. (6). This expression indeed relates the energy-weighted $M1$ sum rule with the non-energy-weighted $E2$ sum rule. The quantity c is introduced to match dimensions of the left- and right-hand sides of this equation. This relation was discussed and illustrated more explicitly in Heyde *et al.* (1992) in which it is shown under what approximations the above relation reduces to the non-energy-weighted $M1$ sum rule. There it is also shown that the effect of the Majorana term can be incorporated to a large extent.

It is important though to study analogous sum rules for the magnetic dipole strength but now starting from a shell-model formulation of the problem. Using protons and neutrons explicitly, Zamick and Zheng (1992) derived an energy-weighted magnetic sum rule which was refined subsequently (Moya de Guerra and Zamick, 1993) with the more general result

$$\sum B(M1)E_x(1^+) = \frac{9\chi}{16\pi}[B(E2)_{\mathrm{IS}} - B(E2)_{\mathrm{IV}}], \qquad (16)$$

which is indeed close to the form of the IBM-2 result in Eq. (15), except for the additional isovector (IV) contribution. Here χ denotes the strength of the quadrupole-quadrupole interaction and the $B(E2)$ values are in units of e^2 fm^4. For many of the transitional and definitely for the strongly deformed nuclei, the second term is small and thus one recovers the IBM-2 result exactly. For a number of cases though Zamick and Zheng (1992) explicitly showed the need for the isovector term in order to have the correct physics in connecting $M1$ and $E2$ electromagnetic properties. It is important to note that, similar to the collective IBM-2 formulation and the TRM treatment, the residual two-body forces may contain besides the strong quadrupole forces, pairing interactions among identical nucleons. The sum rule is not affected by the addition of the latter term.

Moreover, one can relate the non-energy-weighted $M1$ sum rule to the nuclear monopole properties (Heyde *et al.*, 1993). Starting from the IBM expression for the monopole operator

$$T(E0) = \gamma_0\hat{n}_s + \beta_0\hat{n}_d = \gamma_0\hat{N} + \beta_0'\hat{n}_d, \qquad (17)$$

with $\hat{n}_s$, $\hat{n}_d$, $\hat{N}$ representing the s, d, and total boson number operators, respectively, and $\beta_0' \equiv \beta_0 - \gamma_0$, one derives the mean-square radius as

$$\langle r^2\rangle = \gamma_0 N + \beta_0'\langle\hat{n}_d\rangle. \qquad (18)$$

Thus, the $M1$ sum rule of Eq. (12) can be recast in the form

$$\sum B(M1) = \frac{9}{4\pi}(g_\pi - g_\nu)^2\frac{1}{\beta_0'}\frac{P}{N-1}[\langle r^2\rangle - \gamma_0 N]. \qquad (19)$$

This latter expression (see Fig. 25 for a comparison with data) shows the connection between summed $M1$ strength and nuclear radial properties [the latter taken from the compilation of Otten (1989)]. Similar connections have also been suggested by Iachello (1981) and by Otsuka (1992) separately because of the connection between the nuclear radial variation $\Delta\langle r^2\rangle$ for a liquid drop and the variation in quadrupole deformation $\Delta\langle\beta_2^2\rangle$.

d. Deformation dependence and saturation

Starting from a microscopic approach [deformed mean field with residual pairing and quadrupole interactions and even using Hartree-Fock calculations using Skyrme effective forces (Garrido *et al.*, 1991; Smith *et al.*, 1995; Lo Iudice, 1998)], the same dependence between the summed $M1$ strength and nuclear deformation results, as discussed. Remarkably, it is the presence of pairing forces that modifies the dependence of the summed $M1$ strength from linear to quadratic. This was shown to be the case by Hamamoto and Magnusson (1991) in a Nilsson model study and also by Lo Iudice and Richter (1993) using an RPA study of magnetic scissors motion.

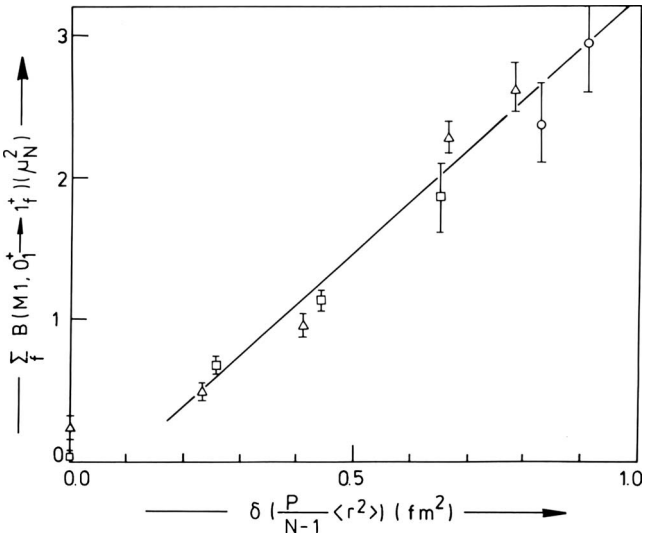

FIG. 25. Relation between the experimental summed $M1$ strength of all 1^+ states below 4 MeV for $^{142,146-150}$Nd (squares), $^{144,148-154}$Sm (triangles), $^{160-162}$Dy (circles), and the variation in the quantity $\delta(\frac{P}{N-1}\langle r^2\rangle)$ related to the isotope shift (Heyde *et al.*, 1993).

The fact that the summed $M1$ strength shows this striking collective behavior immediately leads to saturation because the equilibrium quadrupole deformation (in passing through the rare-earth region from $A=140$ toward the mass $A=180$ region) stabilizes at a value of $\delta\simeq 0.25$ in the region $A\geqslant 160$ of strongly deformed even-even nuclei. The precise origin of this saturation stems from the specific single-particle structure in the deformed mean field and from the balancing effects of shell and pairing corrections to the liquid-drop energy (Heyde *et al.*, 1992). The saturation arises after a steep increase in deformation, which is reflected in a steep rise in both the summed $M1$ strength and $B(E2;0_1^+\rightarrow 2_1^+)$ value when entering the region of deformation, starting from closed-shell nuclei (see Fig. 22). This strong correlation between the summed $M1$ strength and the ground-state equilibrium quadrupole deformation was discussed by De Coster and Heyde (1989).

The dominant role of pairing to obtain the correct deformation dependence for the magnetic summed strength is not straightforward but comes in indirectly. In a quadrupole deformed potential, the strength of $M1$ transitions between Nilsson orbitals, characterized by Ω (the projection of j on the symmetry axis) and shown by the arrows in the top part of Fig. 26, can be expressed as

$$B(M1) = \frac{3}{4\pi}(u_1v_2 - u_2v_1)^2|\langle\Omega_1|g_l\hat{l}_+ + g_s\hat{s}_+|\Omega_2\rangle|^2. \qquad (20)$$

The occupation probabilities v_i^2 (with $u_i^2 = 1 - v_i^2$) of the Nilsson orbitals Ω_i are schematically drawn in the bottom part of Fig. 26 for both small and large quadrupole deformations. The doubly hatched lines indicate the position of the Fermi level (top part) and for an occupation number 0.5 (lower part). For small deformation the pairing factor $(u_1v_2 - u_2v_1)^2$ quenches the $M1$ strength and

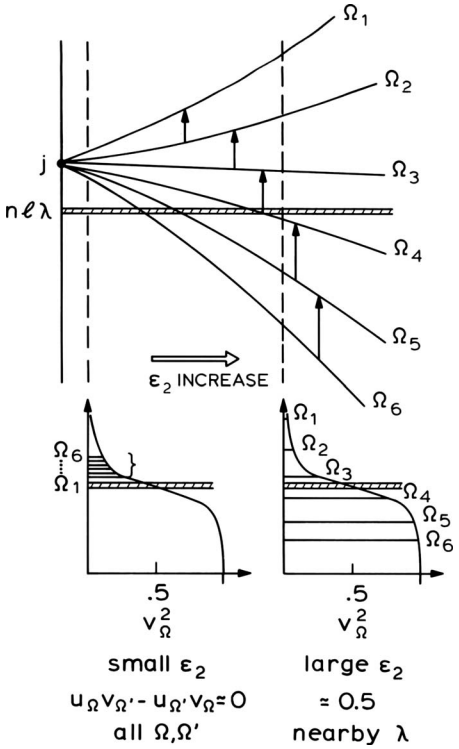

FIG. 26. Schematic representation of the effect of deformation on the orbital $(lj)\rightarrow(lj)$ transition strength. The Fermi level is denoted by the hatched lines (Richter, 1990).

vanishes for zero deformation. With increasing deformation, the Nilsson single-particle orbitals Ω_i originating from a single j shell-model orbital are more spread out and the corresponding occupation probabilities become different resulting in a rather large pairing factor. Then, as deformation does not change much for increasing mass numbers, the pairing factors remain roughly constant, causing saturation before they start to decrease again toward the end of the shell. Using the approximation that the energy of the Nilsson orbitals vary linearly with deformation for not too large values of deformation, it can even be shown that the pairing factor $(u_1v_2-u_2v_1)^2$ becomes proportional to δ^2. This result comes close to what Hamamoto and Magnusson (1991) also obtained.

A particularly interesting example of this deformation dependence has resulted from the study of magnetic dipole strength in superdeformed nuclei (Hamamoto and Nazarewicz, 1992, 1994). The summed $B(M1)$ strength was found to be much larger than in nuclei at normal deformation. This can be understood from the growing proton orbital contribution with increasing deformation and the fact that, for the weak pairing present in the superdeformed configuration, the pairing factor in Eq. (20) becomes maximal. Applications for nuclei in the proton-rich deformed Kr-Zr nuclei showed similar results (Nakatsukasa *et al.*, 1994).

Whereas QRPA calculations for strongly deformed nuclei give rise to the δ^2 dependence of the $M1$ strength and saturation for both the $B(E2;0_1^+\rightarrow2_1^+)$ and summed $M1$ strength due to the importance of pairing correlations among the interacting nucleons, the IBM does not exhibit this characteristic behavior. In both the SU(3) and O(6) limit of the IBM-2, the $B(M1)$ transition into the scissors 1^+ mixed-symmetric state is proportional to the P factor (Casten *et al.*, 1987) which implies an almost linear rise toward midshell before dropping off toward the end of the major shell (Scholten, Heyde, and Van Isacker, 1985). This sheds light on the way in which to count the boson number when highly deformed systems are being described. Casten *et al.* (1988) showed that one should consider in this region an effective boson number, following arguments by Otsuka *et al.* (1990), through which Pauli blocking is taken into account.

e. A comprehensive analysis

Even though it was previously shown that one can obtain a qualitative understanding of the observed behavior of the summed magnetic dipole strength at low energies (deformation dependence, saturation, and relation to other multipoles), a quantitative agreement between the large body of experimental data and theory has still been lacking. Part of the problem is related to the fact that most model approaches use still too idealized assumptions concerning the way in which nucleons behave inside the atomic nucleus: moments of inertia, gyromagnetic ratios, etc. Therefore, a global study in heavy even-even nuclei was carried out in order to obtain as accurate a description of the scissors mode when one uses as input the realistic physical parameters in the calculations (Enders *et al.*, 1999, 2005).

This study makes use of the sum-rule method as described by Lipparini and Stringari (1983, 1989b) and starts from the energy-weighted (S_{+1}) and the inverse energy-weighted (S_{-1}) sum-rule expressions

$$S_{+1}=E_{sc}B(M1)$$
$$=\frac{3}{20\pi}r_0^2A^{5/3}\delta^2E_D^2\frac{m_N}{\hbar^2}(g_p-g_n)^2\mu_N^2\ \text{MeV} \tag{21}$$

and [cf. Eq. (10)]

$$S_{-1}=\frac{B(M1)}{E_{sc}}=\frac{3}{16\pi}\frac{J_{sc}}{\hbar^2}(g_p-g_n)^2\frac{\mu_N^2}{\text{MeV}}, \tag{22}$$

with $r_0=1.15$ fm, A the nuclear mass number, δ the nuclear deformation parameter, E_D the isovector giant electric dipole resonance (IVGDR) excitation energy, m_N the nucleon mass, and g_p (g_n) the g factors for protons (neutrons). With E_{sc} we denote the excitation energy of the scissors mode and J_{sc} describes the moment of inertia associated with the scissors mode vibrations, which are of isovector type. These expressions are rather general and express the fact that the scissors mode and the IVGDR are both of isovector nature and strongly related through the restoring force acting on the deformed proton and neutron bodies and also that the major contribution to S_{-1} comes from the low-lying scissors mode ($0\hbar\omega$ strength in Fig. 1) whereas the high-lying

scissors mode ($2\hbar\omega$ strength in Fig. 1) mainly contributes to S_{+1}.

We first discuss S_{-1} because the low-lying scissors mode after all is well studied by now in heavy nuclei. To begin we use the common relative g-factor values $g_{\rm rel}=g_p-g_n=2Z/A$ (Bohr and Mottelson, 1975) and deduce the moment of inertia (taking the assumption that the scissors $M1$ strength resides in the energy region 2.5–4 MeV). It is interesting to see (Enders *et al.*, 1999, 2005) that the ground-band and scissors motion moments of inertia are very close to each other (except for a systematic deviation in heavier nuclei).

Next we take these two moments of inertia to be equal,[2] i.e., $J_{sc}=J_{gb}$, and evaluate the g factors starting from the sum-rule value of S_{-1}. There appears a striking agreement between these values with only small deviations (of the order of 10%). When recalculating the moment of inertia related to the scissors motion in Eqs. (21) and (22), using the experimentally deduced $g(2^+)$ values and comparing these moments with the ground-state moments of inertia, an almost perfect overlap between the two sets results. We can then draw the conclusion that the g factors acting in the scissors mode are the same as the ones for the ground band.

Since all quantities in the sum rules [Eqs. (21) and (22)] are fixed, we are now in a position to rederive the energies and the strengths for the scissors modes. However, when dealing with S_{+1} one has to take into account that contributions from the $K=1$ component of the isovector giant quadrupole resonance (IVGQR) will dominate, which have to be removed in order to compare with the experimental data. This is achieved with a procedure described by Lipparini and Stringari (1983), which leads to a correction factor $\xi=E_Q^2/(E_Q^2+2E_D^2)$ to Eq. (21), where E_Q denotes the centroid energy of the isoscalar giant quadrupole resonance (ISGQR).

When putting all low-lying (high-lying) $M1$ strength $\Sigma_{\rm low}B(M1)=B_l$ [$\Sigma_{\rm high}B(M1)=B_h$] into a single state with energy E_l (E_h), one obtains

$$S_{-1}\approx B_l/E_l, \quad S_{+1}\approx B_h\cdot E_h, \tag{23}$$

and using the expressions for S_{-1} and S_{+1}, we can derive an average energy

$$\bar{\omega}=\frac{2}{\sqrt{15}}\sqrt{\frac{m_N}{\hbar^2}}r_0\sqrt{\frac{4NZ}{A^2}}A^{5/6}E_D\sqrt{E_{2^+}\xi}\delta, \tag{24}$$

where use was made of the relation between scissors mode and ground-state band moment of inertias established above and the latter is expressed through the energy of the first excited state of the rotational band E_{2^+} by $J_{gb}=3\hbar^2/E_{2^+}$. The centroid energies of the IVGDR and ISGQR are taken from mass-dependent systematics (Harakeh and van der Woude, 2001).

[2]More precisely the moment of inertia of isoscalar and isovector motion differ by a factor $4NZ/A^2=0.96$ (Lo Iudice and Richter, 1993).

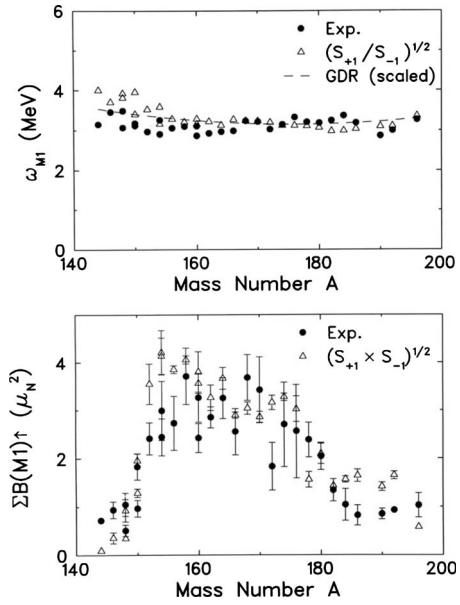

FIG. 27. Sum-rule analysis of the scissors mode in rare-earth nuclei. Excitation energy (upper part) and transition strength systematics (lower part) are presented. Experimental values (solid circles) and parameter-free predictions (open triangles) are shown for the mean excitation energy (upper part) and the summed $M1$ strength (lower part). The deformation dependence of the moment of inertia leads to the proportionality of the excitation energies of the scissors mode and the IVGDR as indicated by the dashed line (Enders *et al.*, 2005).

The values resulting from Eq. (24) are drawn as triangles in Fig. 27 (upper part). Excellent agreement with the experimental data is obtained. When scaled by the ratio of the scissors mode to the liquid-drop moment of inertia, the energy of the isovector giant dipole resonance (dashed line) also shows the proportionality to the energy of the scissors mode predicted in Eq. (24). We note that the observed near constancy of ω could also be explained by Pietralla, von Brentano, Herzberg *et al.* (1998) within a schematic RPA approach after inclusion of the deformation dependence of paring effects analogous to the previous discussion.

Similarly one obtains for the low-lying scissors strength

$$B_l=\frac{3}{\pi}\sqrt{\frac{3}{20}}r_0\sqrt{\frac{4NZ}{A^2}}A^{5/6}E_D\sqrt{\frac{m_N\xi}{\hbar^2E_{2^+}}}\delta g_{gb}^2, \tag{25}$$

with $g_{gb}=\frac{1}{2}(g_p+g_n)$, the g factor of the 2^+ level of the ground-state band. Comparison to the experimental scissors mode strength is shown in the lower part of Fig. 27. The agreement is satisfactory except for some nuclei with $A>180$. The strong deformation dependence is generated by the interplay of E_{2^+} and δ. Indeed the experimentally established quadratic dependence of the scissors-mode strength on the ground-state deformation is easily derived from Eq. (25) recalling (Bohr and Mottelson, 1975) that the moment of inertia J_{gb} is roughly proportional (albeit much larger) to the superfluid moment of inertia $J_{\rm liq}$,

$$J_{gb} \propto J_{\mathrm{liq}} = J_{\mathrm{rig}}\delta^2, \tag{26}$$

where J_{rig} stands for the moment of inertia of a rigid rotor.

f. Sum-rule relation between magnetic dipole and octupole strength

In the spirit of the IBM-2 non-energy-weighted $M1$ sum rule (Ginocchio, 1991), a relation between magnetic dipole and octupole strength could be derived starting from energy-weighted sum rules (Heyde *et al.*, 1994). It has been possible to obtain an approximate, yet simple relation

$$\frac{\sum_f B(M1;0_1^+ \to 1_f^+)E_x(1_f^+)}{\sum_f B(M3;0_1^+ \to 3_f^+)E_x(3_f^+)} \cong \left[\frac{6(g_\pi - g_\nu)}{7(\Omega_\pi - \Omega_\nu)}\right]^2. \tag{27}$$

This relation establishes a link between different parameters of the IBM-2, the gyromagnetic boson factors and octupole boson moments, and hence imposes constraints on choosing them when fitting to other spectroscopic data. One can, on the other hand, also use the relation starting from common values for these parameters $(g_\pi, g_\nu, \Omega_\pi, \Omega_\nu)$ as derived from a phenomenological and/or microscopic starting point and deduce an estimate for the summed $M3$ strength, whenever information on the summed $M1$ dipole strength is available. This was discussed by De Coster *et al.* (1995), where an estimate of the summed $M3$ strength is presented in the mass region $144 \leqslant A \leqslant 164$. Even though it contains a number of approximations, in the absence of systematics on the $M3$ strength, the above method might be a first guide for further experimental studies.

There are few studies on $M3$ transitions carried out by now, both theoretically and experimentally. On the theoretical side, $M3$ transitions were investigated within the framework of the IBM-2 by Scholten *et al.* (1984) and within the context of a schematic RPA study for heavy deformed nuclei by Lo Iudice (1988). There has been an early experimental search for $M3$ strength in ^{164}Dy by Bohle, Richter, *et al.* (1987) that made use of both the electron accelerators at Darmstadt and Amsterdam. Only an upper limit for such strength has been derived. A more systematic search for magnetic octupole strength is called for in light of the above approximate connection with the summed $M1$ strength.

B. Spin-flip mode: Experimental evidence and theoretical description

1. Qualitative nature of the magnetic dipole response

The magnetic dipole operator for a system of protons and neutrons reads

$$T(M1) = \sqrt{\frac{3}{4\pi}}\sum_i \{g_l(i)\hat{l}_i + g_s(i)\hat{s}_i\}\mu_N, \tag{28}$$

with the usual orbital and spin g_l, g_s factors for neutrons and protons [see also Eq. (7)]. Using the isospin labels $t_z(i) = \pm\frac{1}{2}$ for neutron and proton, respectively, the magnetic dipole operator can be split into an isoscalar and isovector term in the following way:

$$T(M1) = \sqrt{\frac{3}{4\pi}}(g_J\hat{J} + g_S\hat{S})\mu_N + T(M1,\mathrm{IV}). \tag{29}$$

Since $\hat{J}$ denotes the total angular momentum operator, this term does not induce any $M1$ transitions and because $g_S = [(g_s^\pi + g_s^\nu) - 1]/2$, the isoscalar spin part only contributes in a minor way to $M1$ transitions. This is a consequence of the opposite signs in the proton and neutron spin g_s factors resulting in a value of $g_S = 0.38$.

The isovector part of the $M1$ operator $T(M1,\mathrm{IV})$,

$$T(M1,\mathrm{IV}) = \sqrt{\frac{3}{4\pi}}\left\{\frac{1}{2}(\hat{L}_\pi - \hat{L}_\nu) + \frac{1}{2}(g_s^\pi - g_s^\nu)(\hat{S}_\pi - \hat{S}_\nu)\right\}\mu_N, \tag{30}$$

splits into two pieces: the first part, describing the relative angular momentum between protons and neutrons, generates the scissors orbital motion whereas the second part, a spin-flip part, is nothing else but the $\Delta T_z = 0$ component of the Gamow-Teller operator. This term can strongly enhance spin-flip $M1$ transitions because of the large factor $\frac{1}{2}(g_s^\pi - g_s^\nu)$ in front (with a numerical value 4.72 using free g_s factors).

The fact that the simple picture of the nuclear magnetic dipole response is approximately correct is shown in Fig. 28 using the three nuclei ^{56}Fe, ^{156}Gd, and ^{238}U as examples. As discussed, the mean excitation energy of the orbital mode scales approximately with deformation as $E_x \simeq 66\delta A^{-1/3}$ MeV. The spin $M1$ strength obtained in inelastic proton scattering (Frekers *et al.*, 1990) lies at $E_x \simeq 41A^{-1/3}$ MeV and thus exhibits a shell-model-like excitation energy dependence. As shown in Fig. 28, the spin strength represents the largest fraction of the $M1$ strength.

It is the residual particle-hole interaction acting in the spin-isospin channel that shifts this spin $M1$ strength to higher energies as can be seen in schematic model (Zawischa, Macfarlane, and Speth, 1990; De Coster and Heyde, 1991a; De Coster *et al.*, 1992; Zawischa and Speth, 1994) and in RPA studies (Sarriguren *et al.*, 1993, 1994, 1996). The orbital part of the $M1$ strength is hardly moved by this force component and so one expects to observe experimentally a good overall separation of the orbital dipole magnetic excitations, at the lower-energy end of 2.5–4 MeV, from the higher-lying spin magnetic dipole excitations.

The experimental detection of spin strength in the energy region above 4 MeV needs a probe that is particularly sensitive to the spin part of the nuclear current.

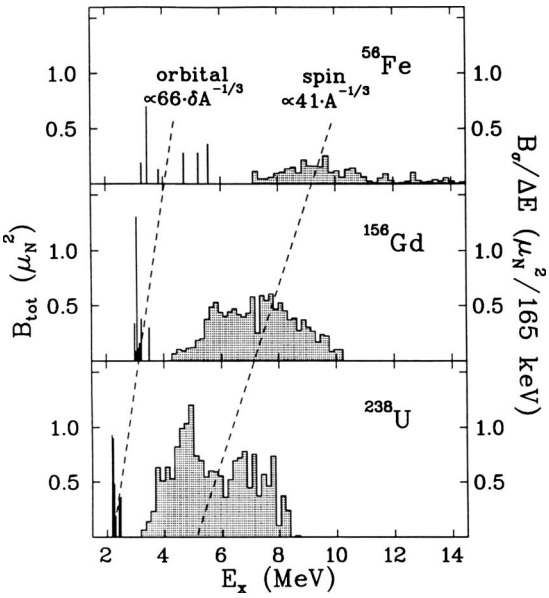

FIG. 28. The nuclear orbital and spin magnetic dipole response in a medium-heavy, a heavy, and a very heavy nucleus, derived from experiments with electromagnetic and hadronic probes, respectively (Richter, 1994).

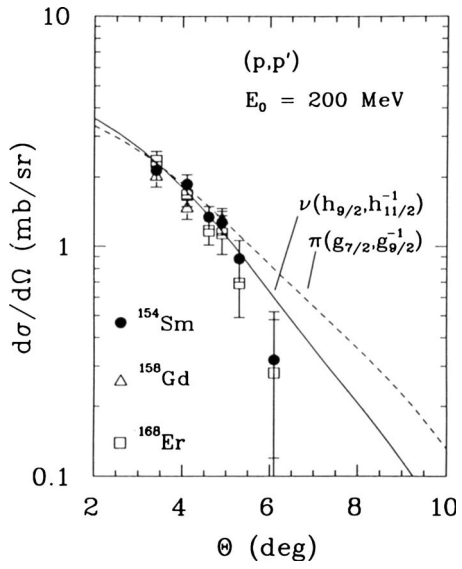

FIG. 30. Angular distribution of the summed double-humped structures observed in ^{154}Sm, ^{158}Gd, and ^{168}Er. The dashed and full curves result from DWBA calculations based on the indicated particle-hole excitations (Richter, 1991).

Intermediate-energy scattering of (polarized) protons at small forward angles should be the optimal selective reaction to carry out such a search. First experiments performed by a Darmstadt-Münster-TRIUMF Collaboration on ^{154}Sm, ^{158}Gd, and ^{168}Er used 200 MeV protons at an angle of 3.4° covering final states up to 12 MeV. Analyzing those data clearly showed in all nuclei the presence of extra strength sitting on the tail of the IVGDR (Fig. 29) with a double-hump structure (Frekers *et al.*, 1990; Richter, 1995). The double hump has centroids around 6 and 8.5 MeV and widths of about 1.5 and 2 MeV, respectively. Even more detailed substructure becomes visible (see inset in Fig. 29). Such a pronounced splitting and fragmentation of magnetic dipole strength has not been observed as yet in spherical nuclei. The selectivity of the (p,p') reaction could be demonstrated at the same time: the orbital $M1$ transition at 3.19 MeV strongly excited in (e,e') and (γ,γ') reactions was not observed with an upper limit $B(M1)<0.1\ \mu_N^2$.

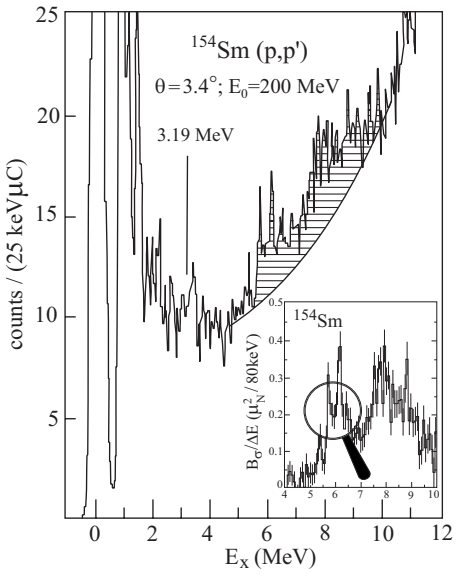

FIG. 29. Forward angle inelastic proton-scattering spectrum taken at 200 MeV incident energy on ^{154}Sm. The shaded area constitutes the giant spin magnetic dipole resonance. In the inset, the extracted $B(M1)$ strength (in units μ_N^2/80 keV) distribution is shown. Adapted from Frekers *et al.*, 1990.

In order to obtain more complete insight in the structure of these excitations, angular distributions have been taken for the three nuclei (Fig. 30). No strong Z nor A dependence shows up. A DWBA fit for a $\Delta S=1$, $\Delta L=0$ transition considering a neutron spin-flip $1h_{11/2}\rightarrow 1h_{9/2}$ or a proton $1g_{9/2}\rightarrow 1g_{7/2}$ transition has been performed. These orbitals are clearly the dominant ones in this mass region and for deformed nuclei; even the Nilsson states are dominated by these particular spherical components. A strength $B(M1)=10.5(2.0)\mu_N^2$ could be extracted, a value in line with expectations for the theoretical spin-flip strength (see Fig. 17).

Complementary experiments detecting the transverse spin-flip probability S_{nn} have been carried out (Wörtche, 1994). Thereby the probability that an incoming proton, interacting with the target nucleus, will leave with its spin flipped ($\Delta S=1$ process) is measured. The results for ^{154}Sm are shown in Fig. 31 where, besides the cross section in the energy interval 4–32 MeV, the corresponding spin-flip probability S_{nn} is given. Here one notices the presence of increased S_{nn} values in the region of the observed spin $M1$ strength (6–8.5 MeV), confirming the spin-flip character of the structures located on the low-energy tail of the GDR, the latter being split in two fragments, due to nuclear deformation. This figure also

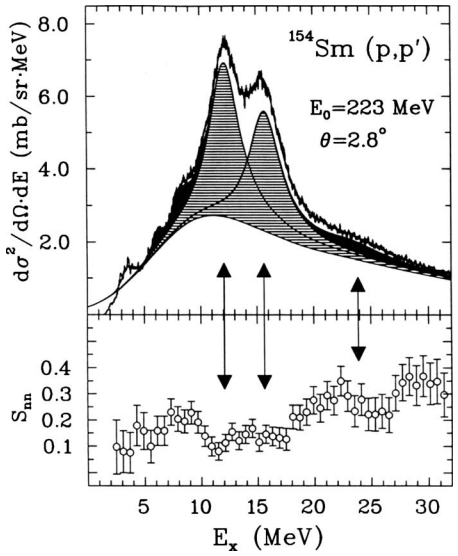

FIG. 31. Differential cross section and transverse spin-flip probability for inelastic polarized proton scattering on ^{154}Sm. The hatched areas show the double-humped GDR. Visible on the low-energy side of the GDR is the spin-flip $M1$ resonance between 5 and 12 MeV excitation energy and at E_x =23.4 MeV for the IVGQR. The arrows visualize the connection between the electric resonances and dips in the spin-flip probability (Richter, 1995).

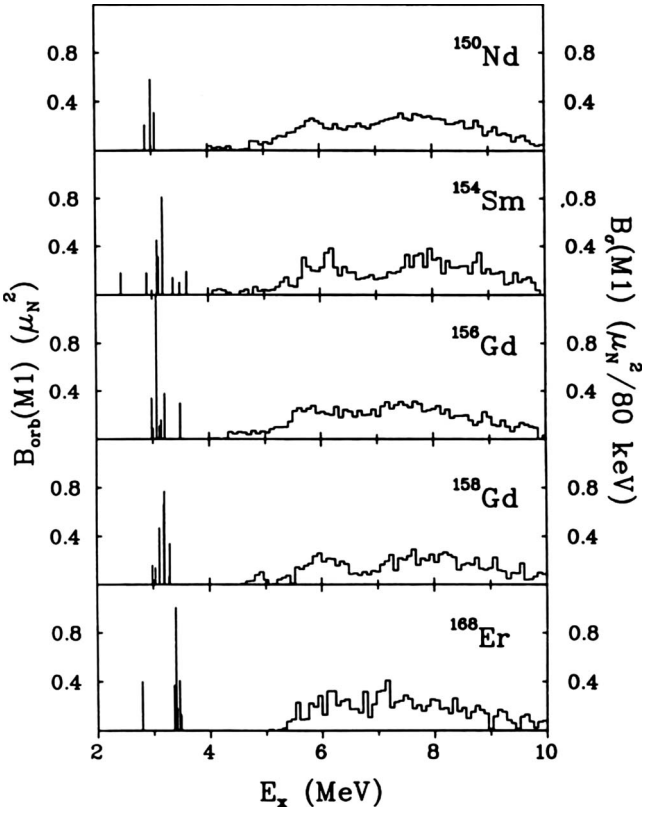

FIG. 32. Magnetic dipole response of several deformed rare-earth nuclei determined by inelastic electron, photon, and proton scattering (Richter, 1995).

shows the presence of an IVGQR derived from a multipole decomposition around 23 MeV, an excitation energy where it is has also been detected in other heavy nuclei (Harakeh and van der Woude, 2001). The analysis of the S_{nn} values is carried out consistently with the DWBA analysis of the angular distributions.

Recently it has become clear that the $E1$ response in heavy nuclei generally exhibits a local concentration of strength [called the pygmy dipole resonance (PDR)] well below the IVGDR overlapping with the excitation energy region of the spin-flip resonance. The PDR has been observed at a variety of shell closures [see, e.g., Kneissl *et al.* (2006), and references therein] but not yet in heavy deformed nuclei. This raises the question whether part of the strength attributed to the spin-flip $M1$ resonance is in fact of $E1$ nature. While this problem needs further experimental investigation, there are immediately two arguments in favor of the present interpretation: the angular distributions shown in Fig. 30 are distinct from those of Coulomb-excited $E1$ transitions and the S_{nn} values in the bottom part of Fig. 31 display a local maximum of the spin-flip strength.

Before concentrating on the theoretical description, we show the $M1$ response for a set of nuclei spanning a wide region of deformed rare-earth nuclei (Fig. 32). In all of these nuclei, a particularly stable pattern is emerging: at the lower energy side, at energies 2.5–4 MeV, a concentration of orbital magnetic dipole strength shows up with a ratio $\sqrt{B_l/B_\sigma} \approx 4$, where B_l and B_σ denote the reduced transition strength of the orbital and spin part of the magnetic dipole operator [Eq. (30)] and $B(M1) = (\sqrt{B_l} \pm \sqrt{B_\sigma})^2$ (Willis *et al.*, 1989). Higher up, starting at 5.5 MeV up to almost 10 MeV, a rather broad and extended region with a clear double-hump structure in most of these nuclei appears in which $\sqrt{B_l/B_\sigma} \leqslant 1$. Figure 32 therefore reflects the magnetic dipole response for strongly deformed nuclei in the rare-earth region to electromagnetic and hadronic probes. The low-energy part corresponds to an orbital magnetic dipole structure, the scissors mode, and the higher part is the spin-flip part mainly caused by proton and neutron single-particle transitions between spin-orbit partners. Whereas the energy of the spin-flip $M1$ mode will be localized at the energy of the gap in closed shells for spherical nuclei, in the region where deformation sets in one expects splitting of the various Nilsson energy levels causing a spreading of the spin-flip strength around the spherical centroid energy. If this argument is correct, one should obtain an $A^{-1/3}$ excitation-energy dependence for the observed peaks of $M1$ strength throughout the whole mass region (cf. Fig. 28). This seems indeed the case and is shown in Fig. 33, in which the double-hump $M1$ spin strength in deformed rare-earth and actinide nuclei is connected (Richter, 1995) to the detailed knowledge of the spin-flip strength in the doubly-magic ^{208}Pb nucleus (Laszewski *et al.*, 1988). Indications of a similar splitting are observed in medium-mass nuclei (Djalali *et al.*, 1982) except for the stable Zr isotopes (Crawley *et al.*, 1982), where the forward-angle (p,p') cross sections exhibit a single bump at $E_x \approx 9$ MeV identified as a spin-flip $M1$

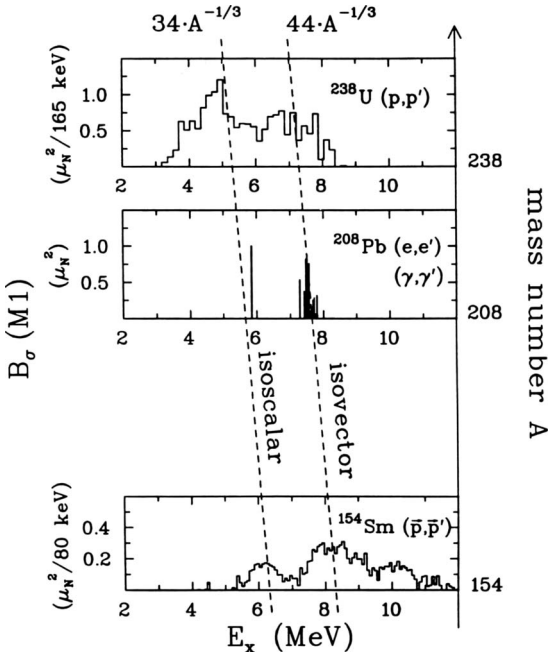

FIG. 33. Spin magnetic dipole strength distributions in ^{238}U, ^{208}Pb, and ^{154}Sm. The center of gravity of the excitation energy of the two peaks representing the main strength follows a simple $A^{-1/3}$ law, characteristic for spin-flip excitations between spin-orbit partners. The experimental strength distribution for ^{208}Pb has been combined from inelastic electron and photon scattering experiments (Richter, 1995).

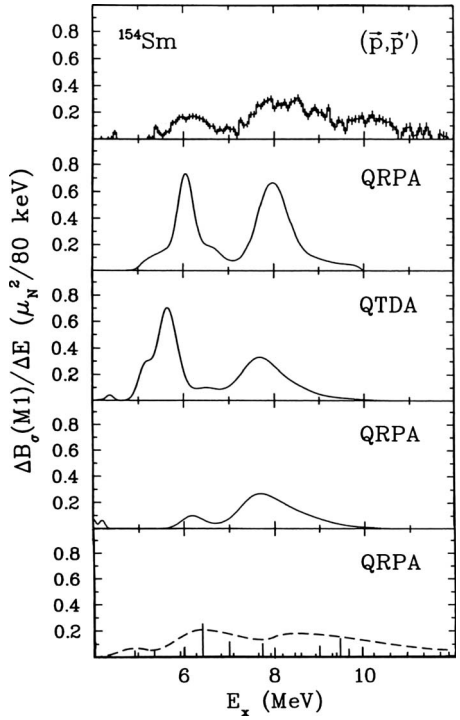

FIG. 34. Experimental and theoretical spin magnetic dipole strength distributions in ^{154}Sm. Underneath the experimental data, theoretical predictions from various calculations are given (in descending order): QRPA from Zawischa, Macfarlane, and Speth (1990); Zawischa and Speth (1990), QTDA from De Coster and Heyde (1991a); De Coster *et al.* (1992), QRPA from Sarriguren *et al.* (1993), and QRPA from Hilton *et al.* (1998).

resonance. This may be related to the special shell structure at $Z=40$, where the high-j orbital near the Fermi surface ($\pi 1g_{9/2}$) is essentially unoccupied and the corresponding $1g_{9/2}\rightarrow 1g_{7/2}$ transition suppressed.

2. Theoretical description

When trying to study the systematics of centroid energy and strength of the spin-flip transitions in rare-earth nuclei, a first approximation is to look at the unperturbed $M1$ strength originating from a deformed single-particle model. In carrying out this procedure, De Coster and Heyde (1991a) studied the summed spin $M1$ strength throughout the whole rare-earth region from ^{140}Ce up to ^{198}Pt. The strongest values are obtained at the end of the major shell near $Z=82$ and $N=126$ through proton $1h_{11/2}\rightarrow 1h_{9/2}$ and neutron $1i_{13/2}\rightarrow 1i_{11/2}$ transitions. The unperturbed energy of these transitions is situated in the energy region 4–10 MeV. With the residual interaction switched on, the $M1$ strength will be redistributed but the total strength should not change much from the unperturbed case.

Comparison of the experimental strength distribution in ^{154}Sm with a number of QRPA and QTDA studies has been carried out (Zawischa, Macfarlane, and Speth, 1990; Zawischa and Speth, 1990; De Coster and Heyde, 1991a; Sarriguren *et al.*, 1993; Hilton *et al.*, 1998) (see Fig. 34). The theoretical results have been folded with a Gaussian of variable width in order to facilitate comparison. One concludes that the agreement between experiment and theory is still on a qualitative level. The position of the two peaks does not vary much but the relative strength of the peaks is changing in a rather important way pointing out the sensitivity of the calculations to both the underlying single-particle structure and the residual interactions used. The QRPA calculations that come closer to the data (Sarriguren *et al.*, 1993; Hilton *et al.*, 1998) have been carried out after the experiments were performed. One also notices that the difference between QRPA and QTDA (Zawischa, Macfarlane, and Speth, 1990; Zawischa and Speth, 1990; De Coster and Heyde, 1991a) are not dramatic pointing out that ground-state correlations do not seem to play a major role in determining both the energy and the strength for these spin-flip transitions.

The specific double structure of the strength distributions is related to the residual spin-spin interaction which changes the unperturbed picture in an important way (De Coster *et al.*, 1992). Besides a shift of the spin strength to higher energies, as expected from schematic p-h models studying isovector excitations, a rather clear separation into a protonlike and a neutronlike collective spin mode remains. As a result, in ^{154}Sm the lower peak mainly originates from the proton $1g_{9/2}\rightarrow 1g_{7/2}$ and the $1h_{11/2}\rightarrow 1h_{9/2}$ excitations whereas the second, higher-lying peak is mainly due to the $1h_{11/2}\rightarrow 1h_{9/2}$ and $1i_{13/12}\rightarrow 1i_{11/2}$ spherical components. These simple p-h configu-

rations act as doorway states for the fragmentation of the resonance in analogy to the discussion for the scissors mode (cf. Fig. 20).

For larger strengths of the spin-spin proton-neutron interaction as used by Sarriguren *et al.* (1993, 1994, 1996), the spin strength becomes more concentrated into a full isoscalar and isovector part with proton and neutron configurations strongly mixed. Zawischa and Speth (1990) obtained results somewhat intermediate between the two more extreme cases of very weak coupling and strong coupling between the individual proton and neutron spin-flip $M1$ configurations. The higher peak shows a structure that is reminiscent of a genuine giant spin-flip (or Gamow-Teller) mode of isovector character. In comparing both the incoherent sum of the separate proton and neutron contributions with the actual calculation where interference effects do play an important role, it seems the lower part is mainly of proton character but also an isoscalar part is present. They come to the conclusion that for the higher peak in ^{154}Sm, using a Landau-Migdal residual interaction, the neutron contributions play the dominant role and come close to the results of De Coster and Heyde (1991a).

It is beyond our discussion that the starting points, i.e., different single-particle deformed potentials (Nilsson, deformed Woods-Saxon, and deformed Hartree-Fock mean field) and different residual interactions, lead to results that differ in an important way in their interpretation of the nature of the double-peak structure (proton and neutron versus isoscalar and isovector); see also Lipparini and Richter (1984). Experiments that are sensitive to the proton-to-neutron content in exciting those states (such as inelastic $\pi^{\pm}$ scattering) can most probably solve this issue and simultaneously give invaluable information concerning the proton-neutron part of the spin-spin component in the effective residual two-body interaction.

In conclusion, the general structure and evolution of spin-flip $M1$ strength can also be studied using schematic models (Zawischa and Speth, 1990, 1994; De Coster and Heyde, 1991b; De Coster *et al.*, 1992) and these results are in general consistent with those from the more detailed QRPA studies. For not too strong spin-spin proton-neutron coupling, while considering a two-level model (or a four-level model) in the rare-earth region, the strength becomes concentrated separately into a pure proton and neutron collective spin-flip state. With increasing strength, all components eventually contribute into an isovector mode at the higher energy and an isoscalar part at the lower-energy side, albeit with the neutron configurations and proton configurations dominating in these two modes, respectively.

C. Magnetic dipole strength at higher excitation energy: Prediction and experimental hints

Experiments have succeeded in studying the response of the nucleus to medium-energy protons toward much higher excitation energies. This was already shown in Fig. 31 in which the cross section and the S_{nn} transverse spin-flip probability in ^{154}Sm up to an energy of 32 MeV are presented. Besides the dominant giant electric dipole resonance state, split by deformation, on the lower side, the spin-flip $M1$ strength has been detected and is discussed in Sec. III.B. On the higher-energy tail though, excess strength is observed, which can be described by a Lorentzian centered at $E_x=23.4$ MeV with a width of 6.8(6) MeV. These parameters as well as an exhaustion of the corresponding energy-weighted sum rule of 76% (11%) agree well with the (scarce) systematics (Harakeh and van der Woude, 2001) of the IVGQR. The arrows indicate dips in the S_{nn} behavior which are directly related to the electric character of the strong states as compared to the other spin magnetic excitations.

The dip is probably the $K^{\pi}=1^{+}$ component of the IVGQR, which is split into various K components for strongly deformed nuclei, and taken as the genuine manifestation of a classical scissors motion. Lo Iudice and Richter (1989) pointed out that the lower RPA 1^{+} solution does not collect the whole $M1$ strength. They showed that a non-negligible fraction is obtained at higher energy. For $A=164$ ($N=Z$), they obtained a value of 25 MeV for the excitation energy of a high-energy mode with a corresponding strength of $B(M1)=4.5\mu_N^2$. The quadrupole component then acquires, through the $M1$ transition, an additional scissors characteristic.

As discussed in Sec. III.A.3, making a comprehensive analysis of $M1$ excitations in atomic nuclei, a relation between the energy and strength of a low- and high-energy scissors state was indicated, i.e., $\omega_h B_h=4\omega_l B_l$ which gives interesting information on both the expected excitation energy and the $M1$ strength for a high-energy mode. Such a mode will be mainly built out of $2\hbar\omega$ quasiparticle excitations for which the $M1$ strength becomes concentrated into a single strong state above 20 MeV. The issue of how well such a strong state at that high energy will remain intact is not clearly settled. A number of calculations (Hamamoto and Nazarewicz, 1992, 1994; Zawischa and Speth, 1994; Nojarov *et al.*, 1995; Zawischa, 1998) using schematic or more realistic forces come to different conclusions. Nojarov *et al.* (1995) and Hamamoto and Nazarewicz (1992) obtained a large concentration in a strong peak if they truncated the 2qp model space up to 20 MeV, in line with calculations within a schematic picture in which the higher-lying $M1$ strength also remains concentrated (see Fig. 35). Using a more extended space spreads out this strength considerably. At this energy, the resonance is highly unbound which will induce further spreading making it a difficult task to unambiguously detect and measure the amount of $M1$ strength. Thus, in view of the largely different theoretical results, the question of a still observable concentrated strong state will be difficult to solve. Moreover, as shown in Fig. 31, there are considerable experimental difficulties arising from a strong background mainly due to quasifree scattering, whose exact shape and strength are unknown and had be approximated by a semiempirical approach (Lisantti *et al.*, 1984).

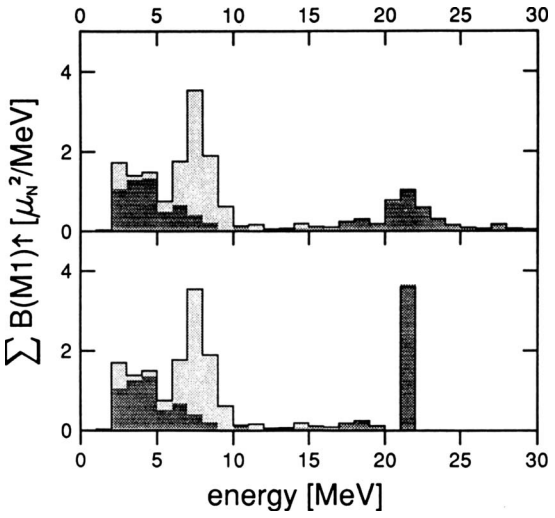

FIG. 35. Prediction of the full $M1$ strength distribution (summed in bins of 1 MeV) including the high-energy part in ^{160}Gd. The dark-hatched zone represents spin strength, the light-hatched one orbital strength. In the lower part, only 2qp configurations up to 20 MeV are taken into account. In the upper part, a much higher energy cutoff for these 2qp configurations is imposed. From Nojarov *et al.*, 1995.

The identification of the IVGQR permits an interesting test of the energy-weighted $M1$ sum rule given in Eq. (16) relating the summed $M1$ strength on the lhs to the difference of the isoscalar and isovector $E2$ summed strengths on the rhs of Eq. (16). With the experimental numbers for ^{154}Sm (Ziegler *et al.*, 1993) one obtains for the energy-weighted $M1$ sum rule a value of $(7.71\pm0.44)\mu_N^2$ MeV whereas the right-hand part (the difference of summed $E2$ strength) becomes $(9.32\pm0.31)\mu_N^2$ MeV. This is a rather good indication that below 4 MeV, the region where the sum of $M1$ strength was carried out, the $M1$ sum rule is exhausted already by 80%, leaving room for about 20% at the high-energy part of $M1$ strength.

IV. MAGNETIC DIPOLE EXCITATIONS IN HEAVY ODD-MASS NUCLEI

A. Experimental results and systematics

Naturally, the issue of what will happen in odd-mass nuclei when a single nucleon (proton or neutron) is coupled to the scissors mode in the even-even underlying core system arises. From the concept of particle-core coupling and considering the low-lying isoscalar quadrupole and octupole vibrational excitations in spherical and transitional nuclei, ample evidence for all states and a sharing of electromagnetic strength among the particle-core coupled multiplet members has been shown (Bohr and Mottelson, 1975). In the situation where the scissors mode $M1$ strength at the low-energy region is already spread out over a large energy span (2.5–4 MeV), it is clear that an experimental verification of (i) the presence of particle- (hole-) scissors coupled configurations and, more compelling, (ii) if the total $M1$ strength summed up in the appropriate energy interval in the odd-mass nucleus is consistent with the observed $M1$ strength in the even-even adjacent nuclei, will not be easy.

The problem is one of detecting all $M1$ strength, in particular the $M1$ strength residing in the background of many and complex configurations. On the other hand, the challenge for a good description from the theoretical side is also not an easy one. From a more phenomenological approach and taking the core $M1$ strength to be concentrated in one state, one will clearly not be able to correctly reproduce the strong fragmentation, however, the summed strength puts a constraint on this kind of model studies. From a more microscopic approach, odd-mass nuclei can be studied using a quasiparticle-phonon nuclear model (QPNM) (Soloviev, 1992). Here one needs to take into account the fact that the QRPA phonons themselves are partly constructed from the quasiparticle configurations one is coupling to. This so-called Pauli blocking has been treated for deformed nuclei (Soloviev, 1992). For spherical odd-mass nuclei, a detailed study of the transition strength from core-coupled configurations provided quantitative evidence for Pauli blocking (Scheck *et al.*, 2008). Ultimately, one aims at exact shell-model calculations but for the strongly deformed rare-earth region this is at present outside reach.

The experimental work covering a large part of the deformed rare-earth region has mainly been carried out by groups at Stuttgart, Köln, and Darmstadt, using inelastic photon scattering through the excited states in these odd-mass nuclei. The first search in the odd-proton ^{165}Ho nucleus using photon scattering with an end point of about 2.5 MeV did result in appreciable amounts of $M1$ strength (Huxel *et al.*, 1992) albeit to be associated with transitions among single one-quasiparticle proton excitations in this particular nucleus. Partly due to the low end point energy, no clear evidence for the presence of $M1$ strength into the mixed-symmetric configurations, to be expected beyond 2.5 MeV, was detected. Using a higher end point energy of 4.8 MeV and an EUROBALL cluster module (von Neumann-Cosel, 1997), spectra of much higher quality could be measured at the S-DALINAC (Huxel *et al.*, 1999) and we give an illustration for the case of ^{165}Ho (Fig. 36).

The first and quite clear indication for such $M1$ excitations was obtained in the ^{163}Dy odd-neutron nucleus (Bauske *et al.*, 1993). Here a concentration of $M1$ strength near to 3 MeV excitation energy was detected and the summed strength fits with the observed $M1$ strength in the neighboring even-even ^{162,164}Dy nuclei. Subsequent experiments on ^{161}Dy and ^{157}Gd (Margraf *et al.*, 1995), however, showed a large fragmentation of strength in the latter nucleus. This is quite difficult to understand in light of the proximity to ^{161}Dy (just a difference of two protons and two neutrons). Further experiments on some key nuclei in order to build up systematics in this region of the rare-earth nuclei were

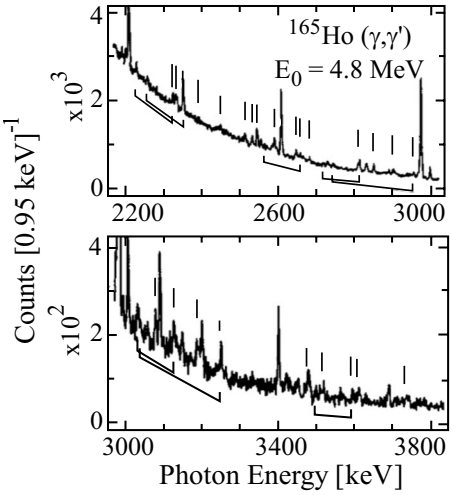

FIG. 36. Spectra of the ^{165}Ho(γ,γ') reaction in the energy region E_γ=2.2–3.8 MeV observed with a Euroball Cluster detector placed under 130° with respect to the incident beam with an end point energy of 4.8 MeV. Only the strongest transitions assigned to ^{165}Ho are marked with lines; brackets connecting two peaks indicate decay branches to low-lying excited states. Other transitions are due to the calibration standard ^{27}Al or result from background sources (Huxel *et al.*, 1999).

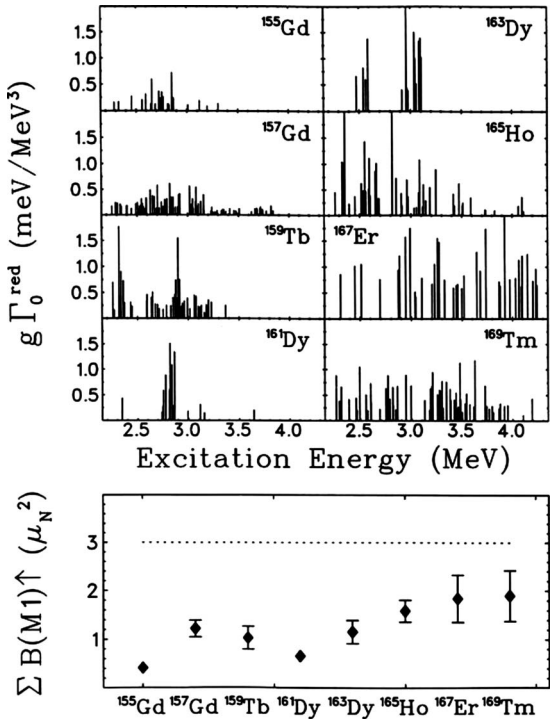

FIG. 37. Comparison of the magnetic dipole strength in the odd-mass rare-earth nuclei (Enders *et al.*, 1997). Upper part: Distribution of reduced ground-state decay widths. Lower part: Summed $B(M1)$ strengths assuming magnetic dipole character of all observed transitions in the energy range between 2.5 and 3.7 MeV. Large differences in total strength, fragmentation, and the number of detected ground-state transitions is observed. Data are from Bauske *et al.* (1993), Margraf *et al.* (1995), Nord *et al.* (1996), Schlegel *et al.* (1996), and Huxel *et al.* (1999).

performed on ^{155}Gd and ^{159}Tb (the latter an odd-proton nucleus), and on the heavier ^{167}Er (Schlegel *et al.*, 1996) and ^{165}Ho, ^{169}Tm (Huxel *et al.*, 1999) nuclei.

Bringing these data together in Fig. 37, one observes that starting from ^{155}Gd, passing over the odd-mass Dy nuclei and progressing toward heavier nuclei, $M1$ strength seemed to become more concentrated, precisely in those regions that were expected from the knowledge of the $M1$ scissors mode strength in the nearby even-even nuclei (Enders *et al.*, 1997). In Fig. 38 the full systematics of the Gd nuclei combining mass-even and -odd isotopes is shown (Kneissl *et al.*, 1996; Nord *et al.*, 1996). Recent experimental data on ^{151,153}Eu, and with increased sensitivity, on ^{163}Dy and ^{165}Ho, have been provided by Nord *et al.* (2003). Conclusions from all these data are (i) the fragmentation pattern is at best rather badly understood and (ii) even worse only about half to one-third of the $M1$ strength observed in the even-even nuclei (when summing the strength in the odd-mass nuclei in the interval 2.5–3.7 MeV) could be detected firmly (see lower part of Fig. 37).

One notable exception is the study of ^{167}Er (Schlegel *et al.*, 1996), where experiments have been carried out with end point energies up to 5.8 MeV at the S-DALINAC. The summed strength reaches $3.49(1.15)\mu_N^2$, a value that is at variance with many of the former experiments by a factor of about 3. This experiment gave a first hint that one needed to look for $M1$ fragments at energies higher than was first thought. As discussed below, the calculated $M1$ strength using the interacting boson-fermion model (Iachello and Van Isacker, 1991) accounts well for this total strength although in the theoretical study only two major peaks are obtained below 4 MeV.

B. Missing strength: Experimental problem and its solution

Comparison between odd-mass and even-even nuclei immediately poses the question: Where has the $M1$ strength gone in the odd-mass nuclei? The search was on for the observation of a large part of $M1$ strength residing in a large number of complex states but with very small $B(M1)$ values and hidden in the background of the spectra. A detailed statistical model analysis of the high-quality data in ^{165}Ho and ^{169}Tm, obtained with an EUROBALL cluster module, indeed revealed that a significant part of the $M1$ strength is carried by the background states (Enders *et al.*, 1997, 1998; Huxel *et al.*, 1999). It has been shown (Enders *et al.*, 1997) that the statistical assumptions underlying the fluctuation analysis approach are also capable to explain the large variations in the measured dipole distributions shown in Fig. 37. Monte Carlo distributions have been generated taking into account the properties of $M1$ and $E1$ distributions in even-even neighboring nuclei and allowing for the energy dependence of the experimental sensitivity

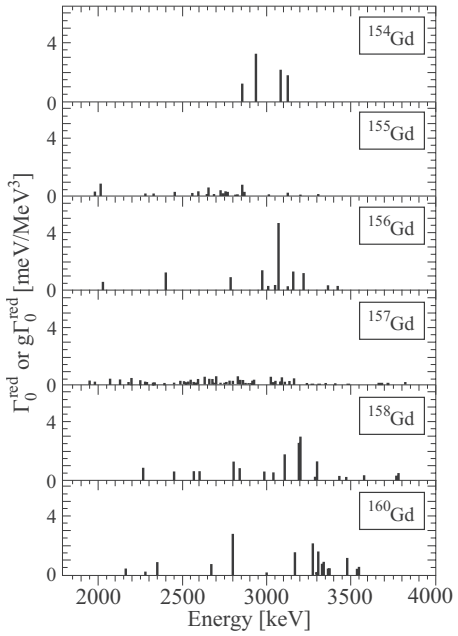

FIG. 38. Ground-state decay width distributions for ^{154,155,156,157,158,160}Gd extracted from photon scattering experiments. For the even-even nuclei all $\Delta K=1$ transitions are shown. In a number of cases, the $M1$ character has been determined by Compton polarimetry. Information from (e,e') form-factor measurements has also been considered. From Nord *et al.*, 1996.

limits. These results are shown in Fig. 39 and compared to the data (Enders *et al.*, 1997; Huxel *et al.*, 1999). Overall, the large variations of the total number of observed levels and the summed dipole strengths can be simultaneously reproduced in a very satisfactory manner.

Subsequent experiments with unrivaled sensitivity confirmed these results for the cases of ^{163}Dy and ^{165}Ho (Nord *et al.*, 2003). The experiments showed a wealth of previously unresolved weak transition as demonstrated

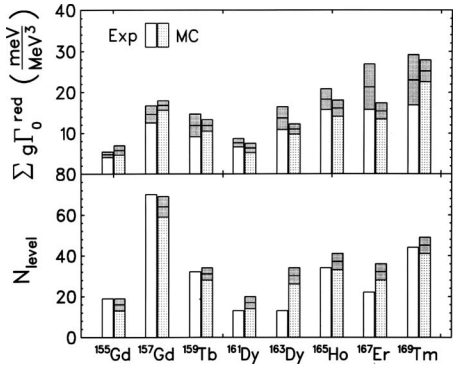

FIG. 39. Number of ground-state dipole transitions and their summed reduced width in deformed odd-mass rare-earth nuclei. Open bars refer to the data. Dotted bars stand for Monte Carlo generated strength distributions based on a statistical approach. Uncertainties of the random spectra have been estimated by 1000-fold repetition of the calculation. Error bars denote a 1σ deviation (Huxel *et al.*, 1999).

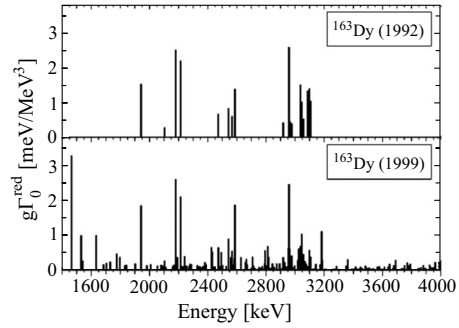

FIG. 40. Ground-state decay width distributions for ^{163}Dy from Bauske *et al.* (1993) and Nord *et al.* (2003). The latter experiment had an order-of-magnitude improved sensitivity. While transition strength agree well for prominent excitations, many previously unresolved weak transitions are visible.

in Fig. 40, where the strength distribution deduced for ^{163}Dy is compared to the first measurement (Bauske *et al.*, 1993). The sum of the reduced dipole strength is roughly doubled. However, the fragmentation pattern into a few rather strong and many very weak transitions in ^{163}Dy seems to be peculiar, since a fluctuation analysis cannot explain the still missing strength. On the other hand, for ^{165}Ho good agreement with previous work (Huxel *et al.*, 1999) was obtained when combining the strength of resolved and unresolved transitions. It may also be noted that a recent NRF measurement on ^{235}U also showed good agreement of the total $M1$ strength deduced from a comparable statistical analysis with that in the even-mass neighbor ^{236}U (Yevetska *et al.*, 2010).

In conclusion for the present-day situation on scissors states and scissors $M1$ strength in odd-mass nuclei one can say that in the deformed odd-mass rare-earth (and probably also actinide) nuclei, the mode seems to be present with a strength expected from the even-even systematics but a significant part—which can change quite importantly from nucleus to nucleus depending on the respective level densities and the photon scattering end point energy—escapes detection in the photon scattering experiments because of the very large fragmentation.

C. Theoretical description

As discussed coupling an odd particle or hole (proton or neutron) to the collective modes of the even-even core nucleus generally results in the observation of core-coupled multiplets (Bohr and Mottelson, 1975). Because of the subsequent fragmentation of $M1$ scissors strength, it is clear that in comparing theoretical results with data at most indications for the total summed $M1$ strength will be the guiding principle to judge the level of agreement.

Within the context of the interacting boson-fermion model (IBFM), a sum rule was derived by Ginocchio and Leviatan (1997) in which they studied the coupling of a single j-shell particle (the unnatural parity orbital in

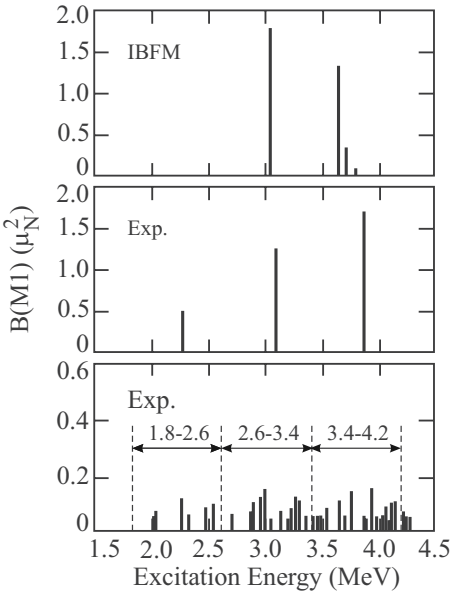

FIG. 41. Theoretical and experimental $M1$ strength distribution in ^{167}Er. Bottom to top: Experimental $M1$ strength distribution, strength distribution summed up in the indicated energy bins, comparison with an IBFM calculation, and expected splitting of the energy spectrum through coupling of the unpaired particle (Schlegel *et al.*, 1996).

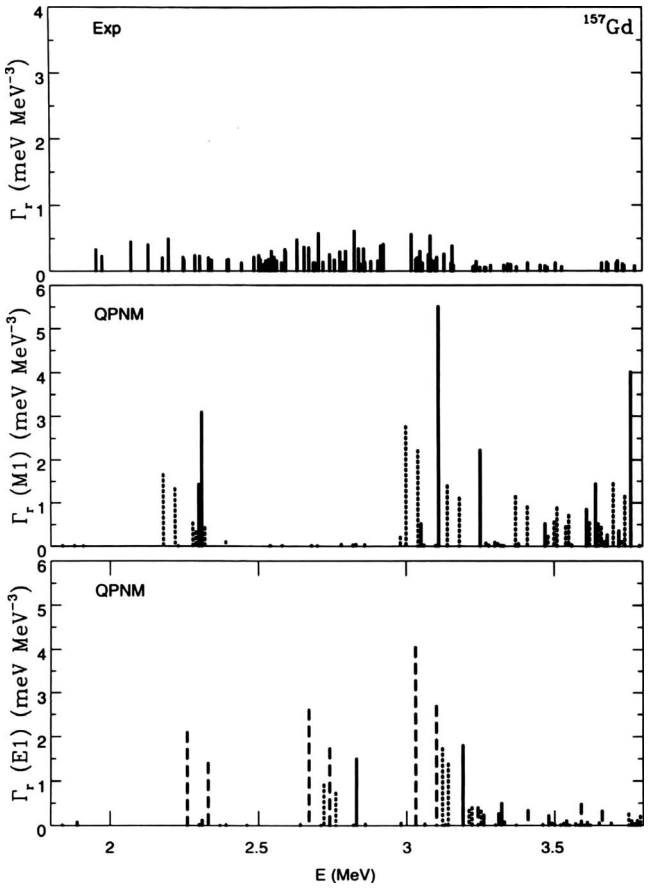

FIG. 42. Experimental and theoretical reduced width distributions. Experimental ground-state reduced width distribution in ^{157}Gd (top), together with the QPNM predictions (Soloviev, 1992) for $M1$ (middle) and $E1$ (bottom) transitions to $K=1/2,3/2,5/2$ final states displayed by full, dashed, and dotted lines, respectively (Soloviev *et al.*, 1997).

fact) to the underlying scissors mode. In the limit of good F spin and large boson number N, the resulting new sum rule has been compared with a similar sum rule derived for even-even nuclei (Ginocchio, 1991; von Neumann-Cosel *et al.*, 1995). These results yield upper limits and in the case of the odd-neutron $1i_{13/2}$ particle coupled to the scissors for the nuclei ^{161}Dy and ^{167}Er as some extremes (see data), it is observed that the theoretical sum rule in ^{167}Er is consistent with the data but for ^{161}Dy definitely largely overestimates them.

A number of interesting results were derived by Van Isacker and Frank (1989) and by Frank *et al.* (1991) using the more general IBFM. Analytical results could still be derived under the assumption of good F spin and considering a single-j shell. Calculations were performed for ^{169}Tm and ^{165}Ho (Huxel *et al.*, 1992). A more detailed study has also been carried out for ^{163}Dy and ^{167}Er. In the case of ^{167}Er, where the $1i_{13/2}$ odd-neutron determines the ground-state structure, this orbital only is considered and again comparisons with summed strengths are possible, as shown in Fig. 41. The multiplet structure resulting from coupling the odd-particle to the scissors excitation always underestimates fragmentation. Within the algebraic formulation, Devi and Kota (1992a, 1992b, 1996) studied group-theoretical reductions for odd-A nuclei now including the g boson. By introducing an extra boson degree of freedom, the effect of fragmentation of course increases.

Microscopic studies in the deformed rare-earth region have also been carried out using the coupling of a 1qp excitation with the underlying collective phonon structure. Calculations have been performed by Raduta and Lo Iudice (1989) and Raduta and Delion (1990) using a coherent-state formalism to describe the collective phonons. A more extensive calculation of this kind also exists for a number of odd-mass nuclei (Soloviev, Sushkov, and Shirikova, 1996, 1997a; Soloviev *et al.*, 1997). In the particular case of ^{157}Gd shown in Fig. 42, the $M1$ strength is localized mainly between 2 and 2.5 and between 3 and 3.7 MeV, clearly overestimating the observed $M1$ strength. The strongest concentration of $M1$ strength is situated near 3 MeV with a subsequent large fragmentation (i) due to the fact that from the $J;K$ ground state, $M1$ excitations are possible into $J+1, J, J-1; K-1$ and $J+1; K+1$ excited states and (ii) the 1qp-phonon coupling mechanism also redistributes strength. The calculations indeed give support to the presence of scissors particle-core coupled configurations in the odd-mass strongly deformed rare-earth nuclei, albeit with a varying character of splitting and further fragmentation over a background of complex microscopic configurations.

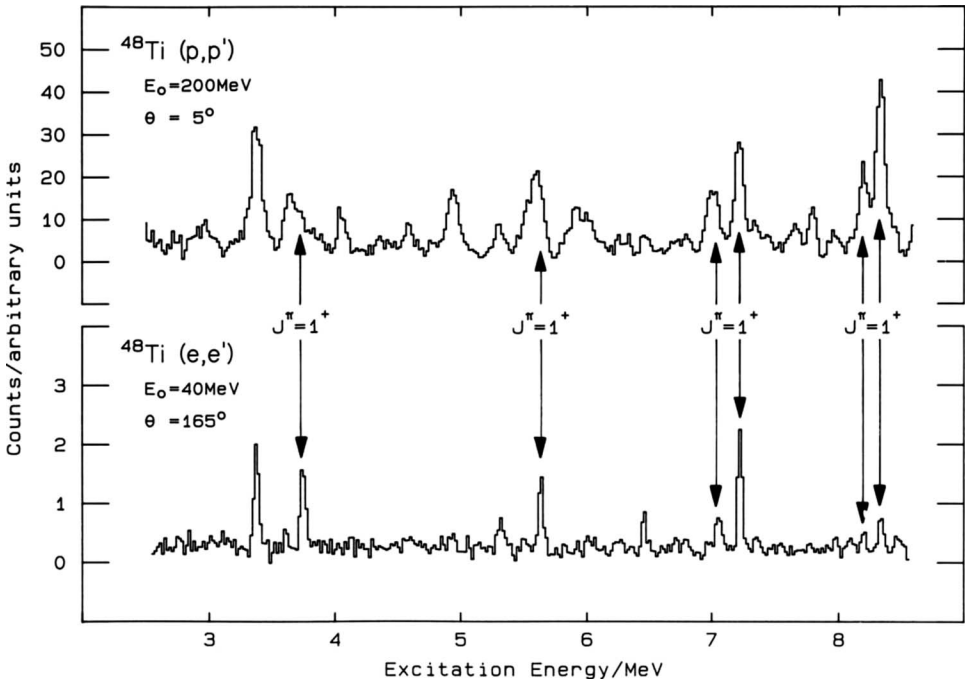

FIG. 43. High-resolution (p,p') and (e,e') spectra in ^{48}Ti. The $J^\pi=1^+$ states are marked by arrows (Richter, 1990).

V. MAGNETIC DIPOLE EXCITATIONS IN LIGHT AND MEDIUM-HEAVY NUCLEI

A. Experimental data

As in heavier nuclei, most experimental information on ground-state isovector magnetic dipole transitions comes from inelastic photon and electron scattering experiments. A particularly interesting technique for the study of even-mass nuclei is electron scattering at 180° (Fagg, 1975) because of the dramatic suppression of the background due to the radiative tail of elastic scattering. If combined with a large-acceptance spectrometer, it represent a powerful tool for the study of the $M1$ response (Lüttge *et al.*, 1995; Lüttge, von Neumann-Cosel, Neumeyer, and Richter, 1996). Data from (γ,γ') in lighter nuclei are limited. Summaries have been provided by Berg and Kneissl (1987) and Raman *et al.* (1991). The most exhaustive studies of $M1$ strength distributions are available from (e,e') data covering all stable nuclides in the p shell, $N=Z$ and $Z+2$ nuclides in the sd shell, the stable Ca isotope chain, the $N=28$ isotones, the open-shell nuclei ^{46,48}Ti, ^{50}Cr, ^{56}Fe, and finally ^{58}Ni.

Complementary information on the spin part of the $M1$ strength stems from inelastic proton-scattering experiments. As an example, in Fig. 43 spectra of the (p,p') and (e,e') reactions off ^{48}Ti under kinematics favoring $M1$ excitations are compared (Richter, 1990). All transitions identified to have $M1$ character (marked by arrows) are seen in both spectra although with different relative intensities due to the interference of orbital and spin strength in the latter reaction. Another case, ^{56}Fe, highlighting the close resemblance of spectra obtained with both probes (Richter, 1994) is shown in Fig. 44. Here all transitions observed above $E_x=6$ MeV possess $M1$ character and represent the spin-$M1$ Gamow-Teller resonance. At lower excitation energies mostly 2^+ states are populated except for the prominent transition seen in the (e,e') spectrum at about 3.5 MeV, which again carries most of the orbital $M1$ strength.

B. Theoretical description: The shell model and random phase approximation

Contrary to the problems encountered to describe the magnetic dipole excitation modes in strongly deformed heavy nuclei within a shell-model framework, for the

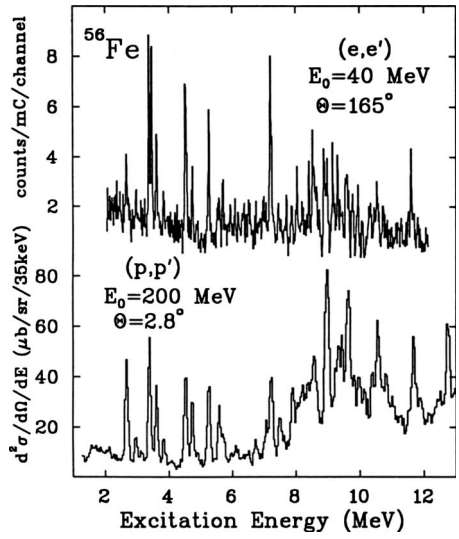

FIG. 44. High-resolution inelastic electron and proton-scattering spectra in ^{56}Fe measured at TRIUMF. Lines above 6 MeV correspond to the excitation of $J^\pi=1^+$ states under the kinematic conditions of the two experiments (Richter, 1994).

light nuclei large-scale shell-model calculations have been performed and used to study $M1$ excitation properties in detail. Concentrating on mixed-symmetry states, Zamick and co-workers studied such excitations for nuclei in the $1f_{7/2}$ shell-model region (Zamick, 1985, 1986a, 1986b; Liu and Zamick, 1987a, 1987b, 1987c). We treat ^{48}Ti with two proton particles and two neutron holes outside of the closed shell nucleus ^{48}Ca as an example (analogous arguments hold for other nearby nuclei). The wave functions within the $1f_{7/2}$ model space solely are expanded as

$$\Psi(J^\pi) = \sum_{L_p,L_n} D_J(L_p,L_n)|(1f_{7/2})^2_{L_p},(1f_{7/2})^{-2}_{L_n};JM\rangle, \quad (31)$$

in which the notation is self-explanatory and where the coefficients $D_J(L_p,L_n)$ denote the amplitudes that the two protons couple to L_p and the two neutron holes to L_n. The $M1$ operator now induces transitions from the 0^+ ground state into the 1^+ states with a corresponding $B(M1)$ value of

$$B(M1) = \frac{3}{4\pi}(g_j^\pi - g_j^\nu)^2 \left| \sum_L D_0(L,L) D_1(L,L) \right|^2 \times L(L+1)\mu_N^2, \quad (32)$$

in which g_j^π and g_j^ν are the conventional single-particle gyromagnetic factors $g_j^\rho = [(2j-1)g_l^\rho + g_s^\rho]/2j$ and $g_j^\rho = [(2j+3)g_l^\rho - g_s^\rho]/2(j+1)$ for $j = l+\frac{1}{2}$ and $l-\frac{1}{2}$, respectively, and $\rho = \pi, \nu$ (Brussaard and Glaudemans, 1977). One can derive a sum rule for the strength into all possible final 1^+ states

$$\sum B(M1) = \frac{3}{4\pi}(g_j^\pi - g_j^\nu)^2 \left| \sum_L D_0(L,L) \right|^2 L(L+1)\mu_N^2. \quad (33)$$

For the case of ^{48}Ti the mixed-symmetric 2^+ state results from the mixed-symmetric combination of the $L_p = 0$, $L_n = 2$ and $L_p = 2$, $L_n = 0$ components, whereas the 1^+ scissors counterpart originates from the combinations $L_p = 2$, $L_n = 2$; $L_p = 4$, $L_n = 4$, etc. While the use of a single $1f_{7/2}$ orbital keeps the $M1$ strength concentrated in a single strong excitation, gradually increasing the shell-model space with the inclusion of the $1f_{5/2}$, $2p_{3/2}$, and $2p_{1/2}$ orbitals opens the way into many new states and fragmentation starts to set in, as shown in Fig. 45 (Liu and Zamick, 1987c). One notices that the low-lying $J^\pi = 1^+$ state is always well separated from the other 1^+ states at higher excitation energy. It is mainly of orbital nature and can be associated with an experimental state at $E_x = 3.74$ MeV which carries a strength of $B(M1)\uparrow = 0.52(8)\ \mu_N^2$ (Guhr *et al.*, 1990). We also emphasize that within this single $1f_{7/2}$ shell-model space, the orbital $M1$ strength is a measure of dynamical quadrupole correlations in the ground state since it depends on the $(2_p^+ 2_n^+)$ configuration admixture in the ground state.

An important issue in the study of scissors mode excitations in the open-shell nuclei situated in the Ti, Cr, Fe region is the orbital-to-spin ratio for the low-lying 1^+ states. In contrast to heavy nuclei, only a few orbitals determine the structure of the wave functions and, therefore, a non-negligible spin contribution will be present, even in the lowest 1^+ state. This can be studied by comparing (e,e') and (p,p') experiments (cf. Figs. 43 and 44). However, a quantitative analysis of the (p,p') data is hampered by the dependence of the extracted spin-$M1$ strengths on the choice of the effective projectile target interaction, which can lead to variations up to about 40% (Hofmann *et al.*, 2007).

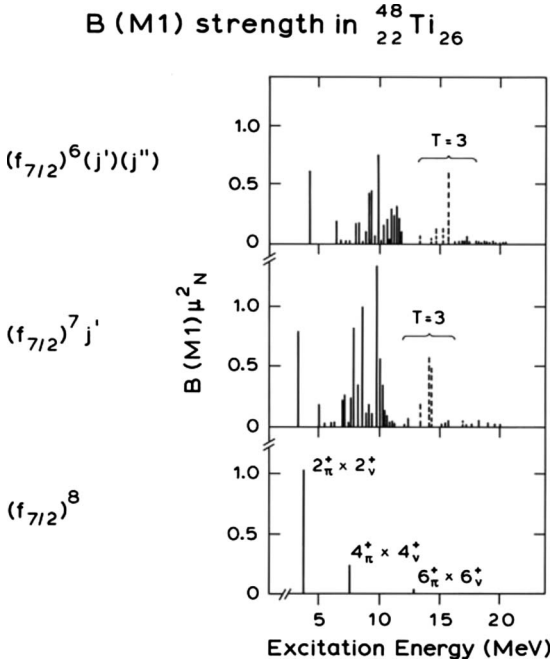

FIG. 45. Magnetic dipole strength distributions for ^{48}Ti as calculated for the model spaces given on the lhs of the figure. From Liu and Zamick, 1987c.

Thus, it is important to find other means to disentangle the spin and orbital parts. Abdelaziz and Elliott (1987) discussed that the GT matrix element in β decay might be used to estimate the spin contribution to a collective isovector $M1$ transition. Such matrix elements can also be measured in charge-exchange reactions populating analog states in the odd-odd neighboring nuclei. A wealth of high-resolution data on the GT strength distributions has recently become available (Frekers, 2006; Fujita *et al.*, 2008) and the dependence on the effective projectile-target interaction in hadronic reactions can partly be circumvented by normalizing to β-decay results. However, isospin selection rules limit the applicability to special cases (some of which are discussed below). Electron scattering form factors present another method to derive bounds on the relative importance of orbital versus spin magnetism in a number of transitions. In Fig. 46 we show two form factors in ^{48}Ti for transitions to the 3.74 and 7.22 MeV 1^+ states (Guhr *et al.*, 1990). Whereas the first transition seems to proceed through the $1f_{7/2}$ orbital only (recoupling), the second transition is consistent with a spin-flip transition $1f_{7/2} \rightarrow 1f_{5/2}$.

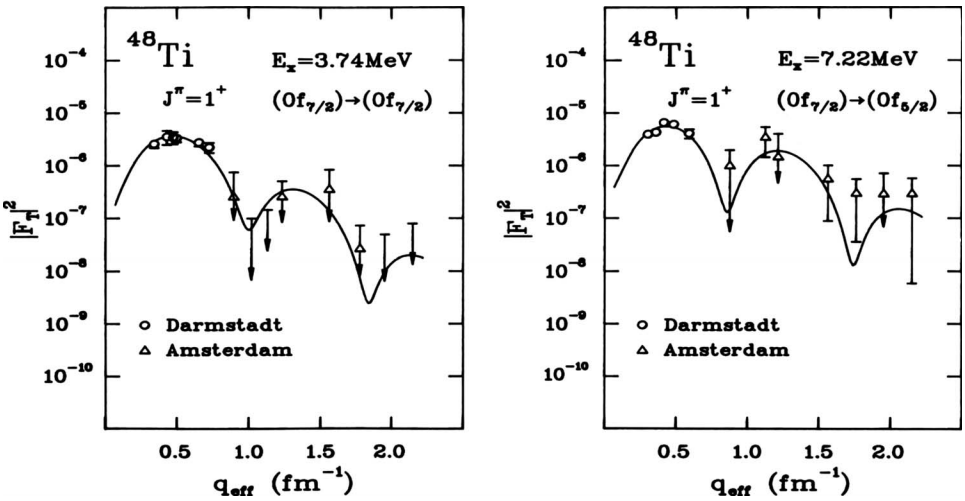

FIG. 46. Inelastic electron scattering form factors for a predominantly orbital (left-hand side) and predominantly spin-flip (right-hand side) $M1$ transition (Richter, 1990).

A systematic study of the orbital-to-spin ratio was carried out by Oda, Himo, and Muto (1987) in which a dependence on both the model space and the use of effective g factors was explored. The result is that including excitations from the $1f_{7/2}$ orbital into the higher-lying $1f_{5/2}$, $2p_{3/2}$, $2p_{1/2}$ orbitals increases the orbital part over the spin part in a systematic way for a number of Ti, Cr, and Fe isotopes. Moreover, quenching the g factors from the free-nucleon values further reduces the spin strength and reinforces the model space extension. The latter result was also derived independently by Heyde and Sau (1984); see also Heyde (1989). Studies of the $M1$ response for the light Ti nuclei have been carried out using the QRPA approach with similar results and conclusions concerning the orbital-to-spin ratio (Nojarov *et al.*, 1987, 1991; Faessler and Nojarov, 1988; Faessler *et al.*, 1989).

Truncations of the large-scale shell-model space and choosing a specific proton-neutron force, on the other hand, may lead to a symmetry-based approach to study $M1$ properties. For light nuclei, the SU(3) shell model has been used and applied to both *sd*- and *fp*-shell nuclei (Chaves and Poves, 1986; Poves *et al.*, 1989; Retamosa *et al.*, 1990). Comparison of shell-model and IBM calculations was performed for the light Sc, Ti, and V *fp*-shell nuclei (Abdelaziz *et al.*, 1988). A particular symmetry-dictated truncation to realistic shell-model calculations, emphasizing the importance of S, D, and G pairs, was used for ^{54,56}Cr and $^{56-60}$Fe (Halse, 1990, 1991b). Moreover, a pseudo-SU(3) model was suggested to describe rotational properties in this mass region (Halse, 1991a).

Recent computational progress allows shell-model studies of the $M1$ strength in large model spaces to describe details of the fragmentation of the mode. For example, unrestricted calculations in the full *fp* model space are possible now for ^{46,48}Ti (Fearick *et al.*, 2006). As an example of the state of the art, a study of the stable $N=28$ isotones ^{48}Ca, ^{50}Ti, ^{52}Cr, and ^{54}Fe (Langanke *et al.*, 2004) is discussed, whose experimental $M1$ strength distributions have been measured (Steffen *et al.*, 1980; Sober *et al.*, 1985). In Fig. 47, the results for ^{52}Cr are shown together with calculations based on two widely used shell-model interactions called KB3G (Poves *et al.*, 2001) and GXPF1 (Honma *et al.*, 2004) derived in a G-matrix approach from nucleon-nucleon interaction potentials. Because of the $N=28$ shell closure a spherical ground state can be expected. Correspondingly, no low-lying orbital transitions are observed. In the energy region above 6 MeV, shown in Fig. 47, a resonance structure arising from spin-flip transitions is visible. The shell-model results are quite successful in reproducing the features of the strength distribution qualitatively and also quantitatively when analyzing the resonance centroid and total strength, but in detail differences remain.

The comparison made in Fig. 47 raises an important and nontrivial question: How can one quantify the degree of correspondence between data and calculation? One possible way may be the extraction of scales char-

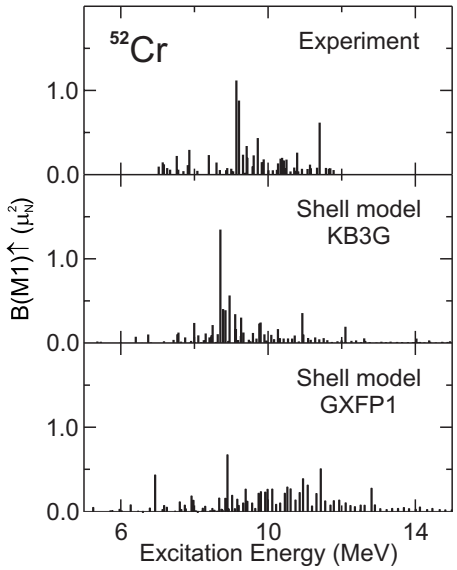

FIG. 47. $M1$ strength distribution in ^{52}Cr from (top to bottom) high-resolution (e,e') experiments (Sober *et al.*, 1985) and large-scale shell-model calculations using the KB3G (Poves *et al.*, 2001) and GXPF1 (Honma *et al.*, 2004) interactions, respectively.

acterizing the fine structure of the mode by means of a wavelet analysis (Shevchenko *et al.*, 2008). Fine structure has been shown to be a global phenomenon of giant resonances (Shevchenko *et al.*, 2004, 2009; Kalmykov *et al.*, 2006). Recent application of this method to $M1$ strength distributions in fp-shell nuclei (Petermann *et al.*, 2010) indeed reveals considerable differences in the characteristic scales extracted from the $M1$ strength functions obtained with different effective interactions including those shown in Fig. 47, and in the case of ^{52}Cr the results from the KB3G calculation are found to be closer to the data.

The capability of large-scale shell-model calculations to describe the interference of spin and orbital parts has been investigated in a detailed study of the electron scattering form factor of the prominent $M1$ transition at E_x=3.449 MeV in ^{56}Fe, which contains spin and orbital matrix elements of comparable size (Fearick *et al.*, 2003). While different effective shell-model interactions describe the strength reasonably well, the predicted q dependence differs considerably. Clearly, the spin-orbit interplay remains a challenge to shell-model studies even in very large model spaces.

It also became clear in the above studies that a reduction of the g factors from the free-nucleon values is generally increasing the orbital-to-spin matrix element ratio. An independent approach to understand the g-factor quenching has been carried out in this region of medium-heavy and light nuclei, concentrating on the comprehensively studied N=28 nuclei. Shell-model calculations require in all cases a reduction in the spin part of the magnetic dipole operator. A consistent description for the stable N=28 isotones can be reached using a value $g_s^{\rm eff}=0.75(2)g_s^{\rm free}$ (von Neumann-Cosel *et al.*, 1998). The required reduction is remarkably close to the quenching factor 0.744(15) obtained from a recent shell-model analysis of GT β-decay transitions in the lower fp-shell region (Martínez-Pinedo *et al.*, 1996). Indeed, the most important mechanism responsible for the quenching is, viz., the mixing with two-particle two-hole configurations at high excitation energies, expected to be the same as in the GT case (Bertsch and Hamamoto, 1982; Ichimura *et al.*, 2006).

C. Some astrophysical implications

Knowledge of the magnetic dipole strength in fp-shell nuclei is also crucial in supernova modeling. It permits one to determine cross sections of inelastic neutrino-nucleus scattering, a process whose importance for supernova dynamics was recognized only recently (Hix *et al.*, 2003). Under the conditions of a supernova type II in massive stars, neutrino-nucleus reactions are dominated by GT transitions (Langanke and Martínez-Pinedo, 2003). The description of inelastic scattering processes requires knowledge of the $T_0 \rightarrow T_0$ isospin component of the GT strengths, where T_0 denotes the ground-state isospin. Except for an overall factor relating the weak and electromagnetic interaction this is nothing but the spin part of the $M1$ strength. Orbital strength is negligible in the stable N=28 isotones due to the shell closure; thus, the measured $M1$ distribution represents to a good approximation the needed GT_0 strength. Figure 48 shows differential cross sections of inelastic neutrino scattering on ^{52}Cr calculated under this assumption for two typical neutrino energies E_ν=15 and 25 MeV (solid line).

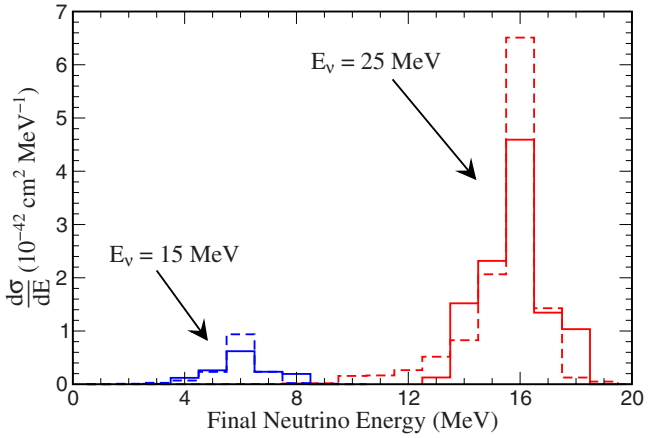

FIG. 48. (Color online) Differential inelastic neutrino cross sections for ^{52}Cr and initial neutrino energies E_ν=15 and 25 MeV. The solid histograms are obtained from the $M1$ data, the dashed ones from shell-model calculations. The bumps represent the GT_0 strength shifted by the centroid energy of the resonance. The final neutrino energies are given by $E_f = E_\nu - E_x$ (Langanke *et al.*, 2004).

Since the reaction network calculations in a supernova require information on the GT_0 strength in many nuclei, one has to rely on model calculations. The set of highly precise data in the N=28 isotones (Sober *et al.*, 1985) was used to demonstrate the capability of large-scale shell-model calculations to describe $M1$ strength distributions (Langanke *et al.*, 2004). If applied to the present problem, differential neutrino scattering cross sections shown by the dashed line in Fig. 48 result. These are indeed in good agreement with the data, and it was concluded that present-day shell-model calculations can provide the necessary GT_0 strengths needed as input to the supernova simulations. Inclusion of inelastic neutrino-nucleus scattering increases the neutrino opacities noticeably and strongly reduces the high-energy tail of the neutrino spectrum emitted in the neutrino burst at shock breakout. Relatedly, the expected event rates for the observation of such neutrinos by earthbound detectors are reduced by up to about 60% (Langanke *et al.*, 2008).

D. Selected problems in light and medium-heavy nuclei

In light nuclei, magnetic dipole transitions have been measured in almost all stable nuclei and detailed theoretical studies (mostly shell model) have been performed. We do not attempt an exhaustive discussion of these results. Rather, we highlight a few topics accessible

only in light nuclei or extending beyond the range of physics questions discussed so far.

1. Quenching of the spin $M1$ strength: The case of ^{48}Ca

A classical example of a clear-cut isovector $M1$ transition with a remarkably large transition strength $B(M1)\uparrow = 3.9(3)\mu_N^2$ was found in ^{48}Ca in electron scattering experiments (Steffen *et al.*, 1980). It was interpreted as a rather pure neutron $1f_{7/2} \rightarrow 1f_{5/2}$ excitation (Richter, 1985). The (e,e') form factor of this transition serves as a another prime example to study the problem of quenching of the spin part of the isovector $M1$ response. Since GT and $M1$ strengths are quenched by comparable amounts, one can expect that the responsible processes are the same. Two major mechanisms are expected to contribute (Ericson and Weise, 1988). On the one hand, a polarization of the nuclear core by the nucleon undergoing a spin-isospin transition occurs, which leads to a virtual excitation of high-lying states by the tensor force in second order; hence it is named second-order core polarization. Alternatively, the GT and $M1$ operators are modified by virtual Δ-hole excitations, analogous to the Lorenz-Lorentz correction in dielectrics (Delorme *et al.*, 1976). Both mechanisms lead to different redistributions of the strength. Thus, by measuring the response up to high excitation energies, the former mechanism was shown to dominate for GT transitions (Ichimura *et al.*, 2006). The study of the (e,e') form factor permits one to delineate the contributions in the case of the $M1$ response (Richter, 1991). The most refined calculations (Takayanagi *et al.*, 1988), although still not able to fully explain the amount of quenching, confirm the dominant role of core polarization leading to mixing with $2p$-$2h$ states over the Δ-hole part, which contributes about 10% to the strength reduction. This value is in agreement with an analysis of the Δ-hole contributions to the quenching of GT strength (Ichimura *et al.*, 2006).

2. Cross-shell transitions in ^{36,38,40}Ar

Magnetic dipole strength distributions in ^{36}Ar and ^{38}Ar deduced from electron scattering experiments (Foltz *et al.*, 1994) reveal marked differences. Calculations in a $0\hbar\omega$ model space (sd shell) with a phenomenological interaction, generally successful in the description of $M1$ and GT strengths (Brown and Wildenthal, 1988), work well for ^{36}Ar (with a closed neutron sd shell) but fail completely for ^{38}Ar (with two neutrons in the fp shell), indicating the importance of $sd \rightarrow fp$ cross-shell contributions. This problem was recently studied by Lisetskiy *et al.* (2007) based on an effective interaction including the coupling of sd to the $1f_{7/2}2p_{3/2}$ orbitals (Caurier *et al.*, 2001). Such cross-shell calculations present a limit of present-day computational capabilities and still require a significant truncation of the model space. The first results support the importance of an inclusion of cross-shell transitions and make specific predictions for the even more neutron-rich ^{40}Ar. Some information on $M1$ strength in ^{40}Ar has recently been reported (Li *et al.*, 2006), but a measurement of the full $M1$ strength distribution would be important.

3. l-forbidden transitions

In sd-shell nuclei, an effective shell-model $M1$ operator has been determined by an empirical fit to the large body of data on magnetic and $M1$ transitions (Brown and Wildenthal, 1987). The deviations from the bare operator are incorporated in correction factors for the spin and orbital parts and an induced-tensor term. Microscopic calculations (Arima *et al.*, 1987; Towner, 1987) are in good agreement except for an isovector tensor correction. Tensor corrections are generally weak and therefore buried in the dominant spin strength for most $M1$ transitions. However, experimental information on the tensor correction terms can be obtained from l-forbidden transitions ($1d_{3/2} \leftrightarrow 2s_{1/2}$ in the sd shell). The term "l forbidden" refers to a selection rule for the one-body operator of $M1$ or GT transitions which does not allow a change of the orbital quantum number. The higher-order corrections to the l-forbidden transitions are theoretically expected to be dominated by Δ resonance admixtures into the nuclear wave functions (Arima *et al.*, 1987; Towner, 1987) and they are a unique observable in this respect. The problem has been studied extensively in $1d_{3/2} \rightarrow 2s_{1/2}$ single-hole transitions in $A = 39$ nuclei. One finds an order of magnitude larger $M1$ strength (Grundey *et al.*, 1981) relative to the GT strength (Hagberg *et al.*, 1994), while the microscopic results predict the tensor correction governing the strength to be the same. However, the interpretation could be blurred by weak cross-shell admixtures of the type discussed in Sec. V.D.2. Therefore, data away from the end of the sd shell are important. One such example is an (e,e') study of the l-forbidden transition to the 1^+ state in ^{32}S at $E_x = 7.003$ MeV (Reitz *et al.*, 1999). The form factor exhibits an anomalous momentum-transfer dependence compared to allowed $M1$ transitions because its finite strength results from higher-order terms only. The shell-model analysis reconfirms the discrepancy between empirical and microscopic approaches to determine the tensor correction, and the problem remains unresolved so far.

Of course, l-forbidden transitions are not restricted to the case $1d_{3/2} \leftrightarrow 2s_{1/2}$ but can appear between all pairs of shell-model orbitals with quantum numbers $(n,l,j=l+1/2)$ and $(n-1,l+2,j'=(l+2)-1/2)$, where n is the radial quantum number, and l and j are the orbital and total angular momenta. Experimentally, the single-particle energies of corresponding pairs of states show a near degeneracy in many nuclei. This led to the concept of pseudospin symmetry, where the doublet structure is expressed in terms of a "pseudo"-orbital angular momentum $\tilde{l} = l+1$, in which the two levels represent spin-orbit partners with a "pseudo"-spin $\tilde{s} = 1/2$. While pseudospin symmetry was empirically established 40 years ago (Arima *et al.*, 1969; Hecht and Adler, 1969), a deeper understanding has been lacking. Relativistic corrections

(Bohr and Mottelson, 1969) have been suggested as a possible source and applied with some success to describe magnetic moments of pseudospin partners near the $N=82$ shell closure (Heyde *et al.*, 1977). Recently, pseudospin symmetry has been interpreted as a relativistic SU(2) symmetry of the Dirac Hamiltonian which occurs when the attractive scalar and repulsive vector nuclear mean fields cancel (Ginocchio, 2005). Evaluating this concept, Ginocchio (1999) derived a relation between the magnetic moments of the pseudospin partners and the strength of the l-forbidden $M1$ transition between them. Application to data near a variety of magic numbers reveals overall good correspondence with a few marked deviations (von Neumann-Cosel and Ginocchio, 2000).

4. Enhancement of magnetic dipole strength by meson exchange currents

Direct signatures of mesonic exchange currents (MECs) in experimental observables are usually restricted to few-body nuclear systems (Ericson and Weise, 1988) with the exception of magnetic dipole properties (moments and transition strengths) as discussed previously. One such example is discussed here. It is well established in sd-shell nuclei that full $0\hbar\omega$ shell-model calculations with an effective operator are able to describe the $M1$ and GT matrix elements (Arima *et al.*, 1987; Brown and Wildenthal, 1987; Towner, 1987). In self-conjugate even-even nuclei with ground-state spin and isospin $J;T=0^+;0$ the set of final states populated by isovector $M1$, GT_-, and GT_+ transitions forms a triplet of isobaric analog states. Their transition strengths are directly related, if spin-orbital interference effects are negligible. This is certainly not the case for individual transitions but holds on the level of 10% when studying full strength distributions of sd-shell nuclei (Hino *et al.*, 1988) because of the sign variations of the mixing term.

When comparing $M1$ and GT strength distributions in ^{24}Mg, excellent agreement of the GT strengths among each other and with the shell model result. However, the same calculations significantly underpredict the $M1$ strength. Such an enhancement of the experimental $M1$ strength can be traced back (Richter *et al.*, 1990) to MEC contributions. To make this clear it is convenient to describe the $M1$ and GT strengths in the following form:

$$B(M1) = C[M_\sigma + M_l + M_\Delta + M_V^{\mathrm{MEC}}]^2, \tag{34}$$

$$B(GT) = [M_\sigma + M_\Delta + M_A^{\mathrm{MEC}}]^2. \tag{35}$$

Here M_l and M_σ are the orbital and spin matrix elements, and M_Δ is the contribution of Δ-isobar admixtures to the strength. The numerical factor C in Eq. (34) equals to 2.643 μ_N^2 using free nucleon g factors. Neglecting the orbital part, the main difference between $M1$ and GT excitations lies in the MEC contributions, which are of vector type for the former and of axial-vector type for the latter. Since axial-vector currents are strongly suppressed because of the conservation of G parity (Towner, 1987), deviations of the ratio $R(M1/GT) = \Sigma B(M1)/2.643\Sigma B(\mathrm{GT})$ from unity point toward an enhancement of the $M1$ strength by vector-type MEC contributions. Besides ^{24}Mg, a clear enhancement was also observed in ^{28}Si (Lüttge, von Neumann-Cosel, Neumeyer, Rangacharyulu, *et al.*, 1996; von Neumann-Cosel *et al.*, 1997). In ^{32}S the situation is less clear (Hofmann *et al.*, 2002) because (e,e') form factors indicate significant orbital admixtures in some of the strongest transitions, and the experimental information on the $M1$ strength distribution is limited to an excitation energy of 12 MeV and therefore incomplete. Another problem noted in Richter *et al.* (1990) was that spin-$M1$ strengths in self-conjugate sd-shell nuclei deduced from forward-angle (p,p') data (Crawley *et al.*, 1982) are systematically about 20% larger than the corresponding GT± strengths. However, this discrepancy can probably be resolved utilizing the latest experimental developments allowing true 0° measurements combined with high energy resolution (Tamii *et al.*, 2009).

5. Isoscalar and isovector $M1$ transitions in ^{12}C and isospin mixing

Isospin is an approximate symmetry in nuclei broken by the long-range Coulomb force and also by small charge-dependent components of the nuclear interaction. In light nuclei, Coulomb effects are weak and excited states possess a well defined isospin quantum number T experimentally known in many cases. This allows one to study isospin mixing between states of the same J^π but different T. Evidence for isospin mixing beyond the Coulomb force has been claimed from the observation of very large isospin mixing matrix elements but later it was realized that the predictions exhibit a strong dependence on the poorly known radial wave functions of the involved single-particle states (Auerbach, 1983).

A unique testing ground are the $M1$ transitions to the pair of $J^\pi;T=1^+;0$ and $J^\pi;T=1^+;1$ states in ^{12}C at 12.71 and 15.11 MeV, respectively. These are of $1p_{3/2}\rightarrow 1p_{1/2}$ spin-flip character. Form factors of both transitions (albeit weak for the isoscalar case) at low momentum transfer have been measured with high precision in inelastic electron scattering (von Neumann-Cosel *et al.*, 2000). Analysis in a two-state model determines not only the mixing amplitudes but also the relative sign through the q dependence of the form factors. The resulting Coulomb matrix element $\langle H_c\rangle = 118(8)$ keV, determined with unequaled precision, is large but can be fully explained by Coulomb mixing (Harney *et al.*, 1986).

VI. ISOVECTOR MAGNETIC DIPOLE TRANSITIONS IN VIBRATIONAL NUCLEI

A. Introduction

In most of this review we have concentrated on the magnetic dipole orbital and spin response in stable, deformed nuclei, which has been studied using both elec-

tromagnetic and hadronic scattering off the nuclear ground state (Sec. I.B). In particular, the scissors 1^+ mode was shown to be excited with a summed strength that scales with the square of the nuclear deformation. Therefore, with decreasing deformation entering the region near closed shells, the scissors mode as well as a stable intrinsic quadrupole deformation will cease to be formed. This mass region is characterized by small amplitude quadrupole vibrational oscillations as the major degree of freedom, with typical $B(E2;2_1^+\rightarrow 0_1^+)$ strength of the order a few tens of Weisskopf units (W.u.). The low-energy nuclear structure properties result in a first excited 2_1^+ phonon excitation which is an in phase motion (or symmetric mode) in the proton and neutron collective motion, also called isoscalar (IS) mode. Multiphonon states can then be constructed, as shown in Fig. 3, in which the proton and neutron motion combines into symmetric (or IS) excitations. However, multiphonon states can also arise rise from proton and neutron motion combining into nonsymmetric (or IV) excitations. Besides the 1^+ states, which is the counterpart of the scissors mode in the vibrational nuclei, also 0^+, 2^+, 3^+, 4^+, states result.

The appearance of IV proton-neutron excitations has been proposed in the context of the IBM-2 (Arima *et al.*, 1977; Iachello, 1984; Otsuka and Ginocchio, 1985; Iachello and Arima, 1987). This approach points out that the isovector excitations appear in a natural way by combining the lowest-lying proton and neutron 2_1^+ d-boson configurations (Iachello, 1984; Van Isacker *et al.*, 1986) into states of mixed-symmetry (MS) character (Iachello, 1984). Besides, the shell model constitutes a microscopic framework in order to describe excitations that are nonsymmetric in its proton and neutron coordinates (Heyde and Sau, 1986; Lisetskiy *et al.*, 2000; Boelaert, Smirnova, *et al.*, 2007; Holt *et al.*, 2007). Moreover, it is possible to describe isoscalar and isovector excitations within the framework of a quasiparticle-phonon model which defines RPA phonons and then to construct states in a basis of one-, two-, and three-phonon components. Since this approach has a microscopic (QRPA) underpinning, it allows one to bridge the gap between a fully microscopic shell-model approach and the algebraic IBM-2 (Lo Iudice and Stoyanov, 2000, 2002, 2004, 2006; Lo Iudice *et al.*, 2009, 2008).

In order to locate these mixed-symmetry (MS) states, one can use the particular structure of the $M1$ and $E2$ operators. We have shown that the $M1$ magnetic dipole operator can be separated into its isoscalar and isovector parts (see Sec. III.B.1). In view of the structure of the isovector part, one expects strong magnetic dipole transitions in the decay of the mixed-symmetry states into the low-lying symmetric states. Likewise, one can separate the electric quadrupole operator $T(E2)$

$$T(E2) = e_\pi \sum_{i=1}^{Z} r_{i,\pi}^2 Y_2(\hat{r}_{i,\pi}) + e_\nu \sum_{i=Z+1}^{A} r_{i,\nu}^2 Y_2(\hat{r}_{i,\nu}), \qquad (36)$$

with e_π and e_ν the proton and neutron effective charges into an isoscalar and isovector part

$$T(E2) = \frac{e_\pi + e_\nu}{2} T(E2,\mathrm{IS}) + \frac{e_\pi - e_\nu}{2} T(E2,\mathrm{IV}). \qquad (37)$$

Here $T(E2,\mathrm{IS})$ and $T(E2,\mathrm{IV})$ are the symmetric and antisymmetric combinations of the proton and neutron parts of the $E2$ operator. Because of the specific symmetry character of the IS and IV excitations, strong $E2$ transitions are expected between S and MS states, separately, but rather weak $E2$ transitions from MS to S states. These characteristics are highlighted in Fig. 3.

In view of the above discussion, the key signature, in order to assign mixed-symmetry character to a state, derives from the $E2$ and $M1$ decay properties: (i) strong $M1$ transitions [$B(M1)$ of the order of $\simeq 1\ \mu_N^2$] to low-lying symmetric states restricting to transitions between states with equal number of phonons mainly, (ii) weak collective $E2$ transitions (with transition probabilities about 10% of the strong $E2$ transitions such as $2_1^+\rightarrow 0_1^+$) to low-lying symmetric states, and (iii) strong collective $E2$ transitions among the MS states themselves.

B. Experimental results and theoretical description

From an experimental point of view, the study of MS states in nuclei of vibrational and transitional structure is rather different from the mapping of scissors mode 1^+ excitations in deformed nuclei. In the latter case (see Sec. I.B), electron, photon, and hadron scattering starting from the 0^+ ground state in deformed nuclei allowed to determine orbital and spin-flip $M1$ strength. In the present situation, the identifying elements are both a strong $M1$ transition into the isoscalar (mostly the 2_1^+ state) state accompanied by a weak $E2$ transition into the 0^+ ground state [with a magnitude of the order of a few % of the $B(E2;2_1^+\rightarrow 0_1^+)$ reduced transition probability]. Thus, in order to obtain a unique characterization of the mixed-symmetry states, different types of experiments have to be carried out and combined. Typical experiments will need to probe the lifetime of a given level, the determination of J^π values, γ-decay branching ratios and the $\delta(E2/M1)$ mixing ratios and this for as complete a set of states with given J^π value. Classical γ-ray spectroscopic methods have to be used extensively as well photon-scattering experiments as, e.g., γ decay following β decay that populates levels in nuclei under study. Determining the nuclear lifetimes needs typically the study of Doppler-shifted attenuation techniques (DSAM) in $(n,n'\gamma)$, light-ion induced reactions, and Coulomb excitation in inverse kinematics. Direct excitation as used in electron scattering, photon scattering, and Coulomb excitation on stable nuclei gives rise to lifetimes in a rather straightforward way. A detailed review of these techniques was presented by Kneissl *et al.* (2006) and Pietralla, von Brentano, and Lisetsky (2008).

1. The $Z\sim 40$, $N\sim 50$ mass region

The nucleus ^{94}Mo forms a particularly suitable test case of the above schematic picture because it has four

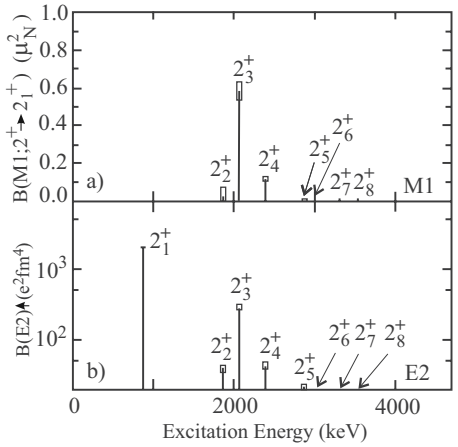

FIG. 49. Measured $E2$ and $M1$ strengths in order to identify the $2^+_{1,ms}$ state in ^{94}Mo. (a) $B(M1;2^+\rightarrow 2^+_1)$ values for the seven lowest-lying identified nonyrast 2^+ states. (b) Corresponding $B(E2;0^+_1\rightarrow 2^+_i)$ values. The error bars are displayed as boxes. From Fransen *et al.*, 2003.

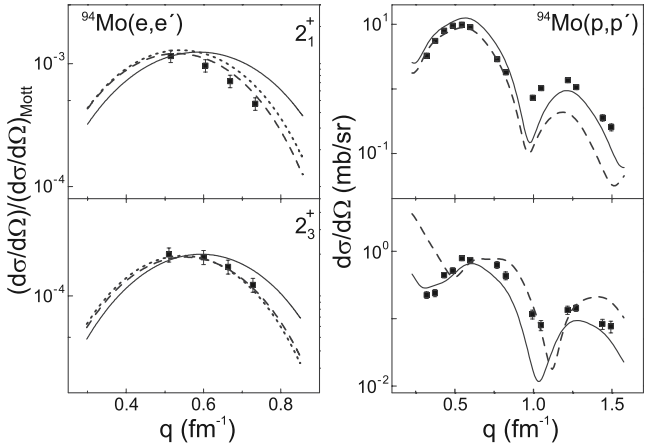

FIG. 50. Inelastic electron and proton scattering off ^{94}Mo. Momentum-transfer dependence of the symmetric (2^+_1, upper part) and mixed-symmetric (2^+_3, lower part) one-phonon excitation cross sections in ^{94}Mo in inelastic electron (left side) and proton (right side) scattering. The data (full squares) are compared to QPM (solid lines), shell-model (dashed lines), and IBM-2 (dotted lines) predictions (Burda *et al.*, 2007).

protons outside of the $Z=38$ subshell closure and two neutrons outside of the $N=50$ closed shell. With these building blocks, ideal conditions show up to form both symmetric and antisymmetric couplings of these pairs. Detailed experimental studies have identified proton-neutron mixed symmetry 2^+ and 1^+ states (Pietralla *et al.*, 1999). In Fig. 49, the specific signatures of a MS 2^+ state [strong $M1$ transition into the 2^+_1 state, weakly collective $B(E2)$ transition from the ground state] are shown. The data point toward the 2^+_3 state as the ideal MS candidate. Experiments in ^{94}Mo have furthermore shown (Pietralla *et al.*, 2000) evidence for two-phonon MS states built from combining a symmetric (2^+_1) and antisymmetric (2^+_3) state, thus forming states with spins in the range 0^+–4^+. Clear-cut identification of the 2^+ (Fransen *et al.*, 2001) and 3^+ (Pietralla *et al.*, 2000) members could be achieved and candidates for the other spins were identified (Fransen *et al.*, 2003) based on the above discussed signatures of MS states.

Independent evidence for one-phonon symmetric and mixed-symmetric states has recently been demonstrated in a combined study of high-resolution inelastic electron and proton scattering off MS 2^+ states in ^{94}Mo (Burda *et al.*, 2007) when comparing with theoretical results derived from quasiparticle-phonon, shell-model, and IBM-2 calculations as shown in Fig. 50. Multiphonon MS states have also been observed in the $N=54$ ^{96}Mo nucleus (Lesher *et al.*, 2007).

The study of the variation in the MS states, keeping the neutron number fixed at $N=52$ but changing the proton number, is quite interesting. In this spirit, experiments have been carried out in ^{96}Ru with $Z=44$ (Pietralla, Barton, *et al.*, 2001; Klein *et al.*, 2002) pointing out a strong similarity with ^{94}Mo. Moreover, evidence for a MS 1^+ state was shown by Linnemann *et al.* (2005). A study of the ^{92}Zr nucleus, with the same number of neutrons, i.e., $N=52$, is quite different because in the core nucleus, ^{90}Zr, two 0^+ states appear resulting from the presence of both $(1g_{9/2})^2_{0^+}$ and $(2p_{1/2})^2_{0^+}$ configurations. The 0^+ ground state therefore acquires extra binding energy which distorts the vibrational spectra as compared with the $N=52$ Mo and Ru nuclei. Still, photon scattering (Werner *et al.*, 2002) and $(n,n'\gamma)$ inelastic neutron scattering have enabled to observe 2^+ and 1^+ states with a MS character. Recent experiments (Elhami *et al.*, 2007, 2008; Werner *et al.*, 2008) concentrated on the special situation in the Zr nuclei.

The nuclei with proton number $40\leqslant Z\leqslant 50$ and neutron number close to $N=50$ (here, $N=52$), with in particular the nucleus ^{94}Mo, form an ideal testing ground for the IBM-2, the QPM, as well as the nuclear shell model. It was shown (Iachello, 1984) that the IBM-2 framework naturally predicts a class of states with MS character in the proton and neutron contributions. Detailed selection and intensity rules have been derived for $E2$ and $M1$ transitions in the various limits of the IBM-2 (Scholten *et al.*, 1985; Van Isacker *et al.*, 1986). Comparison of the IBM-2 results has been carried out in ^{94}Mo as well as the adjacent $N=52$ isotones Ru and Zr with a consistent description of MS states with both a one- (2^+) and two-phonon ($1^+,2^+,3^+,4^+$) character as well as of their decay properties to lower-lying symmetric zero- and one-phonon states [see, e.g., Pietralla, von Brentano, and Lisetsky (2008) for more detail]. Keeping within the context of the IBM-2, a particular scheme (called Q-phonon scheme) was set up by Otsuka and Kim (1994), which allows for the description of these symmetric and MS excitations as phonons, applicable in the U(5) and O(6) symmetry limits and in the transitional nuclei between these two limits.

The IBM-2 has a drawback because the operator only addresses the orbital part and specific spin contributions are only considered in an average way. Therefore, mi-

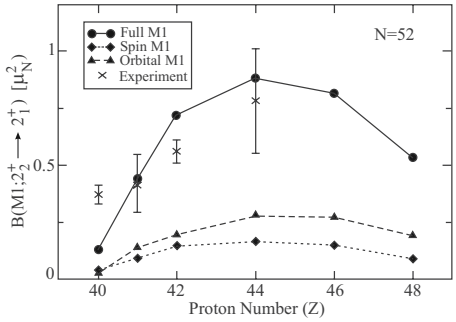

FIG. 51. Evolution of the total, orbital, and spin $B(M1;2_2^+ \rightarrow 2_1^+)$ values for the $N=52$ isotones. The results of recent shell-model calculations are compared with the data. From Holt *et al.*, 2007.

croscopic techniques are needed such as the standard shell-model and quasiparticle-phonon (QPM) approaches. The QPM approach has been applied with considerable success in the region of vibrational nuclei by Lo Iudice and Stoyanov (2000, 2002, 2004, 2006) and Lo Iudice *et al.* (2008). In the $Z=40$, $N=50$ region, it turns out that the 2_1^+ RPA phonon has mainly a symmetric structure in the interchange of proton and neutron labels (or is F-spin symmetric in the IBM-2 language) whereas the 2_2^+ RPA phonon is antisymmetric (or of F-spin MS nature) to a good approximation. The QPM eigenvalue problem is then solved in a basis including up to three-phonon states and considering many phonons of different J^π nature. These results give support to the IBM-2 calculations carried out in which these s and d bosons are the only building blocks. Detailed results are given for ^{94}Mo (Lo Iudice and Stoyanov, 2000, 2002) and for ^{92}Zr (Lo Iudice and Stoyanov, 2004, 2006).

Large-scale shell-model calculations have been carried out for ^{94}Mo (Lisetskiy *et al.*, 2000), ^{96}Ru (Werner *et al.*, 2002), and ^{92}Zr (Klein *et al.*, 2002) in the $Z=40$, $N=50$ mass region using a surface delta interaction and treating all valence protons and neutrons outside of the ^{88}Sr core with $Z=38$ and $N=50$. Here both the orbital and spin matrix elements contribute, the latter part being non-negligible for $M1$ transitions and moments. As in the IBM-2 and QPM, the same structure shows up. The specific characteristics of $M1$ and $E2$ decay characterizing excited states give a microscopic underpinning to the concepts of symmetric and mixed symmetric excitations as used in the Q-phonon classification. The fingerprints that characterize the decay of MS states (see Sec. VI.A) are clearly observed in the results (Lisetskiy *et al.*, 2000). Shell-model calculations for the $N=52$ nuclei have been performed within the same model space but now using matrix elements derived from the low-momentum $V_{\text{low }k}$ nucleon-nucleon interaction (Holt *et al.*, 2007) giving a rather good reproduction of the experimentally observed results. In Fig. 51 besides the calculated total $M1$ strength the orbital and spin contributions, which interfere constructively, are given separately.

2. Nuclei near other doubly closed shell regions

a. The region near $Z\sim50$

The Cd and Te nuclei with two proton holes (two proton particles) away from the $Z=50$ Sn closed core, combined with the neutron filling of the $50<N<82$ neutron shell form an interesting region to expect mixed-symmetry states. In this mass region, a variety of experiments have been carried out, including the $(n,n'\gamma)$ reaction (Garrett *et al.*, 1996; Bandyopadhyay *et al.*, 2003), for ^{112,114}Cd, photon scattering, eventually combined with Compton polarimetry to deduce the parity unambiguously (Lehmann *et al.*, 1999; Gade *et al.*, 2003; Kohstall *et al.*, 2005) for $^{108-116}$Cd, β decay (Linnemann *et al.*, 2007) for ^{106}Cd, and recoil-distance Doppler-shift (RDDS) measurement after fusion-evaporation reactions (Boelaert, Dewald, *et al.*, 2007) for ^{102,104}Cd. Evidence for the presence of MS 2^+ states, slightly above 2 MeV excitation energy, as well as for MS 1^+ states, at the higher excitation energy near 3 MeV, have been obtained in almost all of these nuclei.

Shell-model calculations have also been reported for the light Cd nuclei with $A=98-106$, using the same core as before (^{88}Sr), treating all the available valence protons (10 in the case of Cd) and neutrons (Boelaert, Smirnova, *et al.*, 2007). A detailed mapping of shell-model states onto MS states for both 2^+ and 1^+ states was performed using as criterium strong $M1$ transitions to the 0_1^+ and 2_1^+ symmetric states combined with weak $E2$ transitions to these same states, and strong $E2$ transitions in between the MS $2^+,1^+$ states. Likewise, in the even-even $^{122-130}$Te nuclei, an experimental search for MS 1^+ and 2^+ states was performed by Schwengner *et al.* (1997a, 1997b) using photon inelastic scattering, and in ^{124}Te by Georgii *et al.* (1995) using a variety of reactions. This resulted in the detection of candidates for mixed-symmetry 2^+ states, slightly above 2 MeV excitation energy. Recently Hicks *et al.* (2008) provided detailed results on fragmentation of MS 2^+ states in the $^{122-130}$Te nuclei. The deformation dependence of the ground-state scissors mode strength in these isotopes could by successfully reproduced by QRPA calculations (Guliyev *et al.*, 2002).

b. The rare-earth region: $54<Z\leqslant60$ and $72<N\leqslant82$

Early evidence for the presence of MS 2^+ states in rare-earth nuclei resulted from an analysis by Hamilton *et al.* (1984). They showed that in nuclei with two neutrons outside of the $N=82$ closed neutron shell, with an even number of protons filling the $50<Z<82$ proton shell, 2^+ states near 2 MeV would show up. Experiments at the ILL Grenoble using γ-γ directional correlation experiments (from δ-mixing ratios and branching ratios) allowed one to find in ^{140}Ba, ^{142}Ce, and ^{144}Nd a 2_3^+ state with the typical $M1$ and $E2$ branching into the lower-lying symmetric excitations. Recently these nuclei have been studied using NRF and $(n,n'\gamma)$ scattering, even extending up to ^{148}Sm (Vanhoy *et al.*, 1995; Hicks *et al.*,

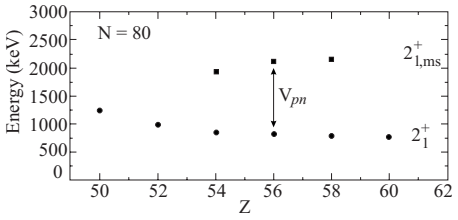

FIG. 52. Excitation energies of the 2^+_1 and 2^+_{ms} states in $N=80$ isotones. The splitting is a measure of the residual proton-neutron interaction (Ahn *et al.*, 2009).

1998; Gade *et al.*, 2000, 2004; Li *et al.*, 2005; Mukhopadhyay *et al.*, 2008) showing evidence for MS 2^+ states, in most cases exhibiting fragmentation over a number of 2^+ states near or just above to 2 MeV excitation energy. Likewise, experiments have been carried out in the $N=80$ nuclei ^{134}Xe, ^{136}Ba, and ^{138}Ce using the same techniques and Coulomb excitation (Pietralla, von Brentano, Gelberg, *et al.*, 1998; Scheck *et al.*, 2004; Rainovski *et al.*, 2006; Pietralla, von Brentano, and Lisetsky, 2008; Williams *et al.*, 2009). They again showed the presence of MS 2^+ states and fragmentation, the latter changing quite drastically with the proton number increasing from $Z=56$ to 58. As shown in Fig. 52 it is even possible to extract the strength of the residual proton-neutron interaction from the energy splitting between lowest symmetric and mixed-symmetric 2^+ state in these $N=80$ nuclei (Ahn *et al.*, 2009).

The $N=80$ nuclei were extensively studied by Lo Iudice *et al.* (2008) within the QPM approach and in a large-scale shell-model study (Sieja *et al.*, 2009). These calculations described rather well both the variation in excitation energy and the changing fragmentation pattern, moving from ^{132}Xe to ^{140}Nd.

A number of nuclei in which both the proton number and neutron number is steadily increasing moving away from the $Z=50$ and $N=82$ shell closure, such as ^{126,128,130}Xe, ^{134}Ba, and ^{136}Ce, have been studied using techniques as discussed before (Fazekas *et al.*, 1992; Wiedenhöver *et al.*, 1997; Gade *et al.*, 2000; Ahn *et al.*, 2007; Bettermann *et al.*, 2009). In these nuclei, the signature of a MS 2^+ state shows up consistently slightly above 2 MeV excitation energy.

c. The $A\approx 60$ region

The region near the doubly magic nucleus ^{56}Ni with proton and neutron hole or particle pairs outside of the $Z=N=28$ core may well give rise to MS couplings of proton and neutron building blocks. The nucleus ^{56}Fe forms an ideal testing case and was studied by Eid *et al.* (1986) using γ-decay studies, and by Hartung *et al.* (1989) in electron scattering. Clear-cut evidence for fragmentation of MS 2^+ strength has been observed around 2.6–2.9 MeV. In nearby nuclei such as ^{54}Cr and ^{66}Zn, candidates for MS 2^+ strength have been detected near 3 MeV excitation energy (Lieb *et al.*, 1988; Gade *et al.*, 2002). It is interesting to note the increase in energy from the heavier nuclei, where the typical energies are closer to 2 MeV.

d. Heavy nuclei in the vicinity of ^{208}Pb

The idea of low-lying 2^+_{ms} excitations appearing in regions where the number of protons and neutrons forms a stable closed shell has been shown to be a general property all through the nuclear mass region. Therefore, the region around $Z=82$ and $N=126$ should be a most interesting region one in order to explore the appearance of states which exhibit a MS character in the protons and neutrons. Early evidence was shown by Ahmad *et al.* (1989) for 2^+ states near 1.5 MeV in ^{200}Hg. Likewise a 2^+ state near 2.2 MeV was observed in ^{196}Pt (von Brentano *et al.*, 1996; Jewell *et al.*, 1997). This region has by now not been studied in a systematic way but the Hg, Pt, and also the Po, Rn nuclei with neutron numbers close to $N=126$ should form an ideal testing ground but require radioactive beams.

C. Summary

To sum up this section, we have presented evidence for isovector proton-neutron excitations in which small amplitude quadrupole oscillations form the basic building blocks. These isovector excitations result in a natural way in both shell-model, collective (geometrical and algebraic), and quasiparticle-phonon theoretical approaches. The characteristic fingerprint of strong $M1$ transitions between MS and symmetric collective states, associated with weak $E2$ transitions from MS states into the symmetric collective states, has allowed us to identify the MS states. They are most clearly observed when a given nucleus only contains a few proton particles (holes) and neutron particles (holes) outside of closed shells. The $Z\approx 40$, $N\approx 50$ region is one of the best studied regions showing besides the lowest MS 2^+ state, more complex MS 1^+, 2^+, 3^+, and 4^+ states (Zr, Mo, and Ru nuclei). Recently the presence of MS states has been accumulated in nuclei near $Z\approx 50$ (such as the Cd, and Te nuclei), in the rare-earth region ($54<Z\leqslant 60$, $72<N\leqslant 82$) and also for lighter nuclei near the $Z=N=28$ closed shells. In view of the very general characteristic of these excitations, one can expect them to appear in nuclei adjacent to any doubly-closed shell nucleus.

VII. SCISSORS MODES IN OTHER MANY-BODY SYSTEMS

A. Rotational magnetic excitations in other fermion systems

1. Deformed metallic clusters

Mass spectra for a particular class of metallic clusters were produced more than 20 years ago (Knight *et al.*, 1984). They exhibit large abundance peaks at $N=8,20,40,58,92,138,\ldots$. These clusters were produced in the expansion of an inert gas (typically argon or xenon) through a 0.1–0.2 mm wide nozzle, in which the random thermal motion of the atoms is converted into a

uniform translational motion, thereby also causing a cooling of the inert gas. Introducing atomic Na vapor into this system results into large clusters with an overall broad size distribution. Details of the mechanism were described by de Heer (1993). The peculiar observation for Na clusters and later shown to exist also for Ag, Au, and Cs, points toward extra stability associated with the delocalized motion of atomic 3*s* electrons, bound in a spherical potential [see de Heer *et al.* (1987) and Bjørnholm *et al.* (1990, 1992) for a detailed discussion]. The observation of quantal effects in clusters of atoms established a deep connection between various fields in physics such as electronic motion in atoms and nucleonic motion in nuclei.

The Hamiltonian describing the neutral cluster consisting of N nuclei with Z electrons each is fully determined through the Coulomb force but is generally too complex to be solved exactly. In simple metals, though, such as Ag, Al, Na, etc., the separation into valence electrons and core electrons (well bound and localized) leads to the simplification of xN interacting electrons (x the number of valence electrons per atom) moving in the field caused by the N ions. A further step results in completely ignoring the nuclear motion, thus leading to an electronic Hamiltonian of the form

$$H_{el} = \sum_{k=1}^{xN} \left\{ \frac{\mathbf{p}_k^2}{2m} + V_I(\mathbf{r}_k) \right\} + \frac{1}{2} \sum_{l \neq k=1}^{xN} \frac{e^2}{|\mathbf{r}_k - \mathbf{r}_l|}, \tag{38}$$

with the ionic potential $V_I(\mathbf{r}_k)$ defined as

$$V_I(\mathbf{r}_k) = -\sum_{i=1}^{N} \frac{xe^2}{|\mathbf{r}_k - \mathbf{R}_i|}. \tag{39}$$

The latter potential most often is replaced by some pseudopotential. At the end, a rather drastic but efficient approximation consists of averaging out the ionic structure and replacing the corresponding charge distribution by a "constant" background charge in a finite (spherical, deformed, vibrating, and/or rotating) volume. This defines the so-called *jellium* model as used in the description of metallic bulk and surface properties (Brack *et al.*, 1991a, 1991b; Brack, 1992).

Collective dipole excitations are well known in alkali-metal clusters (de Heer *et al.*, 1987; de Heer, 1993) which correspond to the classical surface-plasmon oscillations (Ashcroft and Mermin, 1976) of the electron cloud against the positively charged ions forming the cluster. The relative motion of protons versus neutrons in atomic nuclei, giving rise to the giant electric dipole mode is equivalent to the electric dipole mode that results in electron motion in atoms. For deformed metallic clusters, a magnetic excitation of orbital nature was predicted by Lipparini and Stringari (1989b) at an energy much lower than the classical plasmon frequency. A macroscopic illustration of this new magnetic excitation derives from a displacement field $\mathbf{u}$ of the electron motion in the valence cloud. The suggested form is

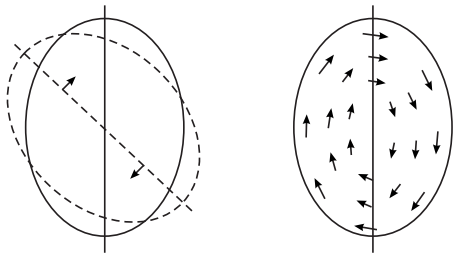

FIG. 53. Displacement field for the magnetic dipole low-lying rotational state. Results shown correspond to (a) a rigid rotation of the electrons with respect to the jellium background and (b) a rotation within a rigid surface. The direction of the unit vector $\hat{\omega}$ (z direction) points out of the plane. From Lipparini and Stringari, 1989a.

$$\mathbf{u} = \hat{\omega}\mathbf{x}\mathbf{r} + \frac{\delta}{1+\delta/3} \nabla(xy), \tag{40}$$

with $\hat{\omega}$ the unit vector in the z direction. The cluster is described with a deformed electron density profile

$$\rho_e = \rho_0(x^2/R_x^2 + y^2/R_y^2 + z^2/R_z^2), \tag{41}$$

with $R_x = R_z$ and the deformation δ defined by

$$\delta = \frac{3}{2} \frac{R_y^2 - R_x^2}{R_y^2 + 2R_x^2}. \tag{42}$$

This displacement field satisfies the condition $\nabla \cdot \mathbf{u} = 0$. The first term solely corresponds to a rigid rotation of the electrons with respect to the jellium background and implies a scissors mode [Fig. 53(a)] with a restoring force that is due to the Coulomb attraction between the electron cloud and the ion positive charged background. This is similar to the proton-neutron symmetry term causing the restoring force in case of atomic nuclei. Including the quadrupole term in the displacement field, i.e., $\nabla(xy)$, the corresponding motion [Fig. 53(b)] corresponds to a rotation within a spheroidal rigid surface with a velocity field such that $\mathbf{v} \cdot \mathbf{n}|_{\text{surface}} = 0$.

In the limit of small deformation, one can determine the frequency of the magnetic mode $\omega_{M1} = \sqrt{K/\theta}$ with K the energy change originating from the displacement field and θ the collective mass parameter (related to the moment of inertia)

$$\omega_{M1} = \delta \sqrt{\frac{4\varepsilon_F}{m r_s^2}} N^{-1/3}. \tag{43}$$

In this section, we use throughout the convention $\hbar = c = 1$. In deriving this result, the approximate relation,

$$\langle r^2 \rangle = \tfrac{3}{5} r_s^2 N^{2/3}, \tag{44}$$

was used. In the particular case of Na clusters, with $r_s = 4$ a.u. and $\varepsilon_F = 3.1$ eV, the frequency becomes $\omega_{M1} = \delta 4.6 N^{-1/3}$ eV. In the range of clusters with $N = 10$–100 and for typical deformations $\delta = 0.2$–0.4, the frequency amounts to 0.2–0.6 eV, much lower than the dipole plasmon frequency of 3.4 eV. This collective state

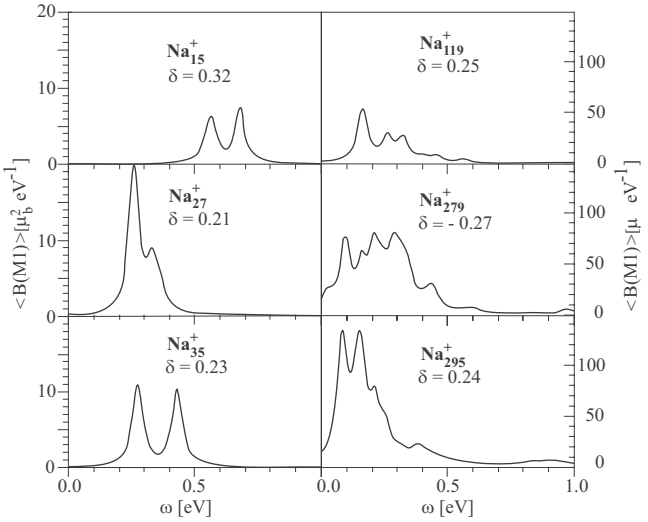

FIG. 54. Energy distribution of the $M1$ strength for Na clusters ranging from $N=15$ to 295. The deformation parameter δ characterizing the specific cluster is also given. From Nesterenko *et al.*, 1999.

carries considerable $M1$ strength $B(M1)\approx\omega_{M1}\theta\mu_B^2$ or using explicit expressions for the frequency and the moment of inertia (Lipparini, 2003) becomes

$$B(M1)=\tfrac{4}{5}\delta\sqrt{\varepsilon_F m r_s^2}N^{4/3}\mu_B^2, \tag{45}$$

which, in the particular case of Na clusters, reduces to the result $B(M1)\approx\delta N^{4/3}\mu_B^2$ with μ_B the Bohr magneton. The particular results for both ω_{M1} and $B(M1)$ have a very similar form as the expressions derived in Eqs. (2) and (3) for the nuclear case.

The above semiclassical results can also be derived starting from microscopic calculations. A schematic two-level RPA model was studied by Lipparini and Stringari (1989a) with results that corroborate the macroscopic approach. More detailed studies of the orbital magnetic dipole mode were carried out by Nesterenko *et al.* (1999), based on a self-consistent RPA approach (Nesterenko *et al.*, 1997; Kleinig *et al.*, 1998). Using a phenomenological Woods-Saxon potential, the results confirm those obtained by Lipparini and Stringari (1989b) discussed before. We show in Fig. 54 the salient features of the $M1$ strength distribution as derived for Na clusters, in which the N dependence (moving from $N=15$ toward $N=295$) becomes particularly clear. In the heavy clusters with $N\sim300$, the $M1$ strength reaches large values of the order of $(350–400)\mu_B^2$ with the strength remaining concentrated in a rather narrow energy interval. Therefore, it is in the heavy clusters that the collective nature of the $M1$ mode becomes particularly clear with a $N^{-1/3}$ frequency dependence as pointed out in Eq. (43). This distinguishes the magnetic mode from the regular electric dipole surface-plasmon mode, which is much better documented experimentally. As pointed out, the strength in exciting this magnetic dipole mode is so much weaker than the electric dipole strength that it has not been observed experimentally as yet, contrary to the nuclear case as discussed in the major part of the present paper.

2. Orbital current modes in deformed quantum dots

Recent advances in semiconductor technology have allowed one to build nanostructures with varying shapes. In these systems, electrons are laterally confined at the semiconductor boundary and form a two-dimensional (2D) quantum dot [see Alhassid (2000)]. Until recently, the vast majority of theoretical and experimental efforts focused on systems with circular symmetry. Many of the properties of these dots are well accounted for when imposing a parabolic potential as confinement or invoking the concept of a jellium disk (see Sec. VII.A.1). Experiments addressing deformed nanostructures using Raman scattering and far-infrared spectroscopy (Sikorski and Merkt, 1989; Demel *et al.*, 1990; Strenz *et al.*, 1994; Schüller *et al.*, 1996; Austing *et al.*, 1999) have been at the origin of theoretical studies relaxing on the circular symmetry (Koskinen *et al.*, 1997; Hirose and Wingreen, 1999; Puente and Serra, 1999).

With the breaking of the rotational symmetry of the system (metallic cluster and quantum dot), in particular by introducing a quadrupole distortion, it turns out that a low-energy orbital current excitation (OCE) is generated in the 2D dot with an energy dependence $N^{-1/2}$ in contrast with the $N^{-1/3}$ dependence for three-dimensional system (Lipparini, 2003). Here N denotes the number of electrons confined in the elliptic quantum dot. Interesting here to remark is the fact that the frequency goes to zero with $N\to\infty$.

One can now perform essentially the same analysis as was used in the description of deformed metallic clusters, but now with an elliptic two-dimensional charge distribution given as

$$\rho_e=\rho_0(x^2/R_x^2+y^2/R_y^2), \tag{46}$$

with R_x and R_y the ellipse radii and a deformation parameter η defined by

$$\eta=\frac{R_y^2-R_x^2}{R_y^2+R_x^2}. \tag{47}$$

The kinetic energy density has an expression analogous to the charge distribution given in Eq. (46). An OCE follows, using a displacement field similar to the one discussed in Sec. VII.A.1 but for the 2D case which is expressed as (Serra *et al.*, 1999)

$$\mathbf{u}=\hat{\omega}\mathbf{x}\mathbf{r}+\eta\nabla(xy). \tag{48}$$

The electronic motion becomes a collective rotating flow along the ellipse contour lines. The frequency for this orbital mode turns out to be

$$\omega_{\mathrm{OCE}}\approx\frac{\eta}{\sqrt{1-\eta^2}}\sqrt{\frac{16\varepsilon_F}{3mr_s^2}}N^{-1/2}, \tag{49}$$

where r_s is the Wigner-Seitz radius (Ashcroft and Mermin, 1976). Carrying out the same analysis but retaining only the quadrupole deformation generating displace-

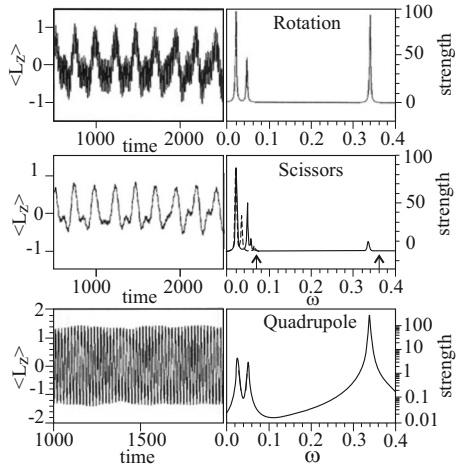

FIG. 55. Results for the time evolution of an elliptic quantum dot with $N=20$ electrons, for a deformation value of $\eta=0.28$, and this using three different initial perturbations: pure rotation, orbital, and quadrupole distortions. In the left-side panels, the simulated $M1$ signal, expressed as $\langle \hat{L}_z \rangle$, is plotted as a function of time. The right-side panels show the corresponding $M1$ excitation strength. The middle right-side panel also shows the independent electron strength function (dashed line) and the small arrows indicate the position of the solutions given by Eqs. (49) and (50). From Serra *et al.*, 1999.

ment term $\mathbf{u}=\nabla(xy)$, the frequency of the corresponding quadrupole charge-density excitation (QCDE) becomes

$$\omega_{\mathrm{QCDE}} \approx \sqrt{2}\omega_0, \tag{50}$$

where ω_0 is the average of the frequencies in x and y directions for the confining parabolic potential. This frequency is much larger than the frequency of the orbital excitation. A most interesting illustration of the effects of both modes is obtained when evaluating the magnetic orbital response. This $M1$ response $\langle \hat{L}_z \rangle$ has been calculated (Serra *et al.*, 1999), as a function of time, by modifying the electron orbitals using the displacement operator of Eq. (48) (left-side part of Fig. 55) as well as the corresponding $M1$ strength (right-side part of Fig. 55). Here the cases of (i) a pure rotational perturbation (rotation), (ii) orbital perturbation (OCE or scissors), and (iii) pure quadrupole perturbation are shown. These results are in line with the simple discussion of the frequencies as presented before. The $M1$ orbital strength is divided in two distinct regions: one at the higher-energy side, which is associated with the quadrupole distortion, and one at the low-energy end, associated with the orbital excitation. An in-depth study was presented by Austing *et al.* (1999). The distribution of scissors $M1$ strength in these elliptic quantum dots is quite similar to the situation in strongly deformed nuclei in which the $M1$ strength is also separated into a low-energy orbital (the scissors mode) part and the higher-lying $K^{\pi}=1^{+}$ component of the isovector giant-quadrupole resonance (see Sec. III.C).

Besides these orbital charge-density excitations, it is also possible to describe spin-density oscillations in quantum dots. When the spin components oscillate in phase, they describe the density modes; however, when oscillating out of phase, spin modes can be created. A particular interesting case is obtained as alternating rotation of spin up and spin down densities in opposite direction, This spin-twist mode is very soft (Puente and Serra, 1999), well below the spin dipole oscillation modes.

3. Other Fermi systems

It turns out that scissor modes can also be realized in a superfluid Fermi gas (Minguzzi and Tosi, 2001). Confining the Fermi gas inside a spherical harmonic trap and solving the equations of motion for the density and concentration fluctuations gives rise to a single scissors frequency for the superfluid situation and results in two scissors frequencies in a normal Fermi gas.

Recently Hatada *et al.* (2005) suggested the possibility that axially symmetric atoms in crystals with ionic bonding can exhibit a scissors excitation. Its signature in this case is the existence of a low-lying collective excitation resulting from precessing atoms around the anisotropy axis of the crystal cells. This excitation has a magnetic dipole character and could be observed through the absorption of incoming photons which should exhibit a differential dichroism. An extension to also cover crystals with cubic symmetry was presented by Hatada *et al.* (2010a).

Other ways of observing scissors modes in crystals start from a recent experiment that studied magnetic properties of rare-earth systems (van der Laan *et al.*, 2008). If one considers crystals in which the internal electrostatic field is small with respect to the electron spin-orbit coupling in the atoms, the so-called "spin-orbit locking" situation, an applied external magnetic field will rotate both the spin and charge density profiles simultaneously. Switching off the magnetic field, the atoms will start oscillating around the axes of the crystal cells (Hatada *et al.*, 2010a). Experiments have been proposed that may be sensitive enough to detect the photons emitted when deexciting the scissors excitation (Hatada *et al.*, 2010b).

B. Scissors modes of a trapped Bose-Einstein condensate

By now there exists a vast literature on trapped Bose-Einstein condensates (Pitaevskii and Stringari, 2003; Giorgini *et al.*, 2008). Superfluidity in these condensates is one of the most spectacular consequences. It is, however, not easy to obtain unambiguous evidence for the superfluid characteristics. Because superfluidity will affect the moment of inertia of the trapped condensate (such as a reduction over the classical rigid value), one could expect that a study of rotational properties of such condensates can give rise to experimental evidence for the existence of superfluidity. Guéry-Odelin and Stringari (1999) studied the oscillatory behavior caused by rotating a condensate with respect to the symmetry axis when trapped in a deformed external potential of para-

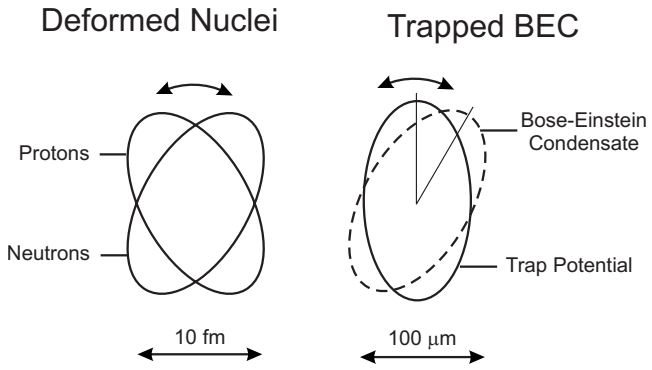

FIG. 56. Schematic comparison of the scissors motion in atomic nuclei with protons and neutrons generating the scissors motion, on a length scale of 10 fm (left side), and in Bose-Einstein condensates trapped in an external potential, the latter acting on a length scale of 100 μm (right side).

bolic type. They concentrated in particular on the superfluid effects in the condensate. The restoring force associated with such a rotation in the x-y plane is proportional to δ^2, with the trapping potential given by

$$V_{\text{ext}}(\mathbf{r}) = \frac{m}{2}\omega_x^2 x^2 + \frac{m}{2}\omega_y^2 y^2 + \frac{m}{2}\omega_z^2 z^2, \tag{51}$$

with, moreover,

$$\omega_x^2 = \omega_0^2(1+\delta), \quad \omega_y^2 = \omega_0^2(1-\delta). \tag{52}$$

The mass parameter, determined by the moment of inertia, in the superfluid case becomes proportional to δ^2 too (Rowe, 1970; Lipparini, 2003). As a result, even when the deformation of the external potential approaches zero, the frequency keeps a finite value. It is only in the absence of superfluidity that the moment of inertia regains its rigid value, and, therefore, a low-frequency will characterize the oscillatory motion. The outcome of the theoretical study [see Guéry-Odelin and Stringari (1999) and Lipparini (2003)] is that a sudden rotation of the trap symmetry axis by a small angle θ_0 will perturb the condensate from its equilibrium shape and if the angle θ_0 is not too large, will start a scissors-like motion[3] in the x-y plane. This is shown schematically in Fig. 56 (right-hand side) in which both the trapping potential and the condensate are drawn. An idea of the dimensions of such condensates is also given. On the left-hand side in Fig. 56, we compare with the analogous situation in strongly deformed atomic nuclei, in which protons and neutrons can give rise to a scissors motion. Here too the dimension of the system is given in order to stress the large difference in scales but keeping essentially the same physics. Under the above conditions one obtains

[3]The expression scissors mode has been taken over from nuclear physics by the atomic physics and BEC community.

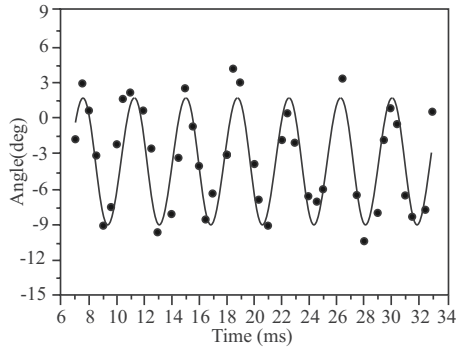

FIG. 57. The classical frequency and the tilt angle for a trapped Bose-Einstein condensate of ^{87}Rb atoms. From Maragò *et al.*, 2000.

$$\theta(t) = \theta_0 \cos(\omega_{sc} t), \tag{53}$$

in which $\omega_{sc} = \sqrt{2}\omega_0$ or $\omega_{sc} = \sqrt{\omega_x^2 + \omega_y^2}$. In the absence of a superfluid condensate and entering a high-temperature regime, analytic solutions become possible (Guéry-Odelin and Stringari, 1999) which, for small rotation angles of the trap axis, are described by a differential equation for $\theta(t)$. This equation now allows for different solutions, propagating at high and low frequencies. In a collisionless regime, the higher frequency becomes $\omega_+ = \omega_x + \omega_y$ and can be identified with an irrotational quadrupole oscillation. The lower frequency $\omega_- = |\omega_x - \omega_y|$, however, corresponds to the rotational mode of the system, a component which is absent in the superfluid case.

Maragò *et al.* (2000, 2001) reported on a clear observation of the scissors mode with a Bose-Einstein condensed gas of ^{87}Rb atoms brought into a magnetic trap. They highlighted the importance of the discovery of the scissors mode in atomic nuclei stating, "The experimental discovery of the scissors mode (Bohle, Richter, *et al.*, 1984), first predicted in a geometrical model (Lo Iudice and Palumbo, 1978; Lipparini and Stringari, 1983), has been one of the most exciting findings in nuclear physics during the past two decades."

The scissors mode has also been excited by a sudden rotation of the deformed trapping potential (with the constraints $\omega_x \approx \omega_z > \omega_y$). The condensate cooled to well below the critical temperature for the Rb gas contains of the order of 10^4 atoms. The time evolution of the scissors oscillation (Fig. 57) exhibits a single undamped mode corresponding to 265.6 ± 0.8 Hz, which agrees with the theoretical value of 265 ± 2 Hz as deduced from $\omega_{sc} = \sqrt{\omega_x^2 + \omega_y^2}$. This observation thus provides an unambiguous demonstration of the superfluid nature the Rb condensate. In Fig. 57 we show the classical frequency and the tilt angle for the trapped Bose-Einstein condensate of ^{87}Rb atoms, which correspond to $\nu = 265.6 \pm 0.8\ \text{s}^{-1}$ and $\alpha = 7.2°$, respectively.

It is instructive to compare the condensate result with the scissors mode in the deformed nucleus ^{156}Gd (Bohle, Richter, *et al.*, 1984). We can extract both the frequency (using the experimental energy of the 1^+ state at $E_x = 3.075$ MeV) and a classical tilt angle identifying the re-

storing force with the symmetry energy and making use of the expression $\alpha=(CJ_{\rm intr}/\hbar^2)^{-1/4}$ deduced from the proton-neutron collective model (De Franceschi *et al.*, 1984; Nojarov *et al.*, 1986) discussed in Sec. III.A.2. This results in $\nu=7\times10^{20}$ s^{-1} and $\alpha\sim6°$. Thus, comparable tilt angles are found characterizing the scissors motion, albeit in different regimes of physics. A striking difference between the two systems, however, is the fact that in the condensate the deformation of the trap can be varied by choosing appropriate frequencies as well as the temperature giving a large range to study the intricate properties of quantum fluids and their transition from the irrotational (superfluid case) to the rotational regime. In the atomic nucleus, the deformation is fixed for a given (Z,N) combination.

Compared to the observation of scissors modes for trapped Bose-Einstein condensates, scissorslike oscillations have also been observed in a quantum-degenerate mixture of two such condensates consisting of different atomic species, i.e., ^{41}K and ^{87}Rb (Modugno *et al.*, 2002). In this case, the scissors mode is induced by interactions between the two atomic species present in the trap. Therefore, this situation is even closer to the nuclear physics case where proton and neutron fluids are present.

C. Rounding up

The above theoretical and experimental studies both in fermionic (metallic clusters, quantum dots, Fermi gas, and crystals) systems in which the electronic motion in some "external" potential has been studied and in bosonic systems (Bose-Einstein condensates in the superfluid phase trapped in an external anisotropic potential) show the existence of scissors modes with properties in line of those observed in atomic nuclei. The arguments can even be turned around: the observation of low-lying scissors modes in these systems is a proof of the superfluid characteristic of proton and neutron fluids in the nuclear rotational motion.

VIII. CONCLUSIONS AND OUTLOOK

A. Conclusions

The study of the response of nucleons, moving inside the atomic nucleus, to external (electromagnetic and hadronic) probes in the magnetic dipole channel, discussed in depth in the present article, can be crystallized and summarized in a succinct way. Here we take Figs. 1–3 as our guide.

(i) At the lower-energy side, orbital nucleonic motion is strongly excited by the $\hat{L}_\pi-\hat{L}_\nu$ part of the $M1$ operator (contrarotational or scissorslike motion of protons versus neutrons). This does not show up, however, as a single collective state but the orbital strength is fragmented within a rather limited energy interval between 2.5 and 4 MeV. In light nuclei, the strength distribution looks more simple since it is contained mainly in the $2^+(\pi)\otimes2^+(\nu)$, $4^+(\pi)\otimes4^+(\nu)$, etc. configurations. In strongly deformed rare-earth nuclei, there is more spreading of strength which has been detected using (e,e') and (γ,γ') reactions and not or very weakly with proton scattering. A number of interesting results are connected to the fact that the non-energy-weighted $M1$ sum rule strength in the interval 2.5–4 MeV exhausts the larger part of the orbital $M1$ strength. Moreover, it was discovered that this summed $M1$ strength correlates strongly with deformation and thus with the $B(E2;0_1^+\rightarrow2_1^+)$ strengths, indicating saturation when progressing through the strongly deformed rare-earth region.

(ii) Spin $M1$ strength is concentrated at higher excitation energies because the spin-flip part of the $M1$ operator is mainly a $1\hbar\omega$ excitation in the shell model and has been studied throughout the region of deformed rare-earth and actinide nuclei. In light nuclei, the strength is particularly associated with the spin-flip transition between spin-orbit partners. In the heavier nuclei, it is the spin-spin isospin-dependent part of the residual interaction $(\vec{\sigma}\cdot\vec{\sigma}\vec{\tau}\cdot\vec{\tau})$ that rules the concentration or fragmentation of spin $M1$ strength.

(iii) At still higher excitation energies $(2\hbar\omega)$, theoretical predictions indicate the presence of a $K^\pi=1^+$ component of the isovector giant quadrupole resonance (IVGQR), a state that could rightly be associated with a collective scissors mode. Because of the high excitation energy, no systematic experimental studies exist yet exploring such a mode. Knowledge of the IVGQR strength, connected to this response, allows the evaluation of an energy-weighted sum rule to constrain the orbital $M1$ strength, which is exhausted to more than 80%.

(iv) In nuclei with just a few valence protons and neutrons outside of closed shells, it has been experimentally proven that low-lying mixed-symmetry (isovector) 2^+ excitations exist. They are characterized by strong $M1$ decay into the first excited 2_1^+ state, a symmetric (isoscalar) mode in the proton and neutron motion, accompanied by weak $E2$ decay into the 0^+ ground state. The quadrupole degree of freedom dominates the low-energy structure, resulting in energy spectra with a vibrational character. However, isovector combinations can also give rise to a 1^+ state which is related to the scissors 1^+ state as it appears in strongly deformed nuclei.

(v) In odd-mass nuclei, the study of the $M1$ strength distribution is more complicated because of the odd-particle (-hole) coupling to the 1^+ modes which induces a large fragmentation. There occurred a number of early problems in accounting

for the observation of the $M1$ strength but the present situation is such that, through careful studies of the highly fragmented background structures, the full summed $M1$ strength in odd-mass nuclei is consistent with the summed $M1$ strength obtained in the adjacent even-even nuclei. Much more work needs to be done from the side of theoretical studies in order to understand the major mechanisms that can explain the fragmentation and the sometimes sudden important changes in the observed fragmentation when going from nucleus to nucleus.

(vi) In the even-even nuclei, a number of general features have resulted from detailed experimental studies of the $M1$ response over many nuclei, spanning the region from light to very heavy nuclei. One of the most important observations is a strong correlation of the orbital magnetic dipole response with other multipoles, in particular with the $E2$ strength but also, be it in an indirect way, with the nuclear charge radii, i.e., with the $E0$ strength. This connection has been formulated in a more quantitative way using various $M1$ sum rules that are proportional to the ground-state expectation value of the quadrupole-quadrupole force and thus lead to new $E2$ sum rules. Lipparini and Stringari (1989a) already pointed out such a connection. The microscopic understanding of this intimate relation between the $M1$ properties on one side and the quadrupole and monopole properties on the other side are more indirect. It has been shown that the quadrupole deformation of the nucleus spreads the individual single-particle states (breaking the spherical symmetry) and, with pairing included, the shell-model description of $M1$ strength is indirectly connected to the $E2$ ground-state deformation characteristics of the nucleus. This gives at the same time a natural explanation of the $M1$ orbital summed strength saturation in the midshell region of the rare-earth nuclei. It is a consequence of the fact that the deformed rare-earth nuclei also exhibit a saturation in the quadrupole deformation value ($\delta \simeq 0.25–0.30$).

(vii) At the present stage, the magnetic $M1$ strength seems to be rather well understood and there appears a clear-cut concentration of orbital strength at lower energies using various theoretical approaches: shell-model, QRPA and QPM calculations, and collective geometric and algebraic models all account rather well with the experimental situation on a qualitative level. This is a highly comforting situation with respect to the theoretical understanding of how $M1$ strength builds up at the lower-energy side as mainly orbital in character. Collective model approaches, however, by their specific nature fail in accounting for the detailed fragmentation. This holds for both the geometrical and algebraic collective models. In order to bridge the gap between the various theoretical approaches, one will have to address and explore the possibilities of large-scale shell-model calculations as a way to extract collective effects starting from a microscopic basis.

B. Outlook and future perspectives

Having formulated a number of concluding elements on how the nucleus responds when excited with electromagnetic and hadronic probes in the magnetic dipole channel, a number of clear-cut problems remain to be solved in the coming years. We also present a number of topics that will deserve intensive thought and future experimental efforts such as to bring us closer to a quantitative level of understanding the magnetic dipole channel (and some related other multipoles).

(i) It will be particularly interesting to connect the scissors 1^+ mode, which was shown to be strongly excited using electron and photon scattering off deformed nuclei, to the recent observation of 1^+ states in nuclei when approaching closed shells. In the latter nuclei, the quadrupole mode determines the dominant low-lying proton-neutron isoscalar and isovector excitations. The exploration of a full class of isovector (also called mixed-symmetry states) excitations with spins ranging from 0^+ to 4^+ has begun but is clearly in need of still more systematic studies. In this quest, it is of utmost importance to combine as many complementary probes as possible [Coulomb excitation, lifetime measurements, detailed γ-spectroscopy measuring branching ratios and $\delta(E2/M1)$ mixing ratios, etc.] so as to be able to pin down the nuclear wave functions of these states.

(ii) The spin-flip magnetic dipole response that has been studied using (polarized) proton-scattering off nuclei in the energy region 5–10 MeV poses some specific challenges. A particularly important and unsolved problem at present concerns the precise character of the two humps observed in the spin-flip $M1$ strength distribution in many deformed nuclei. Theoretical studies come to opposing conclusions and only a more detailed experimental survey of the precise charge character of the two humps (proton or neutron versus isoscalar or isovector) can resolve this issue. From the theoretical side and with the present-day numerical capacities to perform large-scale shell-model calculations, a precise survey of the $M1$ response in both the *sd*-shell nuclei, in particular along the $N=Z$ line with nuclei such as ^{20}Ne, ^{24}Mg,…, ^{36}Ar, ^{40}Ca as well as in the heavier *fp*-shell nuclei would be important, also in the light of existing high-quality data in some of these light and medium-heavy nuclei. Recent experimental developments (Tamii *et al.*, 2009), which combine for the first

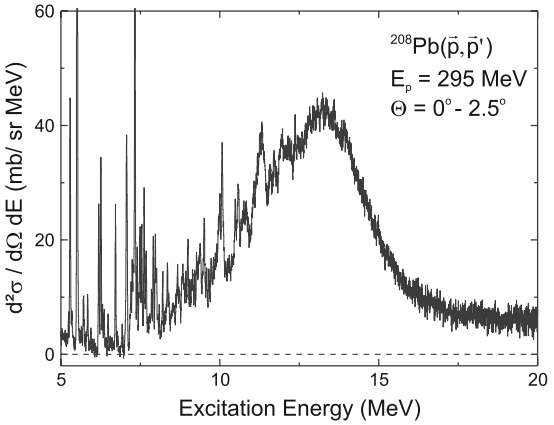

FIG. 58. Spectrum of the ^{208}Pb($\vec{p},\vec{p}'$) reaction at $E=295$ MeV and $\Theta=0°$ (von Neumann-Cosel *et al.*, 2009) measured with an energy resolution $\Delta E \simeq 25$ keV (full width at half maximum).

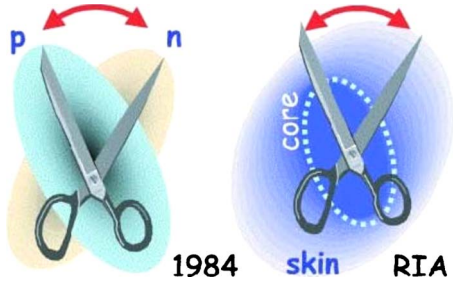

FIG. 59. (Color online) Schematic representation of the scissors mode in stable deformed nuclei (left) as compared to exotic nuclei with a weakly bound neutron skin (right). From RIA, 2003.

time high-resolution measurements of the ($\vec{p},\vec{p}'$) reaction at proton energies of several hundred MeV with measurements at 0°, should allow one to tackle all of these questions. Indeed, the feasibility of such experiments has been proven for the heaviest nuclei as shown in Fig. 58 for the example of ^{208}Pb (von Neumann-Cosel *et al.*, 2009).

(iii) The spin-flip magnetic dipole response, which is connected to the axial-vector part of the Gamow-Teller operator, may well be extended toward higher excitation energies using the fact that the spin-flip part probed in proton scattering is also connected to the neutrino (axial-vector term) scattering contribution. So, proton scattering may provide valuable information concerning neutrino scattering off nuclei in the giant resonance region and, subsequently, give insight in neutrino-nucleus cross sections and their importance in supernova processes.

(iv) There are other magnetic modes to be explored besides the dipole one, which formed the major part of the present review. There has been a search for magnetic quadrupole excitations of $J^\pi=2^-$ states in ^{48}Ca and ^{90}Zr using high-resolution backward angle inelastic electron scattering (von Neumann-Cosel *et al.*, 1999), extended to ^{58}Ni (Reitz *et al.*, 2002). Macroscopically, the orbital $M2$ mode can be viewed as a vibrational counter-rotation of different fluid layers in the upper and lower hemispheres, hence the name "twist" mode (Holzwarth and Eckart, 1977, 1979). As for the scissors mode, occurrence of an orbital $M2$ mode is a general feature of quantum many-body systems as discussed, e.g., for the cases of metallic clusters by Nesterenko *et al.* (2000) and ultracold Fermi gases by Viñas *et al.* (2001). Therefore this mode deserves more intensive and systematic exploration.

(v) The proportionality of the summed $M1$ strength to the nuclear deformation, more in particular showing a δ^2 dependence, opens the possibility to make use of measured magnetic dipole strengths as a new fingerprint for exploring sudden shape-phase transitions. Since there appear a number of regions in the nuclear mass table that look like potential places where sudden changes in nuclear shape may occur, an in depth study of magnetic dipole excitations in those regions can lead to extra information.

(vi) Last, but not least, a point of current interest is to study the scissors mode moving away from the valley of β stability. Because the nuclei to be explored are highly unstable, one will have to resort to reactions in inverse kinematics such as Coulomb excitation, inverse proton scattering utilizing radioactive ion beam facilities such as RIKEN, FAIR-GSI, SPIRAL II, and further on, FRIB. New phenomena are expected (RIA, 2003) in very neutron-rich nuclei when coupling a weakly bound neutron skin to a well-bound deformed core (cf. Fig. 59). A soft scissors mode due to the presence of a neutron skin, analogous to the soft electric dipole mode, has been proposed within both a geometrical approach by Van Isacker *et al.* (1992) at an energy approximately half of the scissors mode energy and within the IBM-2 (Warner and Van Isacker, 1997; Caprio and Iachello, 2004). Considering the plans at FAIR, one may even think about electron scattering on unstable nuclei. These and more exotic possibilities may materialize at future RIB facilities, as discussed, e.g., in recent report on upgrading the NSCL facility at MSU (RIA, 2006). The new generation facilities should also allow one to systematically explore mixed-symmetry states in the $N \approx 50$ and ≈ 82 region by providing beams of high enough luminosity.

To sum up, in the present review we have shown that (i) the 1^+ orbital scissors mode at low excitation energy, (ii) the 1^+ spin-flip mode at higher excitation energy, and (iii) the 1^+ component originating from the still higher-lying isovector quadrupole mode are universal realizations of the nuclear many-body system. It turns out that

these modes are not specific to nuclei only. On the contrary, the scissors mode also shows up in other many-body systems. There is compelling evidence for $M1$ excitations in deformed metallic clusters, in elliptically deformed quantum dots and in Bose-Einstein condensates of superfluid nature, and we have stressed the fascinating interplay between nuclear physics and other highly correlated many-body systems.

ACKNOWLEDGMENTS

During all the years working on magnetic dipole excitations we have benefited much from discussions with many colleagues, in particular (in alphabetical order) B. A. Brown, R. Casten, C. De Coster, A. E. L. Dieperink, J. Enders, A. Faessler, D. Frekers, J. Ginocchio, I. Hamamoto, F. Iachello, J. Jolie, U. Kneissl, K. Langanke, E. Lipparini, N. Lo Iudice, M. Macfarlane, G. Martínez-Pinedo, B. Mottelson, E. Moya de Guerra, T. Otsuka, F. Palumbo, N. Pietralla, A. Poves, C. Rangacharyulu, P. Sarriguren, O. Scholten, J. Speth, S. Stringari, P. Van Isacker, P. von Brentano, L. Zamick, and A. Zilges. One of the authors (K.H.) thanks the "FWO-Vlaanderen" and the University of Ghent for financial support during the years this review was written. This work was also performed in the framework of the BriX network (IAP P5/07, P6/23) funded by the InterUniversity Attraction Policy Programme—Belgian State—Belgian Science Policy. Furthermore, the work of the two other authors (P.v.N.C. and A.R.) was supported generously by the DFG under Contract No. SFB 634.

REFERENCES

Abdelaziz, M., and J. P. Elliott, 1987, Phys. Lett. B **197**, 505.
Abdelaziz, M., M. J. Thompson, J. P. Elliott, and J. A. Evans, 1988, J. Phys. G **14**, 219.
Ahmad, S. T., W. D. Hamilton, P. V. Isacker, S. A. Ahmad, and S. J. Robinson, 1989, J. Phys. G **15**, 93.
Ahn, T., M. Coqard, N. Pietralla, G. Rainowski, A. Costin, R. F. V. Janssens, C. J. Lister, M. Carpenter, S. Zhu, and K. Heyde, 2009, Phys. Lett. B **679**, 19.
Ahn, T., N. Pietralla, G. Rainovski, A. Costin, K. Dusling, T. C. Li, A. Linnemann, and S. Pontillo, 2007, Phys. Rev. C **75**, 014313.
Alaga, G., K. Alder, A. Bohr, and B. Mottelson, 1955, K. Dan. Vidensk. Selsk. Mat. Fys. Medd. **29**, 1.
Alhassid, Y., 2000, Rev. Mod. Phys. **72**, 895.
Allaart, K., E. Boeker, G. Bonsignori, M. Savoia, and Y. K. Gambhir, 1988, Phys. Rep. **169**, 209.
Arima, A., M. Harvey, and K. Shimizu, 1969, Phys. Lett. **30B**, 517.
Arima, A., and F. Iachello, 1975a, Phys. Lett. **57B**, 39.
Arima, A., and F. Iachello, 1975b, Phys. Rev. Lett. **35**, 1069.
Arima, A., T. Otsuka, F. Iachello, and I. Talmi, 1977, Phys. Lett. **66B**, 205.
Arima, A., K. Shimizu, W. Bentz, and H. Hyuga, 1987, *Advances in Nuclear Physics* (Plenum, New York), Vol. 18.
Ashcroft, E. W., and N. D. Mermin, 1976, *Solid State Physics* (Saunders College, Philadelphia).
Auerbach, N., 1983, Phys. Rep. **98**, 273.
Austing, D. G., S. Sasaki, S. Tarucha, S. M. Reimann, M. Koskinen, and M. Manninen, 1999, Phys. Rev. B **60**, 11514.
Balbutsev, E. B., 2010, J. Phys.: Conf. Ser. **205**, 012001.
Balbutsev, E. B., L. A. Malov, P. Schuck, and M. Urban, 2009, Phys. At. Nucl. **72**, 1305.
Balbutsev, E. B., L. A. Malov, P. Schuck, M. Urban, and X. Viñas, 2008, Phys. At. Nucl. **71**, 1012.
Balbutsev, E. B., and P. Schuck, 2004, Nucl. Phys. A **731**, 256.
Balbutsev, E. B., and P. Schuck, 2007, Ann. Phys. **322**, 489.
Bandyopadhyay, D., C. C. Reynolds, C. Fransen, N. Boukharouba, M. T. McEllistrem, and S. W. Yates, 2003, Phys. Rev. C **67**, 034319.
Bauske, I., *et al.*, 1993, Phys. Rev. Lett. **71**, 975.
Baznat, M. I., and N. Y. Pyatov, 1975, Sov. J. Nucl. Phys. **21**, 365.
Berg, U. E. P., 1984, J. Phys. (France), Colloq. **45**, C4-359.
Berg, U. E. P., K. Ackermann, K. Bangert, C. Blasing, W. Naatz, R. Stock, K. Wienhard, M. K. Brussel, T. E. Chapuran, and B. H. Wildenthal, 1984, Phys. Lett. **140B**, 191.
Berg, U. E. P., and U. Kneissl, 1987, Annu. Rev. Nucl. Part. Sci. **37**, 33.
Berg, U. E. P., *et al.*, 1984, Phys. Lett. **149B**, 59.
Bertsch, G. F., and I. Hamamoto, 1982, Phys. Rev. C **26**, 1323.
Bes, D. R., and R. A. Broglia, 1984, Phys. Lett. **137B**, 141.
Bettermann, L., C. Fransen, S. Heinze, J. Jolie, A. Linnemann, D. Mücher, W. Rother, T. Ahn, A. Costin, N. Pietralla, and Y. Luo, 2009, Phys. Rev. C **79**, 034315.
Beuschel, T., J. P. Draayer, D. Rompf, and J. G. Hirsch, 1998, Phys. Rev. C **57**, 1233.
Beuschel, T., J. G. Hirsch, and J. P. Draayer, 2000, Phys. Rev. C **61**, 054307.
Bjørnholm, S., J. Borggreen, O. Echt, K. Hansen, J. Pedersen, and H. D. Rasmussen, 1990, Phys. Rev. Lett. **65**, 1627.
Bjørnholm, S., J. Borggreen, K. Hansen, T. Martin, H. D. Rasmussen, and J. Pedersen, 1991, in *Ecole Internationale Joliot-Curie de Physique Nucleaire*, edited by Y. Abgrall (IN2P3, Bordeaux, France), p. 311.
Boelaert, N., A. Dewald, C. Fransen, J. Jolie, A. Linnemann, B. Melon, O. Möller, N. Smirnova, and K. Heyde, 2007, Phys. Rev. C **75**, 054311.
Boelaert, N., N. Smirnova, K. Heyde, and J. Jolie, 2007, Phys. Rev. C **75**, 014316.
Bohigas, O., 1991, in *Les Houches Summer School on Theoretical Physics, Session L II: Chaos and Quantum Physics*, edited by M. J. Giannoni, A. Voros, and J. Zinn-Justin (North-Holland, Amsterdam), p. 87.
Bohle, D., G. Kilgus, A. Richter, C. W. de Jager, and H. de Vries, 1987, Phys. Lett. B **195**, 326.
Bohle, D., G. Küchler, A. Richter, and W. Steffen, 1984, Phys. Lett. **148B**, 260.
Bohle, D., A. Richter, U. E. P. Berg, J. Drexler, R. D. Heil, U. Kneissl, H. Metzger, R. Stock, B. Fischer, H. Hollick, and D. Kollewe, 1986, Nucl. Phys. A **458**, 205.
Bohle, D., A. Richter, C. W. de Jager, and H. de Vries, 1987, Z. Phys. A **328**, 463.
Bohle, D., A. Richter, W. Steffen, A. E. L. Dieperink, N. L. Iudice, F. Palumbo, and O. Scholten, 1984, Phys. Lett. **137B**, 27.
Bohr, A., and B. Mottelson, 1969, *Nuclear Structure* (Benjamin, New York), Vol. 1.
Bohr, A., and B. Mottelson, 1975, *Nuclear Structure* (Benjamin, New York), Vol. 2.
Brack, M., 1991, in *Ecole Internationale Joliot-Curie de Phy-*

sique Nucleaire, edited by Y. Abgrall (IN2P3, Bordeaux, France), p. 325.
Brack, M., O. Henzken, and K. Hanzen, 1991a, Z. Phys. D: At., Mol. Clusters **19**, 51.
Brack, M., O. Henzken, and K. Hanzen, 1991b, Z. Phys. D: At., Mol. Clusters **21**, 65.
Brown, B. A., and B. H. Wildenthal, 1987, Nucl. Phys. A **474**, 290.
Brown, B. A., and B. H. Wildenthal, 1988, Annu. Rev. Nucl. Part. Sci. **38**, 29.
Brown, G. E., and M. Bolsterli, 1959, Phys. Rev. Lett. **3**, 472.
Brussaard, P. J., and P. W. M. Glaudemans, 1977, *Shell-Model Applications in Nuclear Spectroscopy* (North-Holland, Amsterdam).
Burda, O., *et al.*, 2007, Phys. Rev. Lett. **99**, 092503.
Caprio, M. A., and F. Iachello, 2004, Phys. Rev. Lett. **93**, 242502.
Casten, R. F., D. S. Brenner, and P. E. Haustein, 1987, Phys. Rev. Lett. **58**, 658.
Casten, R. F., K. Heyde, and A. Wolf, 1988, Phys. Lett. B **208**, 33.
Caurier, E., K. Langanke, G. Martínez-Pinedo, F. Nowacki, and P. Vogel, 2001, Phys. Lett. B **522**, 240.
Chaves, L., and A. Poves, 1986, Phys. Rev. C **34**, 1137.
Crawley, G. M., N. Anantaraman, A. Galonsky, C. Djalali, N. Marty, M. Morlet, A. Willis, J. C. Jourdain, and P. Kitching, 1982, Phys. Rev. C **26**, 87.
De Coster, C., and K. Heyde, 1989, Phys. Rev. Lett. **63**, 2797.
De Coster, C., and K. Heyde, 1991a, Phys. Rev. Lett. **66**, 2456.
De Coster, C., and K. Heyde, 1991b, Nucl. Phys. A **529**, 507.
De Coster, C., K. Heyde, and A. Richter, 1992, Nucl. Phys. A **542**, 375.
De Coster, C., K. Heyde, S. Rombouts, and A. Richter, 1995, Phys. Rev. C **51**, 3510.
De Franceschi, G., F. Palumbo, and N. Lo Iudice, 1983, Lett. Nuovo Cimento Soc. Ital. Fis. **37**, 61.
De Franceschi, G., F. Palumbo, and N. Lo Iudice, 1984, Phys. Rev. C **29**, 1496.
de Heer, W. A., 1993, Rev. Mod. Phys. **65**, 611.
de Heer, W. A., K. Selby, V. Kresin, J. Masui, M. Vollmer, A. Chatelain, and W. D. Knight, 1987, Phys. Rev. Lett. **59**, 1805.
Delorme, J., M. Ericson, A. Figureau, and C. Thévenet, 1976, Ann. Phys. (N.Y.) **102**, 273.
Demel, T., D. Heitmann, P. Grambow, and K. Ploog, 1990, Phys. Rev. Lett. **64**, 788.
Devi, Y. D., and V. K. B. Kota, 1992a, Phys. Lett. B **287**, 9.
Devi, Y. D., and V. K. B. Kota, 1992b, Nucl. Phys. A **541**, 173.
Devi, Y. D., and V. K. B. Kota, 1996, Nucl. Phys. A **600**, 20.
Dieperink, A. E. L., 1983, Prog. Part. Nucl. Phys. **9**, 121.
Djalali, C., N. Marty, M. Morlet, A. Willis, J. C. Jourdain, N. Anantaraman, G. M. Crawley, A. Galonsky, and P. Kitching, 1982, Nucl. Phys. A **388**, 1.
Eid, S. A. A., W. D. Hamilton, and J. P. Elliott, 1986, Phys. Lett. **166B**, 267.
Eisenberg, J. M., and W. Greiner, 1987, *Nuclear Theory, Vol. 1: Nuclear Models*, 3rd ed. (North-Holland, Amsterdam).
Elhami, E., J. N. Orce, S. Mukhopadhyay, S. N. Choudry, M. Scheck, M. T. McEllistrem, and S. W. Yates, 2007, Phys. Rev. C **75**, 011301(R).
Elhami, E., *et al.*, 2008, Phys. Rev. C **78**, 064303.
Elliott, J. P., 1985, Rep. Prog. Phys. **48**, 171.
Elliott, J. P., 1990, Prog. Part. Nucl. Phys. **25**, 325.
Elliott, P. J., 1958, Proc. R. Soc. London, Ser. A **245**, 128.
Elliott, P. J., 1963, Proc. R. Soc. London, Ser. A **272**, 557.
Enders, J., T. Guhr, N. Huxel, P. von Neumann-Cosel, C. Rangacharyulu, and A. Richter, 2000, Phys. Lett. B **486**, 273.
Enders, J., N. Huxel, U. Kneissl, P. von Neumann-Cosel, H. H. Pitz, and A. Richter, 1998, Phys. Rev. C **57**, 996.
Enders, J., N. Huxel, P. von Neumann-Cosel, and A. Richter, 1997, Phys. Rev. Lett. **79**, 2010.
Enders, J., H. Kaiser, P. von Neumann-Cosel, C. Rangacharyulu, and A. Richter, 1999, Phys. Rev. C **59**, R1851.
Enders, J., P. von Neumann-Cosel, C. Rangacharyulu, and A. Richter, 2005, Phys. Rev. C **71**, 014306.
Ericson, T., and W. Weise, 1988, *Pions and Nuclei: International Series of Monographs on Physics* (Clarendon, Oxford), Vol. 74.
Faessler, A., 1966, Nucl. Phys. **85**, 653.
Faessler, A., Z. Bochnacki, and R. Nojarov, 1986, J. Phys. G **12**, L47.
Faessler, A., and R. Nojarov, 1986, Phys. Lett. **166B**, 367.
Faessler, A., and R. Nojarov, 1987, Prog. Part. Nucl. Phys. **19**, 167.
Faessler, A., and R. Nojarov, 1988, Phys. Lett. B **215**, 439.
Faessler, A., R. Nojarov, and T. Taigel, 1989, Nucl. Phys. A **492**, 105.
Fagg, L. W., 1975, Rev. Mod. Phys. **47**, 683.
Fazekas, B., T. Belgya, G. Molnar, A. Veres, R. A. Gatenby, S. W. Yates, and T. Otsuka, 1992, Nucl. Phys. A **548**, 249.
Fearick, R. W., G. Hartung, K. Langanke, G. Martínez-Pinedo, P. von Neumann-Cosel, and A. Richter, 2003, Nucl. Phys. A **727**, 41.
Fearick, R. W., P. von Neumann-Cosel, A. Richter, S. J. Q. Robinson, and L. Zamick, 2006, J. Phys. Soc. Jpn. **75**, 094201.
Foltz, C. W., D. I. Sober, L. W. Fagg, H. D. Gräf, A. Richter, E. Spamer, and B. A. Brown, 1994, Phys. Rev. C **49**, 1359.
Frank, A., J. M. Arias, and P. Van Isacker, 1991, Nucl. Phys. A **531**, 125.
Fransen, C., N. Pietralla, P. von Brentanon, A. Dewald, J. Gableske, A. Gade, A. Lisetsky, and V. Werner, 2001, Phys. Lett. B **508**, 219.
Fransen, C., *et al.*, 2003, Phys. Rev. C **67**, 024307.
Freeman, S. J., R. Chapman, J. L. Durell, M. A. C. Hotchkis, F. Khazaie, C. J. Lisle, J. N. Mo, A. M. Bruce, R. A. Cunningham, P. V. Drumm, D. D. Warner, and J. D. Garrett, 1989, Phys. Lett. B **222**, 347.
Frekers, D., 2006, Prog. Part. Nucl. Phys. **57**, 217.
Frekers, D., *et al.*, 1990, Phys. Lett. B **244**, 178.
Fujita, Y., *et al.*, 2008, J. Phys. G **35**, 014041.
Gade, A., H. Klein, N. Pietralla, and P. von Brentano, 2002, Phys. Rev. C **65**, 054311.
Gade, A., I. Wiedenhöver, J. Gableske, A. Gelberg, H. Meise, N. Pietralla, and P. von Brentano, 2000, Nucl. Phys. A **665**, 268.
Gade, A., *et al.*, 2003, Phys. Rev. C **67**, 034304.
Gade, A., *et al.*, 2004, Phys. Rev. C **69**, 054321.
Garrett, J. D., J. Q. Robinson, A. J. Foglia, and H. Q. Jin, 1997, Phys. Lett. B **392**, 24.
Garrett, P. E., H. Lehmann, C. A. McGrath, M. Yeh, and S. W. Yates, 1996, Phys. Rev. C **54**, 2259.
Garrido, E., E. Moya de Guerra, P. Sarriguren, and J. M. Udias, 1991, Phys. Rev. C **44**, R1250.
Georgii, R., *et al.*, 1995, Nucl. Phys. A **592**, 307.
Ginocchio, J. N., 1991, Phys. Lett. B **265**, 6.
Ginocchio, J. N., 1999, Phys. Rev. C **59**, 2487.
Ginocchio, J. N., 2005, Phys. Rep. **414**, 165.

Ginocchio, J. N., and A. Leviatan, 1997, Phys. Rev. Lett. **79**, 813.
Giorgini, S., L. P. Pitaevskii, and S. Stringari, 2008, Rev. Mod. Phys. **80**, 1215.
Govaert, K., *et al.*, 1994, Nucl. Instrum. Methods A **337**, 265.
Greiner, W., 1965, Phys. Rev. Lett. **14**, 599.
Greiner, W., 1966, Nucl. Phys. **80**, 417.
Grundey, T., A. Richter, G. Schrieder, E. Spamer, and W. Stock, 1981, Nucl. Phys. A **357**, 269.
Guéry-Odelin, D., and S. Stringari, 1999, Phys. Rev. Lett. **83**, 4452.
Guhr, T., H. Diesener, A. Richter, C. W. de Jager, H. de Vries, and P. K. A. de Witt Huberts, 1990, Z. Phys. A **336**, 159.
Guhr, T., A. Müller-Groeling, and H. A. Weidenmüller, 1998, Phys. Rep. **299**, 189.
Guliyev, E., A. A. Kuliev, P. von Neumann-Cosel, and A. Richter, 2002, Phys. Lett. B **532**, 173.
Hagberg, E., T. K. Alexander, I. Neeson, V. T. Koslowsky, G. C. Ball, G. R. Dyck, J. S. Forster, J. C. Hardy, J. R. Leslie, H.-B. Mak, H. Schmeing, and I. S. Towner, 1994, Nucl. Phys. A **571**, 555.
Halse, P., 1990, Phys. Rev. C **41**, 2340.
Halse, P., 1991a, Nucl. Phys. A **526**, 152.
Halse, P., 1991b, Phys. Rev. C **44**, 2467.
Hamamoto, I., 1971, Nucl. Phys. A **177**, 484.
Hamamoto, I., and S. Åberg, 1984, Phys. Lett. **145B**, 163.
Hamamoto, I., and C. Magnusson, 1991, Phys. Lett. B **260**, 6.
Hamamoto, I., and W. Nazarewicz, 1992, Phys. Lett. B **297**, 25.
Hamamoto, I., and W. Nazarewicz, 1994, Phys. Rev. C **49**, 2489.
Hamamoto, I., and C. Ronström, 1987, Phys. Lett. B **194**, 6.
Hamilton, W. D., A. Irbäck, and J. P. Elliott, 1984, Phys. Rev. Lett. **53**, 2469.
Haq, R. U., A. Pandey, and O. Bohigas, 1982, Phys. Rev. Lett. **48**, 1086.
Harakeh, M., and A. van der Woude, 2001, *Giant Resonances: Fundamental High-Frequency Modes of Nuclear Excitation* (Oxford University, Oxford).
Harney, H. L., A. Richter, and H. A. Weidenmüller, 1986, Rev. Mod. Phys. **58**, 607.
Hartung, G., A. Richter, E. Spamer, H. Wörtche, C. Rangacharyulu, C. W. de Jager, and H. de Vries, 1989, Phys. Lett. B **221**, 109.
Hasse, R. W., and W. D. Myers, 1988, *Geometrical Relationships of Macroscopic Nuclear Physics* (Springer, Berlin).
Hatada, K., K. Hayakawa, and F. Palumbo, 2005, Phys. Rev. B **71**, 092402.
Hatada, K., K. Hayakawa, and F. Palumbo, 2010a, Eur. Phys. J. B (in press).
Hatada, K., K. Hayakawa, and F. Palumbo, 2010b, e-print arXiv:1004.2220.
Hecht, K. T., and A. Adler, 1969, Nucl. Phys. A **137**, 129.
Heil, R. D., H. H. Pitz, U. E. P. Berg, U. Kneissl, K. D. Hummel, G. Kilgus, D. Bohle, A. Richter, C. Wesselborg, and P. von Brentano, 1988, Nucl. Phys. A **476**, 39.
Heyde, K., 1989, Int. J. Mod. Phys. A **4**, 2063.
Heyde, K., and C. De Coster, 1991, Phys. Rev. C **44**, R2262.
Heyde, K., and C. De Coster, 1993, Phys. Lett. B **305**, 322.
Heyde, K., C. De Coster, and D. Ooms, 1994, Phys. Rev. C **49**, 156.
Heyde, K., C. De Coster, D. Ooms, and A. Richter, 1993, Phys. Lett. B **312**, 267.
Heyde, K., C. De Coster, A. Richter, and H. J. Wörtche, 1992, Nucl. Phys. A **549**, 103.
Heyde, K., C. De Coster, S. Rombouts, and S. J. Freeman, 1996, Nucl. Phys. A **596**, 30.
Heyde, K., and J. Sau, 1984, Phys. Rev. C **30**, 1355.
Heyde, K., and J. Sau, 1986, Phys. Rev. C **33**, 1050.
Heyde, K., M. Waroquier, P. Van Isacker, and H. Vincx, 1977, Phys. Rev. C **16**, 489.
Hicks, S. F., C. M. Davoren, W. M. Faulkner, and J. R. Vanhoy, 1998, Phys. Rev. C **57**, 2264.
Hicks, S. F., J. R. Vanhoy, and S. W. Yates, 2008, Phys. Rev. C **78**, 054320.
Hilton, R. R., 1976, talk at International Conference on Nuclear Structure, JINR Dubna (unpublished).
Hilton, R. R., 1995, in *Proceedings of the International Conference on Perspectives of Nuclear Physics in the Late Nineties*, edited by N. Dinh Dang, D. Feng, N. V. Giai, and N. D. Tu (World Scientific, Singapore), p. 86.
Hilton, R. R., W. Höhenberger, and H. J. Mang, 1993, Phys. Rev. C **47**, 602.
Hilton, R. R., W. Höhenberger, and P. Ring, 1998, Eur. Phys. J. A **1**, 257.
Hino, M., K. Muto, and T. Oda, 1988, Phys. Rev. C **37**, 1328.
Hirose, K., and N. S. Wingreen, 1999, Phys. Rev. B **59**, 4604.
Hix, W. R., A. Mezzacappa, O. E. B. Messer, and S. W. Bruenn, 2003, J. Phys. G **29**, 2523.
Hofmann, F., P. von Neumann-Cosel, F. Neumeyer, C. Rangacharyulu, B. Reitz, A. Richter, G. Schrieder, D. I. Sober, L. W. Fagg, and B. A. Brown, 2002, Phys. Rev. C **65**, 024311.
Hofmann, F., *et al.*, 2007, Phys. Rev. C **76**, 014314.
Holt, J. D., N. Pietralla, J. W. Holt, T. T. S. Kuo, and G. Rainovski, 2007, Phys. Rev. C **76**, 034325.
Holzwarth, D., and G. Eckart, 1977, Z. Phys. A **283**, 219.
Holzwarth, D., and G. Eckart, 1979, Nucl. Phys. A **325**, 1.
Honma, M., T. Mizusaki, and T. Otsuka, 1995, Phys. Rev. Lett. **75**, 1284.
Honma, M., T. Mizusaki, and T. Otsuka, 1996, Phys. Rev. Lett. **77**, 3315.
Honma, M., T. Otsuka, B. A. Brown, and T. Mizusaki, 2004, Phys. Rev. C **69**, 034335.
Huxel, N., W. Ahner, H. Diesener, P. von Neumann-Cosel, C. Rangacharyulu, A. Richter, C. Spieler, W. Ziegler, C. De Coster, and K. Heyde, 1992, Nucl. Phys. A **539**, 478.
Huxel, A., *et al.*, 1999, Nucl. Phys. A **645**, 239.
Iachello, F., 1981, Nucl. Phys. A **358**, 89c.
Iachello, F., 1984, Phys. Rev. Lett. **53**, 1427.
Iachello, F., and A. Arima, 1987, *The Interacting Boson Model* (Cambridge University, New York).
Iachello, F., and P. Van Isacker, 1991, *The Interacting Boson-Fermion Model* (Cambridge University, New York).
Ichimura, M., H. Sakai, and T. Wakasa, 2006, Prog. Part. Nucl. Phys. **56**, 446.
Ikeda, A., and T. Shimano, 1993, Nucl. Phys. A **577**, 573c.
Iwasaki, S., and K. Hara, 1984, Phys. Lett. **144B**, 9.
Jewell, J. K., P. D. Cottle, K. W. Kemper, and L. A. Riley, 1997, Phys. Rev. C **56**, 2440.
Kalmykov, Y., *et al.*, 2006, Phys. Rev. Lett. **96**, 012502.
Kasten, B., *et al.*, 1989, Phys. Rev. Lett. **63**, 609.
Klein, H., A. F. Lisetskiy, N. Pietralla, C. Fransen, A. Gade, and P. von Brentano, 2002, Phys. Rev. C **65**, 044315.
Kleinig, W., V. O. Nesterenkov, P.-G. Reinhard, and L. Serra, 1998, Eur. Phys. J. D **4**, 343.
Kneissl, U., N. Pietralla, and A. Zilges, 2006, J. Phys. G **32**, R217.
Kneissl, U., H. H. Pitz, and A. Zilges, 1996, Prog. Part. Nucl.

Phys. **37**, 349.
Knight, W. D., K. Clemenger, W. A. de Heer, W. A. Saunders, M. Y. Chou, and M. L. Cohen, 1984, Phys. Rev. Lett. **52**, 2141.
Kohstall, C., *et al.*, 2005, Phys. Rev. C **72**, 034302.
Koskinen, M., M. Manninen, and S. M. Reimann, 1997, Phys. Rev. Lett. **79**, 1389.
Kurasawa, H., and T. Suzuki, 1984, Phys. Lett. **144B**, 151.
Kuyucak, S., and A. E. Stuchbery, 1995, Phys. Lett. B **348**, 315.
Langanke, K., and G. Martínez-Pinedo, 2003, Rev. Mod. Phys. **75**, 819.
Langanke, K., G. Martínez-Pinedo, B. Müller, H.-T. Janka, A. Marek, W. R. Hix, A. Juodagalvis, and J. M. Sampaio, 2008, Phys. Rev. Lett. **100**, 011101.
Langanke, K., G. Martínez-Pinedo, P. von Neumann-Cosel, and A. Richter, 2004, Phys. Rev. Lett. **93**, 202501.
Laszewski, R. M., R. Alarcon, D. S. Dale, and S. D. Hoblit, 1988, Phys. Rev. Lett. **61**, 1710.
Lehmann, H., *et al.*, 1999, Phys. Rev. C **60**, 024308.
Lesher, S. R., C. J. McKay, M. Mynk, D. Bandyopadhyay, N. Boukharouba, C. Fransen, J. N. Orce, M. T. McEllistrem, and S. W. Yates, 2007, Phys. Rev. C **75**, 034318.
Li, T. C., *et al.*, 2005, Phys. Rev. C **71**, 044318.
Li, T. C., *et al.*, 2006, Phys. Rev. C **73**, 054306.
Lieb, K. P., H. G. Börner, M. S. Dewey, J. Jolie, S. J. Robinson, S. Ulbig, and C. Winter, 1988, Phys. Lett. B **215**, 50.
Linnemann, A., C. Fransen, M. Gorska, J. Jolie, U. Kneissl, P. Knoch, D. Mücher, H. H. Pitz, M. Scheck, C. Scholl, and P. von Brentano, 2005, Phys. Rev. C **72**, 064323.
Linnemann, A., *et al.*, 2003, Phys. Lett. B **554**, 15.
Linnemann, A., *et al.*, 2007, Phys. Rev. C **75**, 024310.
Lipparini, E., 2003, *Modern Many-Particle Physics: Atomic Gases, Quantum Dots and Quantum Fluids* (World Scientific, Singapore).
Lipparini, E., and A. Richter, 1984, Phys. Lett. **144B**, 13.
Lipparini, E., and S. Stringari, 1983, Phys. Lett. **130B**, 139.
Lipparini, E., and S. Stringari, 1989a, Phys. Rep. **175**, 103.
Lipparini, E., and S. Stringari, 1989b, Phys. Rev. Lett. **63**, 570.
Lisantti, J., J. R. Tinsley, D. M. Drake, I. Bergqvist, L. W. Swenson, D. K. McDaniels, F. E. Bertrand, E. E. Gross, D. J. Horen, and T. P. Sjoreen, 1984, Phys. Lett. **147B**, 23.
Lisetskiy, A. F., E. Caurier, K. Langanke, G. Martínez-Pinedo, P. von Neumann-Cosel, F. Nowacki, and A. Richter, 2007, Nucl. Phys. A **789**, 114.
Lisetskiy, A. F., N. Pietralla, C. Fransen, R. V. Jolos, and P. von Brentano, 2000, Nucl. Phys. A **677**, 100.
Liu, H., and L. Zamick, 1987a, Nucl. Phys. A **467**, 29.
Liu, H., and L. Zamick, 1987b, Phys. Rev. C **36**, 2064.
Liu, H., and L. Zamick, 1987c, Phys. Rev. C **36**, 2057.
Löbner, K. E. G., M. Vetter, and V. Hönig, 1970, Nucl. Data, Sect. A **7**, 495.
Lo Iudice, N., 1988, Phys. Rev. C **38**, 2895.
Lo Iudice, N., 1996a, Nucl. Phys. A **605**, 61.
Lo Iudice, N., 1996b, Phys. Rev. C **53**, 2171.
Lo Iudice, N., 1997, Phys. Part. Nucl. **28**, 556.
Lo Iudice, N., 1998, Phys. Rev. C **57**, 1246.
Lo Iudice, N., 2000, Riv. Nuovo Cim. **23**, 1.
Lo Iudice, N., and F. Palumbo, 1978, Phys. Rev. Lett. **41**, 1532.
Lo Iudice, N., and F. Palumbo, 1979, Nucl. Phys. A **326**, 193.
Lo Iudice, N., and A. Richter, 1989, Phys. Lett. B **228**, 291.
Lo Iudice, N., and A. Richter, 1993, Phys. Lett. B **304**, 193.
Lo Iudice, N., and C. Stoyanov, 2000, Phys. Rev. C **62**, 047302.
Lo Iudice, N., and C. Stoyanov, 2002, Phys. Rev. C **65**, 064304.
Lo Iudice, N., and C. Stoyanov, 2004, Phys. Rev. C **69**, 044312.
Lo Iudice, N., and C. Stoyanov, 2006, Phys. Rev. C **73**, 037305.
Lo Iudice, N., C. Stoyanov, and N. Pietralla, 2009, Phys. Rev. C **80**, 024311.
Lo Iudice, N., C. Stoyanov, and D. Tarpanov, 2008, Phys. Rev. C **77**, 044310.
Lüttge, C., C. Hofmann, J. Horn, F. Neumeyer, A. Richter, G. Schrieder, E. Spamer, A. Stiller, D. I. Sober, S. K. Matthews, and L. W. Fagg, 1995, Nucl. Instrum. Methods Phys. Res. A **366**, 325.
Lüttge, C., P. von Neumann-Cosel, F. Neumeyer, C. Rangacharyulu, A. Richter, G. Schrieder, E. Spamer, D. I. Sober, S. K. Matthews, and B. A. Brown, 1996, Phys. Rev. C **53**, 127.
Lüttge, C., P. von Neumann-Cosel, F. Neumeyer, and A. Richter, 1996, Nucl. Phys. A **606**, 183.
Maragò, O., G. Hechenblaikner, E. Hodby, and C. Foot, 2001, Phys. Rev. Lett. **86**, 3938.
Maragò, O. M., S. A. Hopkins, J. Arlt, E. Hodby, G. Hechenblaikner, and C. J. Foot, 2000, Phys. Rev. Lett. **84**, 2056.
Margraf, J., R. D. Heil, U. Kneissl, U. Maier, H. H. Pitz, H. Friedrichs, S. Lindenstruth, B. Schlitt, C. Wesselborg, P. von Brentano, R.-D. Herzberg, and A. Zilges, 1993, Phys. Rev. C **47**, 1474.
Margraf, J., *et al.*, 1990, Phys. Rev. C **42**, 771.
Margraf, J., *et al.*, 1995, Phys. Rev. C **52**, 2429.
Martínez-Pinedo, G., A. Poves, E. Caurier, and A. P. Zuker, 1996, Phys. Rev. C **53**, R2602.
McCullen, J. D., B. F. Bayman, and L. Zamick, 1964, Phys. Rev. **134**, B515.
Minguzzi, A., and M. P. Tosi, 2001, Phys. Rev. A **63**, 023609.
Mizusaki, T., M. Honma, and T. Otsuka, 1996, Phys. Rev. C **53**, 2786.
Mizusaki, T., T. Otsuka, and M. Sugita, 1991, Phys. Rev. C **44**, R1277.
Mizusaki, T., T. Otsuka, Y. Utsuno, M. Honma, and T. Sebe, 1999, Phys. Rev. C **59**, R1846.
Modugno, G., M. Modugno, F. Riboli, G. Roati, and M. Inguscio, 2002, Phys. Rev. Lett. **89**, 190404.
Moya de Guerra, E., and L. Zamick, 1993, Phys. Rev. C **47**, 2604.
Mukhopadhyay, S., M. Scheck, B. Crider, S. N. Choudry, E. Elhami, E. Peters, M. T. McEllistrem, J. N. Orce, and S. W. Yates, 2008, Phys. Rev. C **78**, 034317.
Nakatsukasa, T., K. Matsuyanagi, I. Hamamoto, and W. Nazarewicz, 1994, Nucl. Phys. A **573**, 333.
Nesterenko, V. O., W. Kleinig, F. F. de Souza Cruz, and N. Lo Iudice, 1999, Phys. Rev. Lett. **83**, 57.
Nesterenko, V. O., W. Kleinig, V. V. Gudkov, N. Lo Iudice, and J. Kvasil, 1997, Phys. Rev. A **56**, 607.
Nesterenko, V. O., J. R. Marinelli, F. F. de Souza Cruz, W. Kleinig, and P.-G. Reinhard, 2000, Phys. Rev. Lett. **85**, 3141.
Nojarov, R., Z. Bochnacki, and A. Faessler, 1986, Z. Phys. A **324**, 289.
Nojarov, R., and A. Faessler, 1990, Z. Phys. A **336**, 151.
Nojarov, R., A. Faessler, and O. Civitarese, 1987, Phys. Lett. B **183**, 122.
Nojarov, R., A. Faessler, and M. Dingfelder, 1995, Phys. Rev. C **51**, 2449.
Nojarov, R., A. Faessler, and P. O. Lipas, 1991, Nucl. Phys. A **533**, 381; **537**, 707(E) (1992).
Nord, A., *et al.*, 1996, Phys. Rev. C **54**, 2287.
Nord, A., *et al.*, 2003, Phys. Rev. C **67**, 034307.
Oda, T., M. Himo, and K. Muto, 1987, Phys. Lett. B **190**, 14.
Otsuka, T., 1990, Nucl. Phys. A **507**, 129c.

Otsuka, T., 1992, Hyperfine Interact. **74**, 93.
Otsuka, T., and J. N. Ginocchio, 1985, Phys. Rev. Lett. **54**, 777.
Otsuka, T., M. Honma, and T. Mizusaki, 1998, Phys. Rev. Lett. **81**, 1588.
Otsuka, T., and K.-H. Kim, 1994, Phys. Rev. C **50**, R1768.
Otsuka, T., T. Mizusaki, and M. Honma, 1999, J. Phys. G **25**, 699.
Otsuka, T., X. W. Pan, and A. Arima, 1990, Phys. Lett. B **247**, 191.
Otten, E., 1989, *Treatise on Heavy-Ion Science* (Plenum, New York), Vol. 8.
Peña Arteaga, D., and P. Ring, 2007, Prog. Part. Nucl. Phys. **59**, 314.
Peña Arteaga, D., and P. Ring, 2008, Phys. Rev. C **77**, 034317.
Petermann, I., K. Langanke, G. Martínez-Pinedo, P. von Neumann-Cosel, F. Nowacki, and A. Richter, 2010, Phys. Rev. C **81**, 014308.
Pietralla, N., C. J. Barton III, R. Krücken, C. W. Beausang, M. A. Caprio, R. F. Casten, J. R. Cooper, A. A. Hecht, H. Newman, J. R. Novak, and N. V. Zamfir, 2001, Phys. Rev. C **64**, 031301(R).
Pietralla, N., C. Fransen, P. von Brentano, A. Dewald, A. Fitzler, C. Frießner, and J. Gableske, 2000, Phys. Rev. Lett. **84**, 3775.
Pietralla, N., P. von Brentano, A. Gelberg, T. Otsuka, A. Richter, N. Smirnova, and I. Wiedenhöver, 1998, Phys. Rev. C **58**, 191.
Pietralla, N., P. von Brentano, R.-D. Herzberg, U. Kneissl, N. Lo Iudice, H. Maser, H. H. Pitz, and A. Zilges, 1998, Phys. Rev. C **58**, 184.
Pietralla, N., P. von Brentano, and A. F. Lisetsky, 2008, Prog. Part. Nucl. Phys. **60**, 225.
Pietralla, N., *et al.*, 1999, Phys. Rev. Lett. **83**, 1303.
Pietralla, N., *et al.*, 2001, Phys. Rev. Lett. **88**, 012502.
Pitaevskii, L., and S. Stringari, 2003, *Bose-Einstein Condensation*, International Series of Monographs on Physics Vol. 116 (Oxford Science, Clarendon).
Poves, A., J. Retamosa, and E. Moya de Guerra, 1989, Phys. Rev. C **39**, 1639.
Poves, A., J. Sánchez-Solano, E. Caurier, and F. Nowacki, 2001, Nucl. Phys. A **694**, 157.
Puente, A., and L. Serra, 1999, Phys. Rev. Lett. **83**, 3266.
Raduta, A. A., and D. S. Delion, 1990, Nucl. Phys. A **513**, 11.
Raduta, A. A., and N. Lo Iudice, 1989, Z. Phys. A **334**, 403.
Rainovski, G., N. Pietralla, T. Ahn, C. J. Lister, R. V. F. Janssens, M. P. Carpenter, S. Zhu, and C. J. Barton III, 2006, Phys. Rev. Lett. **96**, 122501.
Raman, S., L. W. Fagg, and R. S. Hicks, 1991, *International Review of Nuclear Physics* (World Scientific, Singapore), Vol. 7, p. 355.
Rangacharyulu, C., A. Richter, H. J. Wörtche, W. Ziegler, and R. F. Casten, 1991, Phys. Rev. C **43**, R949.
Reitz, B., F. Hofmann, P. von Neumann-Cosel, F. Neumeyer, C. Rangacharyulu, A. Richter, G. Schrieder, D. I. Sober, and B. A. Brown, 1999, Phys. Rev. Lett. **82**, 291.
Reitz, B., *et al.*, 2002, Phys. Lett. B **532**, 179.
Retamosa, J., J. M. Udias, A. Poves, and E. Moya de Guerra, 1990, Nucl. Phys. A **511**, 221.
RIA, 2003, *The Intellectual Challenges of RIA: A White Paper from the RIA Users Community* (http://www.orau.org/ria/pdf/intell.pdf).
RIA, 2006, *Isotope Science Facility at Michigan State University* (http://www.nscl.msu.edu/future/nsclwhitepaper2006).
Richter, A., 1983, in *Proceedings of the International Conference on Nuclear Physics*, edited by P. Blasi and R. A. Ricci (Tipografica Compositori, Bologna), Vol. 2, p. 189.
Richter, A., 1985, Prog. Part. Nucl. Phys. **13**, 1.
Richter, A., 1990, Nucl. Phys. A **507**, 99c.
Richter, A., 1991, Nucl. Phys. A **522**, 139c.
Richter, A., 1993, Nucl. Phys. A **553**, 417c.
Richter, A., 1994, in *Proceedings of the 4th International Spring Seminar on Nuclear Physics: The Building Blocks of Nuclear Structure*, edited by A. Covello (World Scientific, Singapore), p. 335.
Richter, A., 1995, Prog. Part. Nucl. Phys. **34**, 261.
Richter, A., and W. Knüpfer, 1980, in *Electron and Pion Interactions with Nuclei at Intermediate Energies*, edited by W. Bertozzi, S. Costa, and C. Schaerf (Harwood Academic, Newark, NJ), p. 241.
Richter, A., A. Weiss, O. Häusser, and B. A. Brown, 1990, Phys. Rev. Lett. **65**, 2519.
Ring, P., and P. Schuck, 1980, *The Nuclear Many-Body Problem* (Springer, Heidelberg).
Rohozinski, S. G., and W. Greiner, 1985, Z. Phys. A **322**, 271.
Rompf, D., T. Beuschel, J. P. Draayer, W. Scheid, and J. G. Hirsch, 1998, Phys. Rev. C **57**, 1703.
Rowe, D., 1970, *Nuclear Collective Motion* (Methuen, London).
Sambataro, M., and A. Dieperink, 1981, Phys. Lett. **107B**, 249.
Sambataro, M., O. Scholten, A. E. L. Dieperink, and G. Picciotto, 1984, Nucl. Phys. A **423**, 333.
Sarriguren, P., E. Moya de Guerra, and R. Nojarov, 1996, Phys. Rev. C **54**, 690.
Sarriguren, P., E. Moya de Guerra, R. Nojarov, and A. Faessler, 1993, J. Phys. G **19**, 291.
Sarriguren, P., E. Moya de Guerra, R. Nojarov, and A. Faessler, 1994, J. Phys. G **20**, 315.
Savran, D., *et al.*, 2005, Phys. Rev. C **71**, 034304.
Scheck, M., S. N. Choudry, E. Elhami, M. T. McEllistrem, S. Mukhopadhyay, J. N. Orce, and S. W. Yates, 2008, Phys. Rev. C **78**, 034302.
Scheck, M., *et al.*, 2004, Phys. Rev. C **70**, 044319.
Schlegel, C., P. von Neumann-Cosel, A. Richter, and P. Van Isacker, 1996, Phys. Lett. B **375**, 21.
Scholten, O., A. E. L. Dieperink, K. Heyde, and P. Van Isacker, 1984, Phys. Lett. **149B**, 279.
Scholten, O., K. Heyde, and P. Van Isacker, 1985, Phys. Rev. Lett. **55**, 1866.
Scholten, O., K. Heyde, P. Van Isacker, J. Jolie, J. Moreau, M. Waroquier, and J. Sau, 1985, Nucl. Phys. A **438**, 41.
Scholtz, F. G., R. Nojarov, and A. Faessler, 1989, Phys. Rev. Lett. **63**, 1356.
Schüller, C., G. Biese, K. Keller, C. Steinebach, D. Heitmann, P. Grambow, and K. Eberl, 1996, Phys. Rev. B **54**, R17304.
Schwengner, R., *et al.*, 1997a, Nucl. Phys. A **620**, 277.
Schwengner, R., *et al.*, 1997b, Nucl. Phys. A **624**, 776E.
Schwengner, R., *et al.*, 2007, Phys. Rev. C **76**, 034321.
Serra, L., A. Puente, and E. Lipparini, 1999, Phys. Rev. B **60**, R13966.
Shevchenko, A., J. Carter, G. R. J. Cooper, R. W. Fearick, Y. Kalmykov, P. von Neumann-Cosel, V. Y. Ponomarev, A. Richter, I. Usman, and J. Wambach, 2008, Phys. Rev. C **77**, 024302.
Shevchenko, A., *et al.*, 2004, Phys. Rev. Lett. **93**, 122501.
Shevchenko, A., *et al.*, 2009, Phys. Rev. C **79**, 044305.
Shimizu, N., T. Otsuka, T. Mizusaki, and M. Honma, 2001,

Phys. Rev. Lett. **86**, 1171.
Shriner, J. F., Jr., G. E. Mitchell, and T. von Egidy, 1991, Z. Phys. A **338**, 309.
Sieja, K., G. Martínez-Pinedo, L. Coquard, and N. Pietralla, 2009, Phys. Rev. C **80**, 054311.
Sikorski, C., and U. Merkt, 1989, Phys. Rev. Lett. **62**, 2164.
Smith, B. H., X.-W. Pan, D. H. Feng, and M. Guidry, 1995, Phys. Rev. Lett. **75**, 3086.
Sober, D. I., B. C. Metsch, W. Knüpfer, G. Eulenberg, G. Küchler, A. Richter, E. Spamer, and W. Steffen, 1985, Phys. Rev. C **31**, 2054.
Soloviev, V. G., 1992, *Theory of the Atomic Nucleus: Quasiparticles and Phonons* (IOP, Bristol).
Soloviev, V. G., A. V. Sushkov, and N. Y. Shirikova, 1996, Phys. Rev. C **53**, 1022.
Soloviev, V. G., A. V. Sushkov, and N. Y. Shirikova, 1997a, Prog. Part. Nucl. Phys. **38**, 53.
Soloviev, V. G., A. V. Sushkov, and N. Y. Shirikova, 1997b, Phys. Rev. C **56**, 2528.
Soloviev, V. G., A. V. Sushkov, N. Y. Shirikova, and N. Lo Iudice, 1997, Nucl. Phys. A **613**, 45.
Steffen, W., H.-D. Gräf, W. Gross, D. Meuer, A. Richter, E. Spamer, O. Titze, and W. Knüpfer, 1980, Phys. Lett. **95B**, 23.
Strenz, R., U. Bockelmann, F. Hirler, G. Abstreiter, G. Böhm, and G. Weimann, 1994, Phys. Rev. Lett. **73**, 3022.
Sugawara-Tanabe, K., and A. Arima, 1989, Phys. Lett. B **229**, 327.
Suzuki, T., and D. Rowe, 1977, Nucl. Phys. A **289**, 461.
Takayanagi, K., K. Shimizu, and A. Arima, 1988, Nucl. Phys. A **481**, 313.
Tamii, A., *et al.*, 2009, Nucl. Instrum. Methods Phys. Res. A **605**, 326.
Towner, I. S., 1987, Phys. Rep. **155**, 263.
Utsuno, Y., T. Otsuka, T. Mizusaki, and M. Honma, 1999, Phys. Rev. C **60**, 054315.
van der Laan, G., E. Arenholz, A. Schmehl, and D. G. Schlom, 2008, Phys. Rev. Lett. **100**, 067403.
Vanhoy, J. R., J. M. Anthony, B. M. Haas, B. H. Benedict, B. T. Meehan, S. F. Hicks, C. M. Davoren, and C. L. Lundstedt, 1995, Phys. Rev. C **52**, 2387.
Van Isacker, P., and A. Frank, 1989, Phys. Lett. B **225**, 1.
Van Isacker, P., K. Heyde, J. Jolie, and A. Sevrin, 1986, Ann. Phys. (N.Y.) **171**, 253.
Van Isacker, P., M. A. Nagarajan, and D. D. Warner, 1992, Phys. Rev. C **45**, R13.
Viñas, X., R. Roth, P. Schuck, and J. Wambach, 2001, Phys. Rev. A **64**, 055601.
von Brentano, P., A. Zilges, N. V. Zamfir, and R.-D. Herzberg, 1994, in *Symmetries in Science VII*, edited by B. Gruku and T. Otsuka (Plenum, New York), p. 123.
von Brentano, P., *et al.*, 1996, Phys. Rev. Lett. **76**, 2029.
von Garrel, H., *et al.*, 2006, Phys. Rev. C **73**, 054315.
von Neumann-Cosel, P., 1997, Prog. Part. Nucl. Phys. **38**, 213.
von Neumann-Cosel, P., and J. N. Ginocchio, 2000, Phys. Rev. C **62**, 014308.
von Neumann-Cosel, P., J. N. Ginocchio, H. Bauer, and A. Richter, 1995, Phys. Rev. Lett. **75**, 4178.
von Neumann-Cosel, P., H.-D. Gräf, U. Krämer, A. Richter, and E. Spamer, 2000, Nucl. Phys. A **669**, 3.
von Neumann-Cosel, P., F. Neumeyer, S. Nishizaki, V. Y. Ponomarev, C. Rangacharyulu, B. Reitz, A. Richter, G. Schrieder, D. I. Sober, T. Waindzoch, and J. Wambach, 1999, Phys. Rev. Lett. **82**, 1105.
von Neumann-Cosel, P., A. Poves, J. Retamosa, and A. Richter, 1998, Phys. Lett. B **443**, 1.
von Neumann-Cosel, P., A. Richter, Y. Fujita, and B. D. Anderson, 1997, Phys. Rev. C **55**, 532.
von Neumann-Cosel, P., *et al.*, 2009, in *Proceedings of the 13th International Symposium on Capture Gamma-Ray Spectroscopy and Related Topics*, edited by J. Jolie, A. Zilges, N. Warr, and A. Blazhev (AIP, Melville, NY), Vol. 1090, p. 404.
Warner, D. D., and P. Van Isacker, 1997, Phys. Lett. B **395**, 145.
Weidenmüller, H. A., and G. E. Mitchell, 2009, Rev. Mod. Phys. **81**, 539.
Weller, H. R., M. W. Ahmed, H. Gao, W. Tornow, Y. K. Wu, M. Gai, and R. Miskimen, 2009, Prog. Part. Nucl. Phys. **62**, 257.
Werner, V., *et al.*, 2002, Phys. Lett. B **550**, 140.
Werner, V., *et al.*, 2008, Phys. Rev. C **78**, 031301(R).
Wesselborg, C., K. Schiffer, K. O. Zell, P. von Brentano, D. Bohle, A. Richter, G. P. A. Berg, B. Brinkmöller, J. G. M. Römer, F. Osterfeld, and M. Yabe, 1986, Z. Phys. A **323**, 485.
Wesselborg, C., P. von Brentano, K. O. Zell, R. D. Heil, H. H. Pitz, U. E. P. Berg, U. Kneissl, S. Lindenstruth, U. Seemann, and R. Stock, 1988, Phys. Lett. B **207**, 22.
Wiedenhöver, I., A. Gelberg, T. Otsuka, N. Pietralla, J. Gableske, A. Dewald, and P. von Brentano, 1997, Phys. Rev. C **56**, R2354.
Williams, E., R. J. Casperson, V. Werner, H. Ai, P. Boutachkov, M. Chamberlain, G. Gürdal, A. Heinz, E. A. McCutchan, J. Qian, and R. Winkler, 2009, Phys. Rev. C **80**, 054309.
Willis, A., M. Morlet, N. Marty, C. Djalali, D. Bohle, H. Diesener, A. Richter, and H. Stein, 1989, Nucl. Phys. A **499**, 367.
Wolf, A., R. F. Casten, and D. D. Warner, 1987, Phys. Lett. B **190**, 19.
Wörtche, H. J., 1994, Doctoral thesis (Technische Universität Darmstadt).
Yevetska, O., J. Enders, M. Fritzsche, P. von Neumann-Cosel, S. Oberstedt, A. Richter, D. Savran, and K. Sonnabend, 2010, Phys. Rev. C (to be published).
Zamick, L., 1985, Phys. Rev. C **31**, 1955.
Zamick, L., 1986a, Phys. Lett. B **167**, 1.
Zamick, L., 1986b, Phys. Rev. C **33**, 691.
Zamick, L., and D. C. Zheng, 1992, Phys. Rev. C **46**, 2106.
Zawischa, D., 1998, J. Phys. G **24**, 683.
Zawischa, D., M. Macfarlane, and J. Speth, 1990, Phys. Rev. C **42**, 1461.
Zawischa, D., and J. Speth, 1990, Phys. Lett. B **252**, 4.
Zawischa, D., and J. Speth, 1994, Nucl. Phys. A **569**, 343.
Ziegler, W., N. Huxel, P. von Neumann-Cosel, C. Rangacharyulu, A. Richter, C. Spieler, C. De Coster, and K. Heyde, 1993, Nucl. Phys. A **564**, 366.
Ziegler, W., C. Rangacharyulu, A. Richter, and C. Spieler, 1990, Phys. Rev. Lett. **65**, 2515.
Zilges, A., P. von Brentano, R.-D. Herzberg, U. Kneissl, J. Margraf, and H. H. Pitz, 1996, Nucl. Phys. A **599**, 147c.
Zilges, A., P. von Brentano, A. Richter, R. D. Heil, U. Kneissl, H. H. Pitz, and C. Wesselborg, 1990, Phys. Rev. C **42**, 1945.